UNIVERSITY OF CALIFORNIA,
IRVINE

Mechanisms of the Exacerbation of Atherosclerosis by Semi-Volatile Organic Constituents of Inhaled Ambient Particulate Matter in apoE -/- Mice

DISSERTATION

submitted in partial satisfaction of the requirements
for the degree of

DOCTOR OF PHILOSOPHY

in Environmental Toxicology

by

Andrew James Keebaugh

Dissertation Committee:
Professor Robert F. Phalen, Chair
Professor Michael T. Kleinman
Professor Stephen C. Bondy
Professor Scott M. Bartell

2017

TABLE OF CONTENTS

LIST OF SYMBOLS

adjCAPs	Concentrated ambient particles diluted to match particle concentration of denuded concentrated particles
ANOVA	Analysis of variance
apoE -/-	Apolipoprotein E gene knockout
CAD	Coronary artery disease
CAPs	Concentrated ambient particles
Cl^-	Chloride
cm	Centimeter
CPC	Condensation particle counter
CRP	C-reactive protein
Cu	Copper
CV	Cardiovascular
DA	Descending aorta
deCAPs	Denuded concentrated ambient particles
°C	Degrees Celsius
EC	Elemental carbon
ECG	Electrocardiogram
EDTA	Ethylenediaminetetraacetic acid
EPA	Environmental Protection Agency
g	Gravity
H:C	Hydrogen to carbon ratio
HDL	High-density lipoprotein

HEPA	High-efficiency particulate arrestance
HF	High frequency
HPLC	High-performance liquid chromatography
HR-ToF-AMS	High-resolution time-of-flight aerosol mass spectrometer
HRV	Heart rate ariability
Hz	Hertz
IACUC	Institutional Animal Care and Use Committee
ICAM-1	Intracellular adhesion molecule 1
IL	Interleukin
kg	kilogram
LDL	Low-density lipoprotein
LF	Low frequency
LPM	Liters per minute
LV-OOA	Low volatility oxidized organic aerosol
M	Molar
m^3	Cubic Meter
MAP	Mitogen-activated protein
MCP-1	Monocyte chemotactic protein 1
MDA	Malondialdehyde
µg	Microgram
µL	Microliter
µm	Micrometer
µM	Micromolar

mg	Milligram
mL	Milliliter
mm	Millimeter
mM	Millimolar
MMP-9	Matrix metalloproteinase 9
NADH	Nicotinamide adenine dinucleotide
NADPH	Nicotinamide adenine dinucleotide phosphate
NF-κB	Nuclear factor kappa-light-chain-enhancer of activated B cells
NH_4^+	Ammonium
nm	Nanometer
NO_3^-	Nitrate
O:C	Oxygen to carbon ratio
OC	Organic carbon
oxLDL	Oxidized low-density lipoprotein
p	P-value
p/cm^3	Particles per cubic centimeter
PAH	Polycyclic aromatic hydrocarbons
PAI-1	Plasminogen activator inhibitor 1
PBS	Phosphate buffered saline
pg	Picogram
PM	Particulate matter
$PM_{0.1}$	Particulate matter with an aerodynamic diameter less than 0.1 micrometers

PM_{10}	Particulate matter with an aerodynamic diameter less than 10 micrometers
$PM_{2.5}$	Particulate matter with an aerodynamic diameter less than 2.5 micrometers
POA	Primary organic aerosol
R	R wave on an electrocardiogram tracing
ROS	Reactive oxygen species
SD	Standard deviation
SEM	Standard error of the mean
SMPS	Scanning mobility particle sizer
SO_4^{2-}	Sulfate
SOA	Secondary organic aerosol
SV-OOA	Semi-volatile oxidized organic aerosol
SVOC	Semi-volatile organic compound
TNF-α	Tumor necrosis factor alpha
TRPA1	Transient receptor potential ankyrin 1
TRPV1	Transient receptor potential vanilloid 1
U	unit
UF	Ultrafine
VACES	Versatile aerosol concentration enrichment system
VCAM-1	Vascular cell adhesion molecule 1

LIST OF FIGURES

Page

LIST OF TABLES

Page

ACKNOWLEDGEMENTS

I would like to start my acknowledgements by thanking the person, Dr. Glenn Gookin, who first invited me into the world of toxicology by giving me an opportunity in the Kleinman lab as an undergrad who was just looking for a research position and knew nothing about the field. Glenn, Dr. Ronald Shank and Dr. Loyda Mendez were instrumental in mentoring me early on and inspiring me to pursue a career in toxicology. And I owe the most appreciation to Dr. Michael Kleinman, who has always strongly supported me as my mentor and has given me all the opportunity I could ever ask for to grow and learn as a scientific researcher.

I appreciate all of the input and critiques that were given to my dissertation project by the committee both for my advancement and defense. Dr. Robert Phalen, Dr. Stephen Bondy, Dr. Scott Bartell, Dr. Nostarola Vaziri, and Dr. Rufus Edwards all helped me create something that I am very pround of. Furthermore, I am thankful for the growth of the program over the course of my graduate studies, and the faculty, in particular Dr. Ulrike Luderer, for working hard to make it better for the students and really strengthen it for the future.

I could not have done the majority of this work without the help of everyone that supported the project. I would like to thank BP and the South Coast Air Quality Management District for funding the work of which my dissertation research was a part. Additionally, thanks to Dr. Lisa Wingen and the lab of Dr. Barbara Finlayson-Pitts, we were able to get some very unique characterization data that really made this a novel project. And none of this would have been possible without everyone in the Kleinman lab that supported the work, including Irene Hasen, Mariyah Saiddudin, Laura Pawlikowski, Steven Chen, and Amanda Ting. Most of all, David Herman, Samantha Renusch and Rebecca Johnson have made great contributions to the research but more importantly to improving the lab and setting it on a path to do some fantastic things in the future.

Finally, there is the support system that allowed me to make it through the seemingly never-ending years of education. Dr. Anthony Biascan and Dr. Raga Avanasi were great friends that I knew that I could always count on. I am most grateful to my parents and my sister for motivating me to improve myself and always instilling the importance of continuing to as high a level of education as I could. I would not have made it to college without them, and I definitely would not have made it through a decade of college without the love of my life, Nichelle Nguyen, who made these the best years of my life.

CURRICULUM VITAE

Andrew James Keebaugh

2007-2009	Undergraduate Researcher, Baram Lab, Department of Anatomy and Neurobiology, University of California, Irvine
2009	B.S. in Biomedical Engineering, University of California, Irvine
2009-2011	Volunteer, University of California, Irvine Outreach Clinic
2009-2011	Lab Technician, Kleinman Lab, Department of Medicine, University of California, Irvine
2011-2017	Graduate Student Researcher, Kleinman Lab, Department of Medicine, University of California, Irvine
2012-2013	Teaching Assistant, Department of Anatomy and Neurobiology, University of California, Irvine
2013	Teaching Assistant, Department of Developmental and Cell Biology, University of California, Irvine
2017	Ph.D. in Environmental Toxicology, University of California, Irvine

PUBLICATIONS

Dubé CM, Ravizza T, Hamamura M, Zha Q, Keebaugh A, Fok K, Andres AL, Nalcioglu O, Obenaus A, Vezzani A, Baram TZ. Epileptogenesis provoked by prolonged experimental febrile seizures: mechanisms and biomarkers. Journal of Neuroscience. 2010;30(22):7484-94.

Keebaugh AJ, Sioutas C, Pakbin P, Schauer JJ, Mendez LB, Kleinman MT. Is atherosclerotic disease associated with organic components of ambient fine particles? Science of the Total Environment. 2015;533:69-75.

Chen B, Roy SG, McMonigle RJ, Keebaugh A, McCracken AN, Selwan E, Fransson R, Fallegger D, Huwiler A, Kleinman MT, Edinger AL, Hanessian S. Azacyclic FTY720 Analogues That Limit Nutrient Transporter Expression but Lack S1P Receptor Activity and Negative Chronotropic Effects Offer a Novel and Effective Strategy to Kill Cancer Cells in Vivo. ACS Chemical Biology. 2016;11(2):409-14.

McCracken AN, McMonigle RJ, Tessier J, Fransson R, Perryman MS, Chen B, Keebaugh A, Selwan E, Barr SA, Kim SM, Roy SG, Liu G, Fallegger D, Sernissi L, Brandt C, Moitessier N, Snider AJ, Clare S, Müschen M, Huwiler A, Kleinman MT, Hanessian S, Edinger AL. Phosphorylation of a constrained azacyclic FTY720 analog enhances anti-leukemic activity without inducing S1P receptor activation. Leukemia. 2016.

ABSTRACT OF DISSERTATION

Mechanisms of the Exacerbation of Atherosclerosis by Semi-Volatile Organic Constituents of Inhaled Ambient Particulate Matter in apoE -/- mice

by

Andrew James Keebaugh

Doctor of Philosophy in Environmental Toxicology

University of California, Irvine, 2017

Professor Robert F. Phalen, Chair

Emissions-related particulate matter exposures are thought to be associated with thousands of excess deaths per year, many of which are related to cardiovascular disease. Ultrafine particles contain a large proportion of redox-active organic compounds that can exist in either the vapor or particle phase and are considered SVOCs. After inhalation, these compounds may be responsible for initiating a cascade of oxidative stress and inflammation in the body that can promote atherosclerotic plaque development that can lead to CAD. The goal of this project was to investigate the mechanisms of how exposure to particle associated SVOCs promotes atherosclerosis. ApoE -/- mice, which are prone to developing atherosclerosis, were exposed to unmodified UF CAPs, deCAPs with the SVOC components removed by a thermodenuder, or adjCAPs that was adjusted to match the concentration of deCAPs. Mice were exposed for nine weeks for five hours per day, four days per week at the UC Irvine campus. A control group was exposed to purified, filtered air. A higher percentage of mice exposed to adjCAPs formed arterial plaques compared to deCAPs and air

exposed mice. Furthermore there was greater vascular wall thickening and fibrosis in the arteries of mice exposed to CAPs compared to deCAPs. IL-6 was increased in the serum of mice exposed to adjCAPs relative to deCAPs, indicating that the SVOCs are promoting atherosclerosis through a pro-inflammatory mechanism. Furthermore, adjCAPs exposure increased the ratio of LDL to HDL cholesterol, so SVOCs may be related to pro-atherogenic alterations to lipid metabolism. The power in the high frequency component of HRV, a measure of cardiac parasympathetic activity, was acutely reduced in mice exposed to CAPs, and daily changes in HF HRV were associated with the O:C ratio of the UF fraction of CAPs. These associations implicated POA, which comprises a major component of SVOCs, as potentially driving the toxic effects. The attenuation of atherosclerostic plaque formation with deCAPs exposure indicates that SVOCs in CAPs exposures are important contributors to toxic cardiovascular effects and these components deserve consideration in discussions of regulation of primary PM emissions and human exposure reduction strategies to protect public health.

1 Literature Review

1.1 Introduction

The impact of the effects of air pollution on human health has been appreciated for a number of decades, especially due to a number of air pollution episodes that occurred during the first half of the 20th century[1]. Much of the appreciation for the relationship between air pollutant exposure and adverse consequences for human health has come from epidemiological studies investigating associations between the levels of pollutant exposure and the incidence and severity of health impacts that follow. Some of the strongest and most consistent associations occur between the exposure to particulate matter and the exacerbation of cardiovascular disease[2,3].

Studies of hospital admissions related to particulate matter (PM) exposure indicated a significant rise in admissions for cardiovascular disease associated with between 10-13 $\mu g/m^3$ increases in ambient PM_{10} (particles <10μm aerodynamic diameter) concentration[4,5]. Long-term exposure to $PM_{2.5}$ (particles<2.5 μm aerodynamic diameter) was also related to cardiopulmonary mortality in a large-scale study of 14-16 year mortality in six United States cities[3,6]. Furthermore, risk ratios for heart disease, heart failure and cardiac arrest were significantly increased for every 10$\mu g/m^3$ increase in $PM_{2.5}$ in an analysis of American Cancer Society mortality data[2].

Although it is evident from epidemiological work that there is a link between PM exposure and CV disease, there is still a lack of understanding of what components of

particles might be driving these effects and the specific mechanisms by which they are acting following inhalation into the lungs. Part of the difficulty in answering these questions is the nature of the particles themselves, which are heterogeneous mixtures of chemicals and can be present in the atmosphere at a distribution of sizes anywhere from <10 nm up to 100 μm. The specific physical and chemical characteristics of particles are spatially and temporally variable and are dependent on their sources and the amount of atmospheric processing they undergo.

Due to the variable nature of both the physical and chemical characteristics of particles, it makes sense that the toxicity of particles at the same concentration could be vastly different depending on the physical and chemical nature of the particles. However, the physical properties of particles have only been minimally taken into account by Environmental Protection Agency (EPA) standards that consider mass concentrations of $PM_{2.5}$ and PM_{10} size fractions. These regulations do not capture the contribution of particle chemistry, or the importance of smaller particles, which are present in greater number but much less mass, to adverse effects on human health.

Therefore, the goal of this research is to test the contribution of particle chemistry and the importance of the ultrafine fraction to the changes in cardiovascular health effects by evaluating acute and long-term cardiovascular changes with the presence and absence of organic species that are thought to play an important role in effects of inhaled particles on cardiovascular health.

1.2 Physical and Chemical Characteristics of Atmospheric Particles

1.2.1 Particulate Matter Size Fractions

Particulate matter is comprised of small particles suspended in the air that come in a variety of sizes, compositions, and from a number of different sources. Particles can range in size from about a few nanometers to tens of micrometers. Particles are primarily classified into three size fractions for both regulatory definitions and studies on the human health effects of aerosols: PM_{10}, particles less than ten micrometers aerodynamic diameter; $PM_{2.5}$, particles less than 2.5 micrometers aerodynamic diameter; and $PM_{0.1}$, particles less than 0.1 micrometers aerodynamic diameter.

The largest ambient particles that are regulated by the EPA are classified as PM_{10}. Particles greater than ten micrometers in diameter are considered to contribute less to pulmonary and cardiovascular particle toxicity because of their inability to penetrate past the upper airways[7]. Consequently, the EPA does not set standards for PM larger than PM_{10}. The current 24-hour PM_{10} standard set by the EPA is 150 $\mu g/m^3$ [8].

PM_{10} particles can originate from re-suspended dust from roads, agriculture, mining, or natural processes such as fires, blowing dust, and pollen release. The composition of PM_{10}, like all fractions of PM, is dependent on the types of regional sources from which it originates. For example, agriculture-related PM_{10} would be expected to contain more ammonia and and/or pesticides while mining related PM_{10} would likely have a higher metal content[9].

$PM_{2.5}$ particles are thought to be of greater concern to human health than the larger PM_{10} fraction because of stronger associations found with both short and long term

health effects of $PM_{2.5}$. (reference) Therefore, the 24-hour EPA standard for $PM_{2.5}$ is 35 $\mu g/m^3$, which is much lower than 150 $\mu g/m^3$ standard for PM_{10}[8]. Also, there has recently been a greater concern with the long-term effects of $PM_{2.5}$ exposure, so the annual standard was lowered in 2012 from 15 $\mu g/m^3$ to 12 $\mu g/m^3$ average annual concentration for $PM_{2.5}$[8].

$PM_{2.5}$ primarily originates as emissions from combustion processes in most urban areas, but natural dust may contribute in certain area with wind blown dust episodes[10]. These emissions can be either from regional sources such as vehicular traffic and industrial processes, or they can be related to personal exposures such as to second-hand smoke, cooking aerosol, or other indoor air contaminants[9].

$PM_{2.5}$ can contain a number of organic compounds, metals, elemental carbon, nitrates and sulfates[9]. The presence and relative amount of these compounds is dependent on the type of source(s) from which PM originates and how long it is suspended in the atmosphere. $PM_{2.5}$ can undergo a variety of chemical changes following emission related to evaporation or condensation of semi-volatile species, photochemical reactions, reactions with vapor phase co-pollutants, or any combination of those changes[9].

The smallest fraction of particles related to the effects of PM on human health is the $PM_{0.1}$ or ultrafine fraction. Because of their small size, ultrafine particles are not present in high mass concentrations, but they make up the majority of the particle number concentration and surface area of the entire $PM_{2.5}$ fraction[9]. The EPA does not set standards for ultrafine particles because their potential importance in the effects of PM exposure on human health has only recently emerged[8]. Furthermore, the

capabilities of most air pollution monitoring sites are not sufficiently able to evaluate measures such as particle number concentration that are more representative of ultrafine concentrations than traditional measures such as particle mass concentration[8].

In outdoor air, ultrafine particles mostly come from primary combustion emissions and can be composed of similar chemicals to what are found in larger fractions of $PM_{2.5}$ ($PM_{0.1}$-$PM_{2.5}$, known as the accumulation mode) but are typically primarily composed of organics. Ultrafine particles are short-lived relative to larger fractions, only lasting minutes to hours in the atmosphere because they have a tendency to grow into the accumulation mode[9].

Transportation related combustion, including gasoline and diesel emissions, can be the primary source of ultrafine PM in urban environments, including one analysis that found up to 97% of primary ultrafine particle concentration related to traffic emissions[11]. New-particle formation from condensing vapors can also make up a large portion of ultrafine PM in both urban and rural environments[12].

1.2.3 Chemical Characteristics of $PM_{2.5}$ in Southern California

Air pollution, especially $PM_{2.5}$, has been a problem for public health in Southern California for decades due to the high amounts of vehicular traffic, unique geography and meteorological effects such as temperature inversions and numerous sunny days. Recent strict regulations on PM emissions by the Environmental Protection Agency and the California Air Resources Board have reduced $PM_{2.5}$ concentrations in Southern California by 20-25% from 2007-2013[13]. However, recent studies indicate that there is still significant excess mortality in Southern California due to $PM_{2.5}$ exposure[14,15].

$PM_{2.5}$ in Southern California is derived primarily from combustion sources, although the dust contribution can be high as well. Most of the particles originate from vehicular emissions, but there is also contribution from natural dust, industrial sources and marine vessels[16,17]. The main components of Southern California $PM_{2.5}$ are organic carbon, nitrate, and sulfate[16,18]. Elemental carbon, ammonium, metals, and other trace elements are also present in smaller quantities[16,18]. In monitoring performed by the Southern California Air Quality Management district, carbonaceous material made up 27-38% of $PM_{2.5}$ with 18-26% of the material present as organic carbon[18]. The OC/EC ratio was measured to be 2.0-2.2 (1.4-2.4 is the ratio for primary emissions), indicating that the majority of OC in Southern California is from primary emissions [18]. However, other more recent studies have identified secondary PM, PM that originates from reactions of vapors in the atmosphere, as the main source of $PM_{2.5}$, with primary emissions as a lesser but still major source[13,16].

Polycyclic aromatic hydrocarbons (PAHs) are a class of semi-volatile organic compounds associated with primary organic aerosol that is of particular concern to the human health effects of $PM_{2.5}$. PAHs are generated by incomplete combustion emissions, primarily vehicle exhaust emissions in Southern California, and are metabolized to bioactive intermediates in the body following inhalation[19]. Most of the PAHs in the Southern California atmosphere exist in the vapor phase[20], however the high molecular weight PAHs contained within $PM_{2.5}$ particles are thought to be more toxic[19]. Particle phase PAHs benzo[a]pyrene and indeno[1,2,3-cd]pyrene, which are considered probable and possible human carcinogens, respectively, by the International

Agency for Research on Cancer, are present in much higher quantities in urban Southern California locations relative to the California rural background[21].

There is a significant spatial variation in the relative proportions of primary and secondary species between the coastal and inland areas. Nitrate and sulfate are indicative of secondary $PM_{2.5}$, and in Southern California air are commonly present as ammonium nitrate and ammonium sulfate. Nitrogen oxides and sulfur oxides emissions are photochemically transformed to nitric and sulfuric acids, and then react with gas-phase ammonia that is common in Southern California air[22]. Concentrations of ammonium nitrate and sulfate are higher farther away from the coast, comprising up to 55-66% of $PM_{2.5}$ mass in areas such as Fontana and Rubidoux[18]. This mainly occurs in the summer months with warmer temperatures and increased wind speeds to transport and age particles from the more heavily trafficked areas of the western portions of the air basin[23].

Toxic metals have been found in Southern California air at relatively low concentrations including vanadium, chromium, nickel, manganese, copper, arsenic and lead[24]. Southern California lacks a major presence of industrial combustion (coal burning, smelting, etc.) compared to other parts of the country, so the proportion of certain metal species in the air would be expected to be lower. However, despite Southern California's lower presence of industrially sourced metal constituents of PM, there are other sources of metal emissions characteristic to the region. Vehicles can be sources of metal in particulate matter, either through tailpipe emissions or brake and tire wear that contribute to ambient dust[25]. Iron, silicone, and aluminum also are found in natural dust[26]. Furthermore, marine vessels, such as ships idling at the port of Long

Beach, burn residual oil and emit higher proportions of vanadium that have been traced in regional air[17,27].

1.2.4 Atmospheric Chemistry of Organic Aerosols

The composition of organic aerosols can vary substantially depending on the amount of aging the particles have undergone following emission. Particles that originate from emissions sources, known as primary organic aerosol, are typically semi-volatile in nature, meaning these particles can partition to the particle or vapor phase[28,29]. The primary organic aerosol concentration decreases farther away from emission sources due to atmospheric dilution, but vapors that either volatize off of the primary particles or are present in the gas phase can condense to form secondary organic aerosol[30]. Therefore, the secondary organic aerosol becomes a higher percentage of the total organic aerosol the farther away one moves from an emission source. Additionally, secondary organic aerosol becomes a more predominant component of total aerosol during the summer months when there are higher levels of photochemical oxidation[31]. The formation of secondary organic aerosol is primarily driven by oxidation of the vapor phase material and often these vapors will condense onto accumulation mode particles[30].

The organic aerosol oxygen content can determine the amount of particle aging. Freshly emitted, primary organic aerosol (POA) has a relatively low oxygen to carbon (O:C) ratio of less than 0.4:1[32]. Highly aged organic aerosol, also known as low volatility oxidized organic aerosol (LV-OOA) will have very high oxygenation, with O:C ratios of 0.6:1 or greater[33]. There are also a range of semi-volatile oxidized organic aerosol (SV-

OOA) that is oxidized but still relatively volatile with O:C ratios of between 0.4:1 and 0.6:1[33]. Both OOA fractions are associated with secondary organic aerosol.

The differences in composition between primary and secondary organic aerosols have consequences for the potential health effects of the particles. An epidemiological study of elderly subjects in the Los Angeles air basin found associations between pulmonary inflammation and secondary organic aerosol markers, while alternatively finding associations between systemic inflammation and primary organic aerosol markers[34]. Furthermore, a toxicogenomic study of the effects of primary and secondary organic aerosols on human lung epithelial cells found substantially more gene expression changes with exposure to the secondary organic aerosol[35].

1.3 Effects of particulate matter exposure on the progression of atherosclerosis

1.3.1 Atherosclerosis Background

Atherosclerosis is the formation of lipid filled lesions in the arterial wall that eventually grow to occlude the artery and can potentially rupture and cause a thrombus. Atherosclerosis is the primary cause of global vascular disease[36]. It is a particularly dangerous chronic disease because it is often mildly symptomatic or asymptomatic until it is in very advanced stages. Occlusion of the arteries of the heart, brain, and periphery often lead to very vague symptoms such as dizziness, shortness of breath, chest pains, or numbness of extremities and may not be properly diagnosed until a more severe event such as a myocardial infarction or ischemic stroke[37,38].

Atherosclerotic plaques are initiated by an accrual of macrophages in the sub-

endothelial space of the arterial wall. This accumulation is initiated by low-density lipoprotein (LDL) that amasses within the arterial wall and becomes oxidized to form oxidized LDL (oxLDL)[39]. OxLDL promotes the release of inflammatory molecules that draw circulating monocytes into the sub-endothelial space. OxLDL increases the level of P-selectin, a molecule that enhances cell adhesion of monocytes to the endothelium[40]. Furthermore, oxLDL promotes monocyte chemoattractant protein 1 (MCP-1) production by endothelial cells that increases monocyte migration to the site [41,42]. This process can be reversed by high-density lipoprotein (HDL), which can transport cholesterol out of the arterial wall and also has been shown to have anti-oxidant and anti-inflammatory effects[43-45].

Upon accumulation of excessive oxLDL, macrophages eventually become “foam cells” as they accrue large quantities of lipids. The inflammation is exacerbated by these macrophages due to their release of reactive oxygen species (ROS) that increase oxidation of LDL and pro-inflammatory cytokines such as interleukin-1β (IL-1β) and tumor necrosis factor-α (TNF-α)[46]. The initial lesion is called a “fatty streak” because the lesion is primarily made up of lipid filled foam cells.

The presence of foam cells damages the endothelium, which initiates cytokine release that causes smooth muscle cell migration into the intima from the media of the arterial wall[47]. The smooth muscle cells produce fibrous tissue with high collagen content within the lesion[48]. The smooth muscle cells and macrophages eventually undergo apoptosis and subsequently necrosis to form a necrotic core in the middle of the lesion that is mostly comprised of cellular debris and lipids[49,50]. The necrotic core is often separated from the lumen of the artery by a fibrous cap that primarily contains

collagen. Calcium granules in the necrotic core can clump together to form larger calcium deposits[51]. The calcification and expansion of fibrosis within the lesion is characteristic of the most advanced stage atherosclerotic plaques.

The most hazardous consequence of atherosclerotic plaque formation is thrombosis due to plaque rupture. Plaque rupture occurs when there is a weakening in the fibrous cap to the point that constituents of the lipid core of the plaque are exposed to the lumen of the artery[52]. Weakening of the fibrous cap occurs in portions of the cap where loss of smooth muscle cells reduces the amount of collagen and more macrophages are present to break down the cap[53]. If the thrombus remains in the sub-endothelial space, platelets can accumulate over it and occlude blood flow[54]. If the thrombus becomes an embolus, it can lead to an infarct in the heart (myocardial infarction), brain (ischemic stroke), or elsewhere.

1.3.2 ApoE -/- Mice as a Model of Atherosclerotic Development in Humans

Atherosclerosis is modeled in mice by knockout of the apolipoprotein E gene (apoE -/-) in C57BL/6 mice. Mice lacking this gene have altered lipid metabolism that results in an accumulation of LDL and a susceptibility to developing atherosclerosis with a mechanism of plaque formation similar to that seen in humans[55]. Blood LDL levels can be further increased in these mice by feeding them a high-fat diet[56].

ApoE -/- mice consistently develop atherosclerotic lesions in the thoracic aorta, abdominal aorta, and adjacent major arteries branching from the thoracic aorta. Monocyte adhesion to the endothelium and minor foam cell formation has been observed in these mice on a normal chow diet as early as eight weeks of age[57]. By ten

weeks of age, there are numerous foam cells present and by 20 weeks the lesions have progressed to highly fibrotic plaques[57]. The timeline of plaque formation can be accelerated by feeding mice a high-fat diet[56]. ApoE -/- mice are not thought to be good models for plaque rupture because high fibrinolytic activity in mice is able to heal small ruptures and prevent thrombus formation that occurs more readily in humans[58].

1.3.3 Particulate Matter Exposure and the Progression of Atherosclerosis

As stated in section 1.1, there is abundant epidemiological evidence linking cardiovascular mortality to $PM_{2.5}$ exposure. To help determine the causal factors behind this increased cardiovascular mortality, investigators have also attempted to determine specific disease states that may be impacted by $PM_{2.5}$ exposure. Atherosclerosis has been one focus of these investigations because of its prevalence in society and its potential to be exacerbated through $PM_{2.5}$ exposure via increased inflammation and oxidative stress.

$PM_{2.5}$ exposure has been linked to enhanced progression of atherosclerosis in multiple epidemiological studies. Significant increases in carotid intima-media thickness, a measure of atherosclerotic development, have been observed in individuals with exposure to higher levels of $PM_{2.5}$[59-61]. Thoracic aortic calcification, another measure of atherosclerosis, has been found to be associated with $PM_{2.5}$ exposure as well[62].

$PM_{2.5}$ exposure has been associated with exacerbation of atherosclerotic lesion development in the transverse aorta and adjacent major arteries in apoE -/- mice. One study found significantly larger atherosclerotic lesions in the thoracic aorta of high-fat chow fed mice exposed to $PM_{2.5}$ concentrated ambient particles (CAPs) for six months

compared to mice exposed to filtered air[63]. The difference in lesion size between CAPs and filtered air exposed mice on normal diet, however, was not significant. There was a significantly greater lesion area in the thoracic aorta in apoE -/- mice exposed to 112 $\mu g/m^3$ ultrafine CAPs compared to those exposed to filtered air and 438 $\mu g/m^3$ $PM_{2.5}$ CAPs for 40 days[64], indicating that ultrafine CAPs by itself may be a more potent enhancer of atherosclerotic plaque formation. In this study, even though the mass concentration of the PM2.5 CAPs was greater, the greater particle surface area and PAH content of the ultrafine CAPs was thought to be responsible for the enhanced plaque formation of the ultrafine CAPs. Furthermore, atherosclerosis was increased in mice exposed to Beijing ambient air pollution for two months at relatively lower concentrations of approximately 17 $\mu g/m^3$ $PM_{2.5}$ and 99 $\mu g/m^3$ PM_{10}, indicating potential for effects only slightly higher than EPA standard levels of $PM_{2.5}$[65].

Although a link between atherosclerosis and particulate air pollution has been established by a number of studies, the components of $PM_{2.5}$ that are responsible for acceleration of atherosclerosis by $PM_{2.5}$ exposure are still unclear. A few studies have attempted to answer this question by exposing mice to separate fractions of $PM_{2.5}$ to determine which fractions retained a similar response to whole $PM_{2.5}$.

The importance of the vapor phase fraction of diesel exhaust in the promotion of atherosclerosis was investigated by comparing responses to whole and filtered diesel exhaust exposed to apoE -/- mice. Plaque composition changes in the aortic leaflet of apoE -/- mice, including peroxidation of lipids, and increased fibrotic deposits, were found to have a dose-response relationship with exposure to low (109 $\mu g/m^3$), medium (305 $\mu g/m^3$), and high (1012 $\mu g/m^3$) concentrations of diesel exhaust [66]. These effects

were attenuated by filtering of the diesel exhaust, implicating the particle phase as responsible for promoting plaque composition changes that are relevant to plaque vulnerability to rupture. Lesions that are high in oxidized lipids are shown to be more vulnerable because they can drive inflammatory responses that cause localized macrophage infiltration and protease release [67].

In our prior study testing the effect of $PM_{2.5}$ semi-volatiles on the progression of atherosclerotic plaque formation, atherosclerosis was significantly elevated in the arteries of CAPs exposed mice compared to that in either air or CAPs that had been stripped of semi-volatile organic compounds (SVOCs) using a thermodenuder [68]. However, the implications of this study were limited because the removal of SVOCs lowered the overall particle concentration, preventing a clear distinction between dose and composition effects of the SVOC removal.

1.4 Mechanisms of progression of atherosclerosis following particulate matter exposure

1.4.1 Reactive Oxygen Species Formation in the Lung and Vasculature

Following inhalation, particles promote oxidative damage in the lung directly through production of reactive oxygen species (ROS). PAHs in particles can be metabolized in the lung by cytochrome p450 to form redox-cycling quinones that can generate ROS that damage lung tissue[69,70]. Transition metals can also generate ROS by catalyzing hydroxyl radical production through the Fenton reaction[70,71]. Synergistic effects on ROS generation have also been observed by the combination of reactive organics and transition metals. Yet other studies have associated ROS formation with the semi-volatile fraction rather than the non-volatile fraction containing transition metals, so the full picture of ROS generation by particles is still unclear[72].

Particles can also stimulate cells of the innate immune system to produce ROS. Alveolar macrophages, neutrophils, eosinophils and bronchial epithelial cells generate ROS in response to inhaled particles that can be responsible for oxidative stress in the lung[70,73]. The lung also has natural antioxidant defenses against ROS production including glutathione peroxidase, superoxide dismutase, catalase, and heme-oxygenase-1[74]. However, these antioxidant defenses can be inadequate if abundant ROS formation exceeds the ability of the cells to detoxify it through antioxidant response[70].

ROS formation caused by particle inhalation in the lungs can promote inflammation through MAP kinase and NF-κB pathways. These pathways lead to the production of a

number of cytokines, acute phase proteins, and activated macrophages that increase airway inflammation[70,73] and these pro-inflammatory molecules may spillover into the systemic circulation. This spillover can lead to a cascade of systemic oxidative stress and inflammation that is thought to be the initiator of multiple forms of CVD, including atherosclerosis[75]. Effects of systemic inflammation on the acceleration of atherosclerosis are detailed in section 1.4.2.

PM related vascular oxidative stress is initiated by ROS formation from a number of different sources. Enzymes such as NADH/NADPH oxidase, xanthine oxidase, or uncoupled endothelial nitric oxide synthase are normally the primary sources of ROS in the vasculature[76]. PM may promote ROS formation by these enzymes through inflammatory signaling, such as in one study that found an increase in ROS derived from NADPH oxidase in infiltrating monocytes and the aorta of mice exposed to $PM_{2.5}$[77]. ROS generation in the vasculature related to PM exposure may also occur via autonomic signaling (see section 1.5.3) or translocated constituents of particles[78]. Vascular ROS promote a number of atherosclerotic processes including lipid oxidation, matrix metalloproteinase activation, expression of cell adhesion molecules, and vascular smooth muscle cell proliferation and migration[76,79].

1.4.2 Systemic Inflammation

Increased systemic inflammation is an established risk factor for atherosclerotic lesion development, so it is a potential mediator of PM-induced promotion of atherosclerosis. A number of both pro- and anti-inflammatory molecules involved in the mechanism of atherosclerotic development are modulated by PM exposure and give

some idea of how PM affects lesion development. These inflammatory molecules have a number of actions that stimulate lesion growth and development, including promoting monocyte recruitment, adhesion, and activation; migration and proliferation of smooth muscle cells; and further exacerbating release of pro-inflammatory molecules. However, understanding of which of these pathways are activated by various components within particles has yet to be fully elucidated.

TNF-α is an important molecule in inflammatory response that is related to induction of cell adhesion molecule expression, apoptosis, and T cell proliferation[80]. Although many of the downstream functions of TNF-α are related to pro-atherosclerotic inflammation, there have been mixed results in its ability to solely promote atherosclerotic plaque formation. Knockout of the TNF-α gene alone was not sufficient to diminish atherosclerotic plaque formation in wild type mice fed a high fat diet[81]. However, lesion formation was reduced by knockout[80] and inhibition[82] of TNF-α in mice that were otherwise genetically susceptible to atherosclerotic plaque development.

IL-6 has been shown to be an important inflammatory player in the progression of atherosclerosis as it promotes endothelial dysfunction, SMC proliferation and migration as well as recruitment and activation of inflammatory cells, thereby perpetuating vascular inflammation [83]. IL-6 affects the local the expression of the scavenger receptors involved in the uptake of modified LDL and thus promotes the formation of macrophage-derived foam cells [84]. Furthermore, treatment with recombinant IL-6 exacerbated atherosclerosis of apoE-deficient mice [85].

IL-1β is a pro-inflammatory cytokine with a variety of activities, produced by activated macrophages and has also been linked to the progression of atherosclerosis.

IL-1β deficiency induced an approximately 33% reduction in atherosclerotic lesions in apoE−/− mice[86]. It appeared that IL-1β exerted an atherogenetic action by enhancing the expression of VCAM-1 and MCP-1 in the aorta, which possibly increased the recruitment of monocytes/macrophages to the intima [86].

C-reactive protein (CRP) is part of the acute phase response to inflammation that is signaled by the cytokines IL-6 and TNF-α, which are produced by macrophages to initiate a pro-inflammatory response [87]. CRP levels are associated with cardiovascular disease and may play a pro-inflammatory role in promoting atherosclerosis through activation of innate immunity via the complement system[88].

In addition to an increase between pro-inflammatory cytokines and atherosclerotic development, a decrease in anti-inflammatory cytokines has been linked to atherosclerotic lesion formation. IL-10 is an anti-inflammatory cytokine that is inhibits macrophage activation, matrix metalloproteinase activity, and pro-inflammatory cytokines that promote atherosclerosis[89]. This anti-atherogenic activity was further supported by reduced plaque formation and inflammation observed in hyperlipidemic mice overexpressing IL-10[90].

Most of these pro-atherogenic inflammatory molecules have been shown to be systemically increased following PM exposure and therefore are probable mediators of PM-induced atherosclerotic enhancement. Circulating concentrations of C-reactive protein (CRP) were increased following PM exposure in humans[91,92,93] and in apoE -/- mice that had accelerated levels of atherosclerosis[65]. Increased levels of pro-inflammatory cytokines TNF-α, IL-6, and IL-1β have consistently been linked to PM exposure in both rodent and human studies. Serum levels of all three cytokines were

associated with PM_{10} levels in a study of Swiss adults[94]. An increase in serum TNF-α was found in $PM_{2.5}$ exposed mice that had increased levels of atherosclerosis[65]. Increased IL-6 was related to higher long-term levels of $PM_{2.5}$ in study of adults from major American cities[91]. IL-6 expression was increased in vascular endothelial cells following exposure to $PM_{2.5}$, and this was linked to an increase in permeability of vascular endothelial cells that could contribute to the development of CVD[95].

Some attempts have been made to relate chemical composition of inhaled PM to markers of systemic inflammation, however there is not a full understanding of how differences in particle composition may alter effects on increasing pro-atherosclerotic inflammatory molecules. Plasma concentrations of CRP and IL-6 were found to be related to primary organic carbon and ultrafine particles in a panel of elderly subjects with coronary artery disease[96]. Also, serum levels of TNF-α and IL-1β were increased in mice intranasally exposed to $PM_{2.5}$ from an area with high particle concentrations of nickel[97].

1.4.3 Cholesterol Modifications

Serum concentrations of low-density lipoprotein (LDL) and high-density lipoprotein (HDL) cholesterol are related to the development of atherosclerosis. Increased levels of LDL promote atherosclerotic progression because the accumulation of oxidatively modified LDL (OxLDL) initiates macrophage foam cell formation. This is supported by studies with both apolipoprotein E and LDL receptor knockout mice that show these mice develop atherosclerosis faster than wild type mice due to high levels of circulating LDL. Increased levels of OxLDL also promote endothelial adhesion of monocytes and

lymphocytes through promotion of adhesion molecules ICAM-1, VCAM-1 and P-selectin[98]. The accumulation of LDL can be reduced by high-density lipoprotein (HDL), which can transport cholesterol out of the arterial wall and has been shown to have anti-oxidant and anti-inflammatory effects[43-45].

PM exposure can modify LDL and HDL and alter their functions to promote atherogenic conditions in the vasculature. Human $PM_{2.5}$ exposure has been associated with oxidative modifications to lipids in the blood[99,100], and assuming HDL and LDL are included in the lipids being oxidized, would implicate pro-atherogenic effects of cholesterol modification as being related to PM-induced systemic oxidative stress. Additionally, PM exposure also led to increased susceptibility of LDL to oxidation in LDL receptor knockout mice[101]. Modified HDL can also become dysfunctional, lose anti-inflammatory and anti-oxidant function, even become and pro-atherogenic following exposure to PM[64,78,102].

The relative amount of LDL to HDL is an important risk factor of CVD with higher levels of LDL to HDL associated with increased CVD risk. Long-term exposures to PM appear to be related to an adverse change in cholesterol ratio, perhaps through alterations to lipid metabolism. In a recent population based cohort study in Israel, three-month average PM10 concentrations were associated with increased blood LDL and decreased blood HDL[103]. Additionally, long-term exposure to Beijing $PM_{2.5}$ increased serum LDL in apoE -/- mice that also had accelerated atherosclerotic plaque formation[65].

1.5 Autonomic Nervous System Mediated Effects of $PM_{2.5}$ Exposure on Atherosclerosis

1.5.1 Autonomic Nervous System Anatomy and Physiology

The autonomic nervous system is suspected to play a role in the transmission of effects of $PM_{2.5}$ exposure to the cardiovascular system. The autonomic nervous system has two branches. The sympathetic branch acts to increase heart rate, blood pressure, cardiac contractility and constrict blood vessels as part of the body's "fight or flight" response[104]. The parasympathetic branch is responsible for activities that counteract the sympathetic effects when the body is at rest[105]. Autonomic effects on the cardiovascular system are regulated through aortic and carotid baroreceptors, peripheral mechanical and chemoreceptors, and polymodal receptors in the lungs[106,107].

Neural transmission through both branches of the autonomic nervous system involves the participation of two efferent neurons each, with both branches using acetylcholine as a neurotransmitter at their initial neural synapse. The sympathetic nervous system uses the catecholamine neurotransmitters epinephrine and norepinephrine to signal adrenergic receptors on its target tissues[104]. The parasympathetic nervous system acts primarily on the heart through the vagus nerve and uses acetylcholine to bind to muscarinic receptors on its target tissues[105].

1.5.2 Mechanisms of $PM_{2.5}$ Exposure Related Effects on Autonomic Balance

Air pollution may induce autonomic imbalance by stimulating afferent nerve fibers and causing excitatory or inhibitory alterations to the sympathetic or parasympathetic

branches of the autonomic nervous system. Autonomic imbalance is caused acutely by the stimulation of transient receptor potential vanilloid 1 (TRPV1) or TRP ankyrin 1 (TRPA1) on C-fibers, irritant sensitive afferent vagal nerve fibers in the lung, due to oxidative stress induced by inhaled $PM_{2.5}$[108,109]. These afferent nerve fibers initiate a reflexive response to alter efferent autonomic nerve activity to the cardiovascular system[106,110]. The nature of the imbalance, either sympathetic or parasympathetic activation, is dependent on the composition of the inhaled toxicant and the segments of the respiratory system that are impacted[107,111,112].

Chronic autonomic imbalance can occur through the effects of $PM_{2.5}$ on baroreflex response either through atherosclerotic plaque formation in the arteries, neuroplasticity, or endothelial dysfunction[106]. Normal baroreflex response is indicative of proper cardiac autonomic regulation through arterial baroreceptors. As discussed earlier in this chapter, atherosclerotic plaque formation can be promoted by exposure to $PM_{2.5}$ through systemic inflammation and oxidative stress. Coronary atherosclerotic plaque formation can alter baroreflex response[113], possibly though atherosclerotic enhanced dysfunction of arterial baroreceptors. Neuroplasticity may also play a role in chronic autonomic imbalance. $PM_{2.5}$ in tobacco smoke has been shown to reduce the excitability of central cardiac vagal neurons, diminishing baroreflex responsiveness[114]. Endothelial dysfunction can also decrease baroreflex sensitivity by reducing the effect of vascular pressure changes to stretch receptors in the arterial wall. $PM_{2.5}$ exposure can increase vascular stiffness and blunt the sensitivity of stretch receptors by either by promoting atherosclerosis[115] or impairing nitric oxide mediated vasomotor function[116].

1.5.3 Autonomic Effects on the Progression of Atherosclerosis

Autonomic imbalance related to $PM_{2.5}$ exposure might be part of a positive feedback loop to accelerate atherosclerotic formation because in addition to atherosclerotic changes that can promote autonomic imbalance, there are autonomic changes that promote atherosclerosis. Autonomic input to the vasculature controls blood pressure through vasomotor effects[117]. Disruptions in normal vascular autonomic control of blood flow may alter shear stress on the vessel walls through increased turbulent flow, which has been linked to the progression of atherosclerosis[118].

The autonomic nervous system is closely tied to regulation of the immune system and inflammation, so modifications to autonomic activity by $PM_{2.5}$ exposure may mediate inflammatory driven effects on atherosclerotic formation. For example, the vagus nerve inhibits pro-inflammatory cytokine release and is protective against systemic inflammation[119]. In contrast, sympathetic tone has been linked to plasma interleukin-6 (IL-6) levels[120] and adrenergic stimulation results in increased production of TNF by macrophages[121]. However, the relationship between the autonomic nervous system and inflammation is complex and dependent on multiple factors, so it cannot be said that either branch is always pro- or anti-inflammatory[122].

$PM_{2.5}$ exposure related autonomic imbalance is also capable of inducing oxidative stress in the cardiovascular system that may promote atherosclerosis through pro-oxidant effects. Pharmacological blockade of sympathetic and parasympathetic innervation of the heart reduced PM induced reactive oxygen species formation and lipid peroxidation in rat hearts, indicating the importance of the function of both branches of the autonomic nervous system in mediating PM exposure induced oxidative

stress[123]. Similar effects were observed upon blockade of TRPV1 receptors, implicating irritation of afferent C-fibers as initiating autonomic promotion of cardiac oxidative stress[124].

1.5.4 Measurement of Autonomic Control of the Heart Using Heart Rate Variability

Heart rate variability (HRV) measures can indicate modulations in sympathetic and parasympathetic nervous system control of the heart. The sympathetic and parasympathetic branches of the autonomic nervous system (ANS) are the primary modulators of heart rate with each branch exerting control over heart rate at separate frequencies. This is reviewed by Task Force, 1996 and briefly described here: Parasympathetic inputs function to decrease heart rate and act rapidly because of the direct activation of potassium channels by acetylcholine, giving the parasympathetic branch of the ANS high frequency (HF) control over heart rate[125]. The lower frequency (LF) modulations in heart rate, however, are not completely attributable to the sympathetic branch of the ANS because pharmacologic blockade only partially diminishes LF HRV, indicating a mix of parasympathetic and sympathetic influences[125]. In mice, LF HRV is represented by frequencies between 0.1 and 1.5 Hz, while HF HRV is represented by frequencies from 1.5 to 5.0 Hz[126].

Heart rate variability has been used in multiple epidemiology and toxicology studies as a measure of changes in autonomic modulations to the heart associated with air pollution exposure. Decreased HRV in humans is a predictor of adverse cardiovascular outcomes including atherosclerosis and increased mortality after myocardial infarctions[125,127]. In humans, the most consistent association of PM

exposure and HRV is a decrease in the HF component that indicates inhibition of the parasympathetic control of heart rate[126]. HRV is also an indicator of the progression of atherosclerosis[128].

Similar effects of PM exposure on HRV are observed in rodents. Most results indicate decreased HRV after particle exposure[123,129-131] although increases in HRV with particle exposure have also been observed[132-134]. Less experimentation has been performed to evaluate HRV changes in in apoE -/- mice over the course of a long-term exposure to particulate matter. One previous study found a biphasic short-term HRV response to $PM_{2.5}$ exposure in apoE -/- mice over 6 months[135]. Our previous research found that SVOCs might play a role in HRV changes. A decrease in HRV and the LF and HF parameters was observed in apoE -/- mice during an eight week exposure to CAPs and an increase was seen in the same parameters in mice exposed to CAPs stripped of SVOCs[68].

2 Objectives

2.1 Hypothesis

The goal of this thesis study was to investigate the mechanism of how SVOC components of PM contribute to accelerated atherosclerosis following particle inhalation. SVOCs were expected to play an important role in plaque formation because many species within particles that are capable of inducing ROS formation, such as PAHs, are SVOCs. Furthermore, prior studies found reduced oxidant potential and diminished biological effects of PM that has been stripped of SVOCs. SVOC components were differentiated from other refractory species that are capable of producing biological responses, such as metals and elemental carbon, by heating the particles with a thermodenuder to 120°C, and then removing the volatized components with activated charcoal. These particles that were stripped of their SVOCs were called denuded CAPs.

This study gave the unique opportunity to study the activation of different interrelated pathways involved in the development of atherosclerosis (systemic inflammation, systemic oxidative stress, blood cholesterol levels, autonomic changes) by SVOCs. It was hypothesized that CAPs containing SVOCs, but not denuded CAPs, would activate these pathways, due to the pro-oxidant potential of SVOCs that could initiate alterations to each pathway and promote atherosclerosis.

Implanted electrocardiogram transmitters allowed for the exploration of daily associations of PM characteristics, including mass and particle concentration and

chemical composition, with changes in heart rate and heart rate variability to identify what characteristics of the particles are responsible for acute autonomic changes. It was hypothesized that chemical species related to the SVOC fraction resulting from primary emissions would be associated with changes in autonomic function.

2.2 Specific Aims

2.2.1 Determine the importance of SVOCs to the development of atherosclerosis by testing if increased atherosclerosis in apoE -/- mice following exposure to CAPs is attenuated by exposure to concentration-matched denuded CAPs that have been stripped of SVOCs.

2.2.2 Characterize the difference in particle composition between whole and denuded CAPs to determine what physical and chemical properties of SVOCs might be implicated in the toxic effects

2.2.3 Determine if SVOC exposure is related to the activation of pro-atherogenic mechanisms such as increases in systemic inflammation and oxidative stress and alterations to circulating cholesterol concentrations in apoE -/- mice exposed to whole and denuded CAPs.

2.2.4 Determine if SVOC exposure is related to effects on the autonomic nervous system by testing the acute and long-term responses of heart rate and heart rate

variability in apoE -/- mice exposed to whole and denuded CAPs and associating daily changes in CAPs particle characteristics with daily changes in acute heart rate and heart rate variability.

2.3 Study Design

2.3.1 Determine the importance of SVOCs to the development of atherosclerosis by testing if increased atherosclerosis following exposure to CAPs is attenuated by exposure to concentration-matched denuded CAPs that have been stripped of SVOCs.

Our previous findings indicated that CAPs exposure was associated with an acceleration of atherosclerotic lesion formation in mice susceptible to developing the disease, and that removal of SVOCs by denuding reduced that effect. However, this claim was weakened by the finding that denuding of the particles reduced the overall particle concentration, so the reduction in effect may have been related to a lower total PM exposure. Therefore, the current study compared arterial lesion formation in apoE -/- mice exposed for two months in August-October 2014 in Irvine, California to either ultrafine denuded CAPs (deCAPs) or CAPs (adjCAPs) that had been diluted to match the concentration of denuded CAPs. It was anticipated from preliminary experiments that the thermodenuder would reduce deCAPs concentration to at least 50% of the unmodified CAPs, so a group of mice was exposed to adjCAPs to account for the effects of particle loss.

Groups of apoE -/- mice exposed to unmodified CAPs (CAPs) and clean, filtered air served as positive and negative controls, respectively. It was unclear if the adjCAPs exposed mice were going to receive a high enough concentration of PM to promote atherosclerotic development, so the exposure to CAPs served as a positive control to

ensure that plaque development would occur at similar PM concentrations used in past studies.

Atherosclerotic lesion progression was evaluated as both changes in the size and composition of the atherosclerotic plaques in the brachiocephalic artery and aortic arch. ApoE -/- mice typically develop lesions in both arteries after 6-8 months of age on a normal diet. In our previous study, only plaque size was used to determine the advancement of atherosclerosis, but plaque composition is also important to the pathophysiology of adverse consequences of atherosclerosis. Differences in lesions between early lipid-filled foam cells and more advanced fibrotic plaques were determined by the amounts of lipids and collagenous material present in the plaques.

2.3.2 Characterize the difference in particle composition between whole and denuded CAPs to determine what physical and chemical properties of SVOCs might be implicated in the toxic effects.

The chemical and physical characteristics of whole and denuded particles were expected to be substantially different due to the removal of semi-volatile species. A previous study indicated that most of the loss was in the organic fraction, including reactive species such as PAHs, while refractory species such as metals and elemental carbon remained in the denuded particles. Investigation of compositional changes of particles within separate size fractions before and after denuding can determine not only what species are being removed, but give an indication of the sources of those species (i.e. freshly emitted vs. aged particles).

A number of instruments were used during the exposure to measure particle concentration and composition. Particle concentrations were determined by quantifying both particle mass and number concentrations real-time and gravimetrically. Elemental and organic carbon measurements were used to determine the ability of the denuder to strip non-refractory (OC) and refractory (EC) species. Particle oxygenation and mass size distributions of major PM species were measured through the use of aerosol mass spectrometry both in denuded and undenuded particles. Particle size distributions were measured using a scanning mobility particle sizer.

2.3.3 Determine if SVOC exposure is related to the activation of pro-atherogenic systemic inflammation, oxidative stress, and alterations to circulation cholesterol concentrations in apoE -/- mice exposed to whole and denuded CAPs.

Increased systemic inflammation, oxidative modifications of lipids, and changes to circulating cholesterol concentrations have been implicated as potential contributors to the progression of arterial plaque formation. These effects have also been demonstrated to be consequences of exposure to particulate air pollution in rodents and humans. It remains to be determined how much of a role that SVOC constituents of particles play in promoting these systemic effects. Therefore, the differences in biomarkers of these effects between whole and denuded CAPs were studied to determine possible mechanisms for SVOC-promoted increased atherosclerotic plaque formation.

The levels of serum pro-inflammatory cytokines IL-1β, IL-6, TNF-α, anti-inflammatory cytokine IL-10, and acute-phase protein CRP were used to evaluate systemic inflammation in mice exposed to whole or denuded CAPs. All of these cytokines have been implicated in mechanisms of atherosclerotic plaque formation. Serum concentrations of cell adhesion molecules ICAM-1, P-selectin, and E-selection were also measured to evaluate pro-atherogenic downstream effects of these cytokines. Other downstream markers of vascular remodeling and thrombogenic formation, MMP-9 and PAI-1, respectively, were also assessed.

Oxidative stress was measured by determining the levels of the oxidation of lipids in the lung, serum and arteries. Lung oxidative damage was determined by measuring levels of malondialdehyde (MDA), a product of the reaction of ROS with polyunsaturated lipids that is a marker for oxidative stress. The concentrations of MDA were also measured in homogenates of the descending aorta to determine vascular oxidative effects related to exposure to particles with and without SVOCs. Oxidized LDL, a primary driver of atherosclerotic lesion formation, was quantified in the serum as a direct measure of PM induced pro-atherogenic oxidative modifications.

Increased concentrations of circulating LDL cholesterol and decreased concentrations of HDL cholesterol are established risk factors of atherosclerosis. The ability of SVOC constituents of PM to alter the relative amounts of LDL and HDL was determined by measuring the each type of cholesterol separately the serum of mice exposed to whole and denuded CAPs.

2.3.4 Determine if SVOC exposure is related to effects on the autonomic nervous system by testing the acute and long-term responses of heart rate and heart rate variability in apoE -/- mice exposed to whole and denuded CAPs and associating daily changes in CAPs particle characteristics with daily changes in acute heart rate and heart rate variability.

Substantial evidence exists that the autonomic nervous system plays in important role in the effects of PM exposure on the cardiovascular system. The role of SVOC constituents of particles in autonomic changes has not been explored, so the comparison of whole and denuded CAPs on heart rate and HRV was used to determine both acute and long-term changes in autonomic function related to SVOC exposure. Acute changes in HRV were measured during the nights following PM exposure while long term changes were assessed by the change HRV measures over the eight week course of the study both on exposure days and days when mice were not exposed.

Daily measures of heart rate variability and particle characteristics can be used to determine what aspects of particles are responsible for autonomic changes that could potentially mediate chronic cardiovascular changes. The associations between particle mass and number concentration, particle oxygenation, relative amounts of ultrafine particles and CAPs-related changes in HRV measures were calculated for mice exposed to whole CAPs to determine which of these factors promote autonomic changes.

3 Methods

3.1 Particle Concentrator

Ambient particles were pulled into the exposure system through an inlet approximately five meters above ground level. Particles were pulled through a Versatile Aerosol Concentration Enrichment System (VACES) that concentrates the particles before exposure to the mice. The VACES was designed and tested for chamber exposure studies using concentrated ambient particles (CAPs)[136,137].

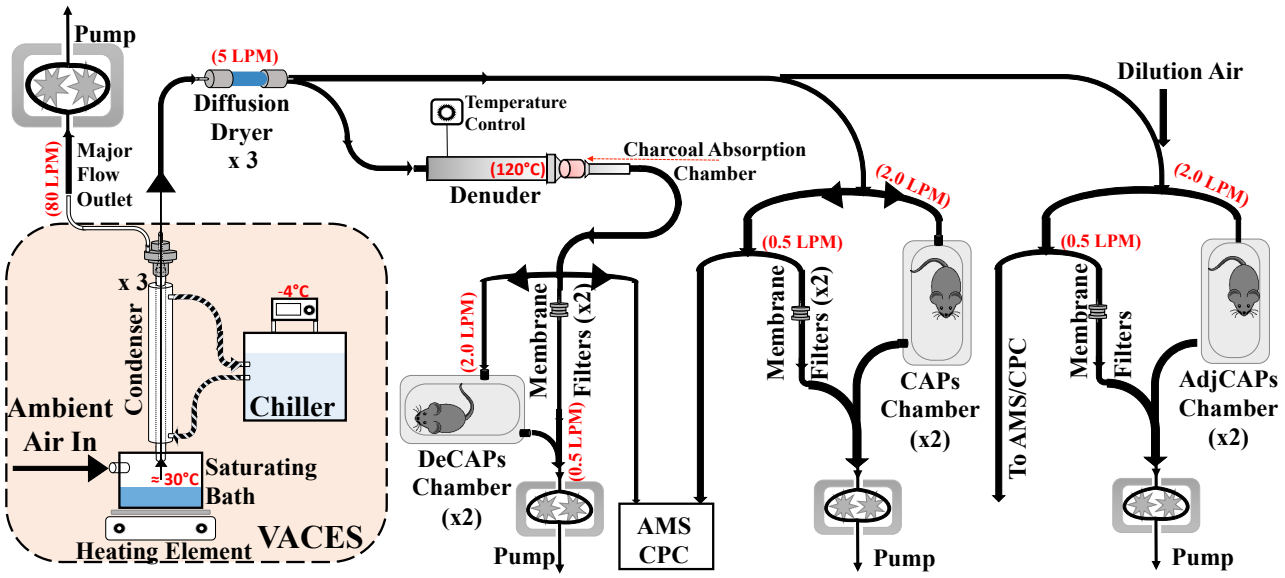

Figure 3.1 VACES Schematic.

As shown in Figure 3.1, the VACES pulls in ambient particles at 85 LPM and saturates them with water molecules by drawing them through humidified air above an approximately 30°C water bath to begin growing the particles. The particles are grown further by next traveling through a condensing tower that is surrounded by a -4°C 1:1

mixture of water and ethylene glycol. Enlarging particles to above 3μm allows them to travel through a virtual impactor with enough inertia to pass straight into a minor outlet that is pulling at 5 LPM, while the main airstream is pulled out of the side through the major outlet at 80 LPM. The particles then pass through a diffusion dryer that removes water molecules by drawing them out of the airstream and into silica surrounding the flow tube. After drying, the concentrated ambient particles (CAPs) are present in the same size distribution as before the VACES, however they were theoretically 17 times more concentrated (~10 times during exposures) because the same amount of particles that were in an 85 LPM flow are now in a five LPM flow.

Following the VACES, ultrafine particles were selected from the overall aerosol by a slit impactor that was placed in-line before the VACES that was intended to remove particles above approximately 180 nm. Although the particle number was insignificant above 100nm, there was still particle mass in the accumulation mode due to the presence of a few large particles.

Separate arms of the concentrator were used for each exposure atmosphere. Each arm included its own condensing tower, virtual impactor, and diffusion dryer and had a flowrate of five LPM. DeCAPs were modified from regular CAPs by placing a thermodenuder (Dekati Ltd.) inline after the VACES. The thermodenuder stripped semi-volatile compounds by heating the aerosol to 120°C and then passing it through an activated charcoal section to remove volatized material. The temperature was chosen based on preliminary experiments that demonstrated adequate removal of semi-volatile compounds without nucleation of new particles[72].

AdjCAPs were modified from regular CAPs by dilution of the CAPs particles with

approximately 2 LPM filtered air to match the number concentration of the deCAPs particles. The clean air atmosphere used room air pulled through a High Efficiency Particle (HEPA) filter, followed by a Chemisorbent media (Purafil Inc.) and charcoal canister that removed vapor phase compounds.

3.2 Animal Exposures

Eleven week old apoE -/- mice (The Jackson Laboratory, Bar Harbor, ME) (n=15 per group) underwent exposure to ultrafine concentrated ambient particles (CAPs), denuded ultrafine CAPs (deCAPs), diluted CAPs (adjCAPs) or purified air (Air) for nine weeks for five hours per day, four days per week (Figure 3.2). Exposures took place from approximately 8:00AM-1:00PM each Monday through Thursday for nine weeks at the Air Pollution Health Effects Lab (APHEL) in Irvine. When not being exposed, mice were housed in the IACUC-approved APHEL vivarium and kept on a 12-hour light/dark cycle and given normal (Harlan 2020X) chow and water ad libitum.

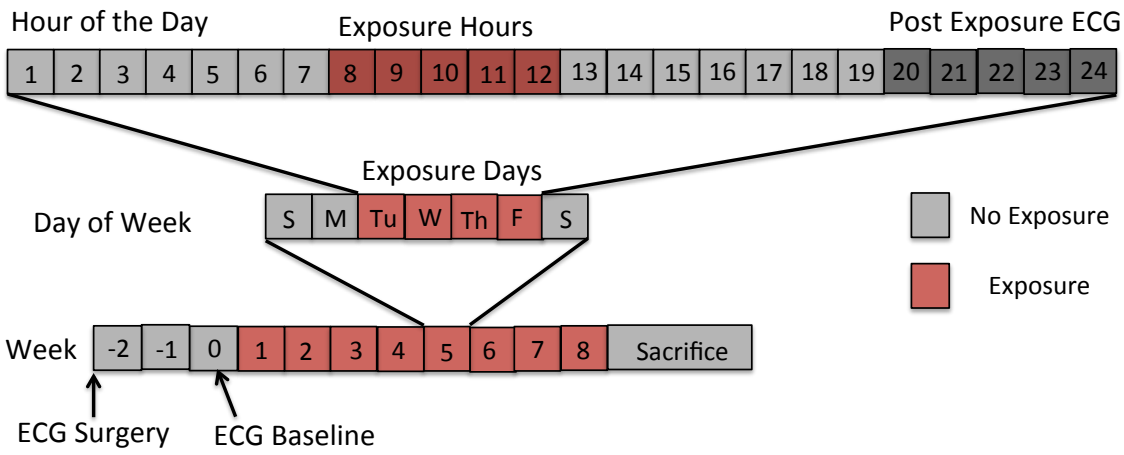

Grouping (n=15/group, 5/group with ECG transmitters):
Clean Air: HEPA and charcoal/purafil filtered air
CAPs: Concentrated ambient particles, 10x ambient concentration
DeCAPs: CAPs denuded at 120C to strip semi-volatile organics
AdjCAPs: CAPs diluted with clean air to match the particle concentration of DeCAPs

Figure 3.2. Exposure and ECG recording schedule.

Each morning of exposure, mice were transferred from their housing cages to exposure chambers pre-designated with the appropriate exposure atmosphere. Stainless steel mesh separators were inserted to keep the mice singly confined. These stainless steel whole-body exposure chambers allowed the mice to move freely within their section of the exposure chamber. Each exposure group had two chambers each and a maximum of eight mice were housed per chamber (Figure 3.1). The exposure chambers were previously designed and validated to ensure uniform distribution of particles within the chamber[138].

After all mice were loaded, chambers were sealed with a plexiglass lid that contained one inlet and one outlet opening. A vacuum pump was attached to the outlet of each chamber, with a buffering tube and rotameters in between the chambers and

the pump to permit a steady pull of two LPM through each chamber (Figure 3.1). At the beginning of the exposure, the flow rate through each chamber was checked with a mass flowmeter to ensure that the mice had adequate airflow, which had previously been determined to be 2 LPM, to freely breathe for the duration of each exposure. The particle line from the VACES (or the HEPA filter for the clean air control group) was attached to the inlet of each chamber (Figure 3.1).

A technician monitored exposure chambers every 15 minutes to check mice health and look for any signs of distress. Flows, temperatures, and pressures were also monitored and recorded with each check. Temperature monitoring strips were placed on the chambers for observation of chamber temperatures and to ensure they stayed within 65-75°F. Rotameters were used to monitor flow through the chambers. If tubing became detached from the chamber, this wouldn't necessarily be reflected on the rotameter (because it would be pulling in room air instead of chamber air) so Magnehelics were used to monitor pressure drop across each chamber as an additional check that mice were receiving sufficient airflow.

3.3 Particle Characterization

3.3.1 Real-time particle concentration monitoring

Particle concentrations were sampled from particle lines just prior to entrance to chambers (Figure 3.1). Ambient and post-VACES particle number concentrations were monitored real-time during the exposure with a Condensation Particle Counter (CPC Model 3022A, TSI Inc). Real-time concentrations were recorded every 15 minutes from

all post-VACES lines and at the beginning of every exposure for the clean air line. The ratio of the CAPs to ambient particle concentrations was the primary measure used during the exposures to determine adequacy of VACES function. CPC measurements of the deCAPs and adjCAPs aerosols were used to match the concentrations of these aerosols during the exposure. Ambient particle mass concentrations were monitored real-time using a Dustrak aerosol monitor (Dustrak Model 8520, TSI Inc).

3.3.2 Aerosol Mass Spectrometry

A high-resolution time-of-flight aerosol mass spectrometer (HR-ToF-AMS or AMS, Aerodyne Research, Inc.) was used to determine composition of non-refractory organic and inorganic particles less than one micron. The aerosol was sampled at 80 mL/minute and the particles were sent as a beam into a time-of-flight vacuum chamber that separated the particles by their aerodynamic diameter. The particles were then vaporized at 600°C and the volatized material underwent electron impact ionization to create small fragments that are separated by their mass-to-charge ratios and detected.

The AMS was able to provide size distributions of the major non-refractory organic and inorganic components of the aerosol. Oxygen to carbon (O:C) and hydrogen to carbon (H:C) elemental ratios were also able to be obtained through AMS measurements. The AMS was not capable of measuring refractory materials such as metals that cannot be vaporized at 600°C. The AMS sampled from predominately the CAPs line each day that it was in operation to get daily averages of CAPs particle characteristics during the exposure. DeCAPs and adjCAPs lines were also intermittently

sampled throughout the time the AMS was available on days when no mice were being exposed to characterize differences in the three groups of aerosols.

3.3.3 Particle Size Distribution

A scanning mobility particle spectrometer (SMPS, TSI Inc.) was used to measure particle size distributions of the CAPs aerosol on a day when the mice were not being exposed. The SMPS measures particle diameter based on electrical mobility of charged particles in a Differential Mobility Analyzer. The Differential Mobility analyzer classifies the particles based on their electrical mobility, with particles of a certain mobility exiting through an output slit to a CPC that determines particle concentration at that size.

3.3.4 Gravimetric Analysis

A particle line was placed in parallel with each exposure chamber (Figure 3.1) to collect particles on in-line 25mm Teflon filters (Zefluor, Pall Corp.) for gravimetric analysis. The flow through each filter was approximately 0.5 LPM for the period of each week (~20 hours) of exposure and the filters were used for gravimetric analysis. Teflon filters were pre- and post- weighed using a microbalance (Model 29, Cahn), with the difference representing the mass of particles collected during one week of exposure. The pre- and post- weights were performed in a temperature and humidity controlled room and filters were given ~24 hours to condition in the room before weights were measured to minimize variability in the measurements. The concentration of particles was determined by dividing the measured mass by the total volume of flow through the filter for each week.

3.3.5 Elemental Carbon and Organic Carbon (EC/OC)

A particle line was placed in parallel with each exposure chamber (Figure 3.1) to collect particles on in-line pre-baked 25mm Quartz filters (Tissuquartz 2500-QAT, Pall Corp.) The flow through each filter was approximately 0.5 LPM for the period of each week (~20 hours) of exposure and the filters were used for EC/OC analysis. Quartz filters were saved in a freezer immediately after exposure in foil-lined petri dishes wrapped with Parafilm (SigmaAldrich) to minimize changes in concentrations of the more volatile species on the filters.

Filters were analyzed for organic and elemental carbon using a Thermal/Optical Transmittance Analyzer (Lab OC-EC Aerosol Analyzer, Sunset). 1.5 square centimeter rectangular punches were made in each filter and each punch was placed in the oven of the analyzer. The sample was heated at four sequentially increasing temperatures to 600°C in an all helium atmosphere to vaporize all the OC off of the filter. The vaporized OC was sent to the oxidizer oven where it was oxidized to carbon dioxide, and then sent to the methanor oven where it was reduced to methane and detected by the flame ionization detector. Some pyrolysis of OC to EC occurred during the vaporization, so the amount of pyrolytic conversion on the filter is monitored optically with a laser within the system.

The detection of EC was performed by the instrument in a similar manner as the OC, except that the sample oven was heated to 850 °C and the oxidation to carbon

dioxide occurred in an oxygen/helium mixture. Both the EC originally on the filter and the EC produced by pyrolysis was detected in this phase. The total sample EC was the detected EC less the EC produced by pyrolysis, and the total sample OC was the detected OC plus the OC that was pyrolytically converted to EC.

The mass of carbon detected was multiplied by the ratio of the total area of the filter to the punch area to determine the total amount of carbon on the whole filter. The total filter mass was divided by the total flow through the filter during each week to determine EC and OC mass concentration in each atmosphere.

3.4 Animal Sacrifices

Mice were sacrificed within three days of their last exposure. Mice were given an injection of ~250 mg/kg pentobarbital sodium and phenytoin sodium (Euthasol, Virbac USA) to suppress neurological control of respiration. After mice were unresponsive to mechanical stimulation, the abdomen was opened and the vena cava was exposed. Blood was drawn out through the vena cava and approximately 0.4-0.6 mL was saved in a serum-separating tube (Vacutainer, Becton Dickinson). The ex-sanguination acted as the final cause of death for the mice. The tubes were allowed to clot for ~1 hour and then spun at 10,000 x g for 10 minutes in a centrifuge. The supernatant fraction containing the serum was removed into a separate tube.

The chest cavity was opened to expose the heart and the aortic tree. The brachiocephalic artery and aortic arch were excised from mice after removing as much fatty tissue from around the arteries as possible. Both vessels were perfused with

phosphate-buffered saline (PBS) to clear blood components and to prevent collapse of the artery upon embedding. Arteries were embedded in Optimal Cutting Temperature compound (TissueTek, Sakura Finetek) and frozen on dry ice.

The lower right lobe of the lung and the descending aorta were removed and snap frozen in liquid nitrogen. All tissues were stored at -80°C for subsequent analysis.

3.5 Histology

5 μm thick frozen sections were cut from the aortic arch and brachiocephalic artery using a cryostat supplied by the UC Irvine pathology department. Six sections were cut from each artery starting at the end of the brachiocephalic artery proximal to the aorta. The aortic arch sections were cut starting at the end proximal to the heart.

Three sections from each vessel were stained with Oil-Red O to visualize lipids with hematoxylin as a background stain. Sections were placed in a solution of Oil-Red O for one hour following pre-treatment with propylene glycol for one minute. Sections were then placed in hematoxylin for five minutes and then mounted with an aqueous mounting media.

Three sections from each vessel were stained with Masson's Trichrome (Trichrome Stain Kit, Abcam), which is a triple stain containing aniline blue that stains collagen. Prior to staining, the sections were fixed in Bouin's fluid for one hour. The sections were first stained for nuclei in Weigert's iron hematoxylin for 5 minutes, then rinsed and stained for muscle fibers with Biebrich scarlet/acid fuchsin solution for 15 minutes. After rinsing, the sections were differentiated in

phosphomolybdic/phosphotungstic acid solution for 15 minutes followed by staining with aniline blue. Slides were then rinsed in acetic acid and dehydrated with alcohol before mounting.

Images of artery sections were captured under a light microscope and digitized with a computer-linked camera (Apollo Instruments). ImageJ (National Institute of Health) software was used to measure structures within the arterial cross-section to quantify area of the structures within the cross-section. The total atherosclerotic lesion area for each artery was calculated as the total lesion area in each cross-section divided by the total cross-sectional area of the artery. The purpose of dividing by total artery cross-sectional area is to normalize the lesion area for different size arteries. The average lesion area for each artery was calculated as the average lesion size from all sections, because the lesions are three-dimensional shapes within the artery and the lesion area is not uniform between sections.

The wall thickness, or intima-media thickness, of the aortic arch and brachiocephalic artery was measured using ImageJ. The measurements were taken as the average distance in pixels from the lumenal wall of the intima to the adventitial surface of the media. A micrometer ruler was measured at the same magnification and used to convert thickness measurements from pixels to micrometers. Wall thicknesses from all sections were averaged to represent the mean wall thickness for each artery.

The presence of lipids and collagen within each lesion were quantified as the total area of red and blue stain, respectively. The compositional analysis was only performed on sections with observable lesions. To determine the total area of a lesion stained for lipids, a Matlab (Mathworks) script was written that converted pixels into binary, either

“red” or “not red”, based on RGB values of each pixel. The red pixels were then counted and divided by total lesion area. The same analysis was done using a Matlab script for “blue” pixels to determine the amount of collagen. The lipid or collagen stained area of each lesion was divided by the total lesion area to normalize for differences in lesion size.

3.6 Serum Biomarkers of Inflammation and Cardiovascular Disease

Biomarkers of inflammation and cardiovascular disease were measured using a Magpix multiplex assay (Milliplex MAP, EMD Millipore) . The following markers were measured:

-Acute phase response: C-reactive protein (CRP)

-Inflammatory cytokines: interleukin-1β, interleukin-6 (IL-6), interleukin-10 (IL-10), and tumor necrosis factor alpha (TNF-α)

-Vascular adhesion molecules: P-selectin, E-selectin, intracellular adhesion molecule 1 (ICAM-1)

-Vascular remodeling: matrix metalloproteinase 9 (MMP-9)

-Pro-thrombotic factor: plasminogen activator inhibitor-1 (PAI-1)

The assay was begun with the addition of 25 µL of each sample to a microplate, followed by addition of 25 µL of buffer solution and 25 µL of antibody-immobilized beads. Samples were incubated overnight at 4°C to allow capture of analytes by antibody-immobilized beads. After washing the plate, 25 µL of detection antibodies were added and the samples were incubated for one hour at room

temperature. 25 µL of streptavidin-phycoerythrin were added to each sample and incubated for 30 minutes. The plate was washed and then 100 µL of operational fluid was added for analyzing the immunoassay using a Magpix (Luminex Corporation) multiplex instrument. The Magpix instrument determined concentrations of each analyte by measuring the excitation of beads within specified regions that corresponded to the analytes. These values were then compared to a standard curve to determine sample concentrations.

3.7 Tissue Malondialadehyde

Malondialdehdye (MDA) was used as a measure of lipid peroxidation in lung and descending aorta (DA) homogenate. Tissues were homogenized in chilled PBS with 0.01 mM EDTA using a FastPrep homogenizer (FastPrep-24, MP Biomedicals). Each sample was homogenized in tubes containing Lysing Matrix A (MP Biomedicals) and 1 mL PBS/EDTA for lung homogenate and 0.5 mL PBS/EDTA for DA homogenate. The tubes were run on the FastPrep three times each for 20 seconds at six m/s and placed on ice for five minutes between each run. Samples were then centrifuged at 10,000 x g to remove cellular debris and the supernatant was diluted 1:10 in PBS/EDTA for MDA and protein analysis.

The MDA analysis protocol was adapted from Folz, et al[139]. 50 µL of each sample was added to 75 µL of 0.44 M phosphoric acid and 25 µL of 0.6% thiobarbituric acid. The mixture was heated at 95°C in a heating block for one hour. Samples were then allowed to cool on ice for 15 minutes and then protein-precipitated and neutralized by

adding 150 µL of 1M sodium hydroxide/methanol (1:11) solution. 200 µL of each sample was filtered through a filter plate with 0.2 µm pore size and then used for HPLC analysis. The mobile phase was 40% methanol/60% 50 mM potassium phosphate buffer (pH 6.8). Detection was accomplished by a fluorescence detector set at emission/excitation of 525 nm/550 nm. The sample concentrations were determined by comparison to a standard curve of MDA ranging from 31.25 nM to 500 nM.

Protein was quantified using a Pierce Bicinchoninic Acid Protein Assay (ThermoFisher Scientific). 25 µL of sample was combined with 200 µL of a reagent that used the sample protein to initiate the reduction of Cu^{2+} to Cu^{1+} and then reacted Cu^{1+} with bicinchoninic acid to form a colored solution that was absorbed at 562 nm. The sample concentrations were determined by comparison to a standard curve for albumin ranging from 25 µg/mL to 2000 µg/mL.

3.8 Serum Oxidized Low Density Lipoprotein

Serum oxidized LDL (OxLDL) was determined by using a enzyme-linked immunoabsorbent assay (ELISA, Cloud-clone Corp.) for mouse OxLDL. Serum was diluted 1:5000 to have OxLDL concentrations within the range of the assay standard curve. 100 µL of sample was added to a microplate that was pre-coated with an antibody specific to OxLDL and incubated at 37°C for one hour. Excess solution was aspirated and 100 µL of reagents containing avidin conjugated to horseradish peroxidase (HRP) was added to each microplate well and incubated at 37°C for one hour. Each well was washed and then tetramethylbenzadine substrate solution was

added to stimulate a color change proportional to the amount of OxLDL, biotin-conjugated antibody and enzyme-conjugated avidin. The enzyme-substrate reaction was terminated by the addition of a sulphuric acid solution and the color change was measured at a wavelength of 450nm. The sample concentrations were determined by comparison to a standard curve of OxLDL ranging from 15.6 to 1000 pg/mL. The OxLDL concentration of each sample was normalized to the concentration of serum LDL in each sample.

3.9 Serum Cholesterol

Serum LDL and HDL were separated using an LDL precipitation buffer (Abcam). 25 µL of serum was mixed with 25 µL of LDL precipitation buffer and incubated at room temperature for ten minutes. Samples were centrifuged at 2000 x g for ten minutes and the supernatant, which is the HDL fraction, was removed into a separate tube. The pellet, the LDL fraction, was re-suspended in 50 µL PBS.

Each fraction was assayed separately for cholesterol using an Amplex Red Cholesterol Assay (ThermoFisher Scientific). LDL samples were diluted 1:100 in PBS and HDL samples were diluted 1:50 in PBS. 50 µL of the diluted samples were added to a microplate. The reaction mixture included 2 U/mL cholesterol esterase to hydrolyze cholesterol esters in the serum, 0.2 U/mL cholesterol oxidase to oxidize cholesterol to hydrogen peroxide, and 300 µM Amplex red (10-acetyl-3,7-dihydroxyphenoxazine) as a probe for hydrogen peroxide in the presence of 2 U/mL horseradish peroxidase. 50 µL of the reaction mixture was added to each sample and the samples were incubated at

37°C for 30 minutes. Amplex red reacted with hydrogen peroxide to produce resorufin that has an excitation/emission fluorescence that was detected at 571 nm/585 nm. The sample concentrations were determined by comparison to a standard curve of cholesterol ranging from 2 μM to 20 μM.

3.10 Electrocardiogram measurements

3.10.1 ECG implantation

Implanted electrocardiogram (ECG) transmitters, model TA-ETAF20 (Data Sciences International) were used to measure electrical activity of the heart in five mice per exposure group. The devices were implanted under isofluorane anesthesia in the abdominal cavity of the mice, with biopotential leads sutured in place in the chest wall in an ECG lead II configuration. The lead II configuration is characterized by placement of the negative electrode near the right shoulder and the positive electrode to the left of the xyphoid space. Buprenorphine (0.05 mg/kg) was administered every 12 hours after surgery for pain management and enrofloxacin (3 mg/kg) was administered twice per day for seven days post-surgery as an antibiotic. Mice were permitted a two-week recovery period after surgery before initiation of baseline telemetry recordings.

3.10.2 ECG Data Collection

The transmitted ECG data was collected and recorded using the EMKA IOX2 telemetry system (EMKA Inc.). Receivers placed under housing cages collected ECG

data from each mouse. Baseline ECG data was collected from each mouse during the week prior to the start of exposures (Figure 3.2). To mimic the chamber stress, the baseline data was recorded while mice were in the exposure chambers receiving filtered air during the same time of day that the mice were recorded during the CAPs exposures. The baseline measurements were taken so that each mouse could serve as its own control to account for individual differences in the ECG traces.

3.10.3 ECG Signal Processing

All ECG analysis was performed with EMKA ECGAuto software (EMKA Inc.). Algorithms in the software label R-waves and permit user verification of proper R-wave labeling.

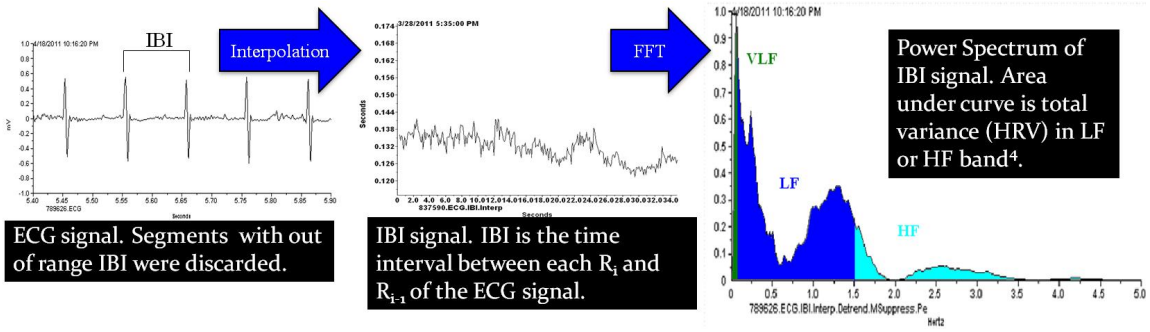

Figure 3.3. Calculation of LF and HF HRV.

Heart rate variability was analyzed from 8PM-1AM both on days when the mice were exposed and days when mice were not exposed. It was determined that this time period would be best to use to minimize the influence of both post-exposure stress and changes in HRV associated with diurnal light/dark changes.

Power spectral analysis of an interpolated signal of R-R intervals using the Fast Fourier Transform was used to obtain frequency domain HRV measures (Figure 3.3).

The guidelines of the Task Force of the European Society of Cardiology (Task Force, 1996) were followed in the selection of short segments of stationary signal and removal of ectopic beats, which was done on the ECGAuto software. After obtaining the HRV spectra, the area under the curve for the frequency bands of interest (low frequency (LF HRV), represented by frequencies between 0.1 and 1.5 Hz, and high frequency (HF HRV), represented by frequencies from 1.5 to 5.0 Hz[126]) was calculated for each recording segment to obtain total power in each band. Values for each R-R signal segment were averaged to obtain one total HRV value for a five-hour analysis period. The relative power in the LF and HF frequency bands was calculated for each five-hour recording in the same by dividing the LF power by the HF power of each frequency band (LF/HF).

Heart rates were calculated from R-R interval lengths of all intervals not excluded due to noise or ectopic beats. Heart rates from all accepted intervals within an analysis period were averaged to obtain a value of heart rate for the five-hour analysis period.

3.11 Statistical Analysis

Group means $\pm$ SEM was determined for the four exposure groups for each of the biological parameters discussed above. SPSS (International Business Machines Corp.) was used for statistical analysis. Analysis of variance (ANOVA) with a Tukey post hoc test was used to assess differences in vascular parameters between exposure groups. 0.05 was set as the significance level.

The averages of heart rate variability and heart rate from each five-hour analysis period were treated as a daily time series. The five-hour analysis periods from the non-exposure days were analyzed separately in the same manner. The time series data was analyzed for exposure effects using a linear mixed model in which time was considered as a random effect within the measurements for each subject. Adjacent measurements in time were expected to be more highly correlated than those that were non-adjacent, so an autoregressive order 1 correlation structure was used for within subject measurements. Estimates were obtained of the effect of each exposure compared to pre-exposure baseline values of the HRV parameters.

4 Results

4.1 Particle Characterization – Physical Characteristics

4.1.1 Particle Number Concentration

Particle number concentrations of the CAPs, deCAPs, adjCAPs and pre-VACES ambient aerosols were sampled every 15 minutes throughout each exposure period and then averaged into daily, weekly, and study averages. The study and weekly averages are shown in Figure 4.1 and Figure 4.2, respectively.

The ratio in particle number concentration between CAPs and pre-VACES ambient was the primary measure used to determine desired concentration factor, approximately ten times ambient. As shown in Figure 4.1, this concentration factor was achieved as the CAPs concentration was 1.0×10^5 compared to 1.0×10^4 for the pre-VACES ambient.

Particle number concentrations for the deCAPs aerosol were approximately half of the CAPs aerosol due to the removal of the more volatile particles by the thermodenuder. The adjCAPs aerosol number concentration was adjusted throughout the exposure to match the deCAPs aerosol number concentration, and the number concentration of the adjCAPs aerosol was also approximately half the CAPs aerosol Figure 4.1.

Figure 4.2 shows that the weekly average particle loss in the deCAPs aerosol relative to the CAPs aerosol was variable, with the CAPs to deCAPs ratio much lower in weeks one through three and week nine compared to weeks four through eight.

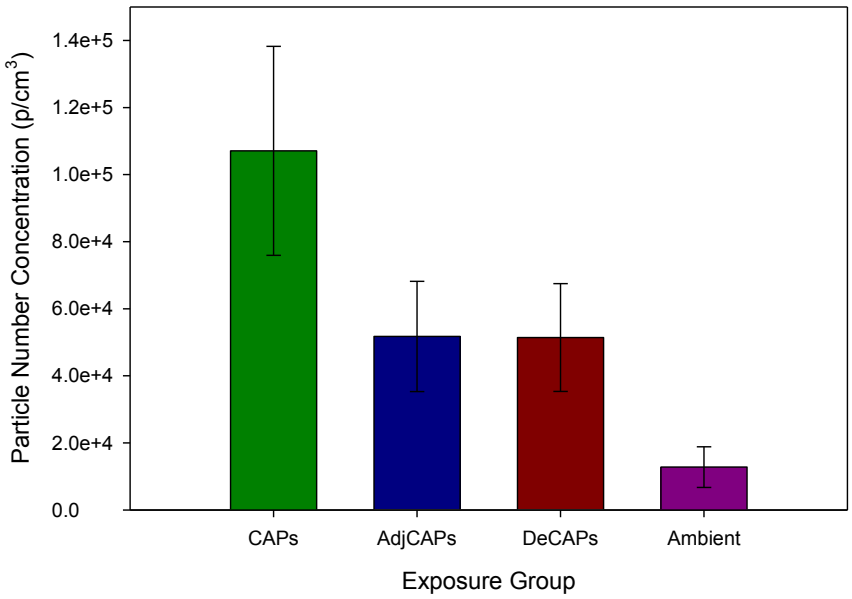

Figure 4.1 Study average Particle Concentration.
Mean of the weekly average particle concentrations measured by CPC of each exposure group and pre-VACES ambient particle concentration for the nine weeks of the exposure. Error bars represent standard deviation of the mean.

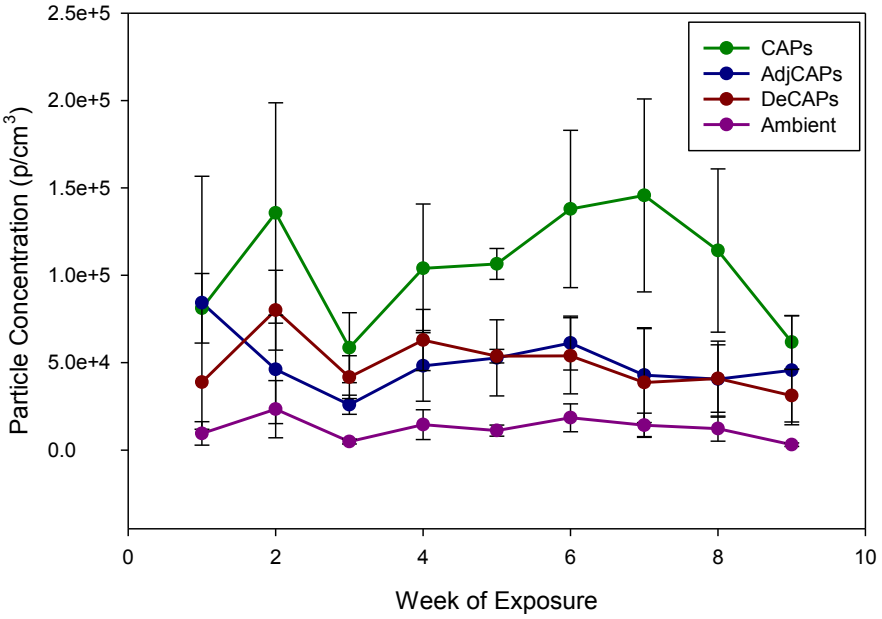

Figure 4.2 Weekly Average Particle Number Concentration.
Mean of the daily average particle concentrations measured by CPC of each exposure group and pre-VACES ambient particle concentration for the nine weeks of the exposure. Error bars represent standard deviation of the mean.

4.1.2 Particle Size Distribution

Particle size distributions of CAPs and ambient were measured on a day when animal exposure was occurring to determine the particle number, surface area, and volume size distribution of the aerosol (Figure 4.3). By particle number, most of the particles were less than 100 nm in diameter. However, the size distribution of particle volume indicated that some larger, more voluminous, particles were present in the aerosol that were above 100 nm in size. The SMPS can only reliably measure particles below 300 nm in size because of large corrections made for particles with multiple charges above this cutoff. Therefore, the volume size distribution of the larger fraction of the accumulation mode was not determined.

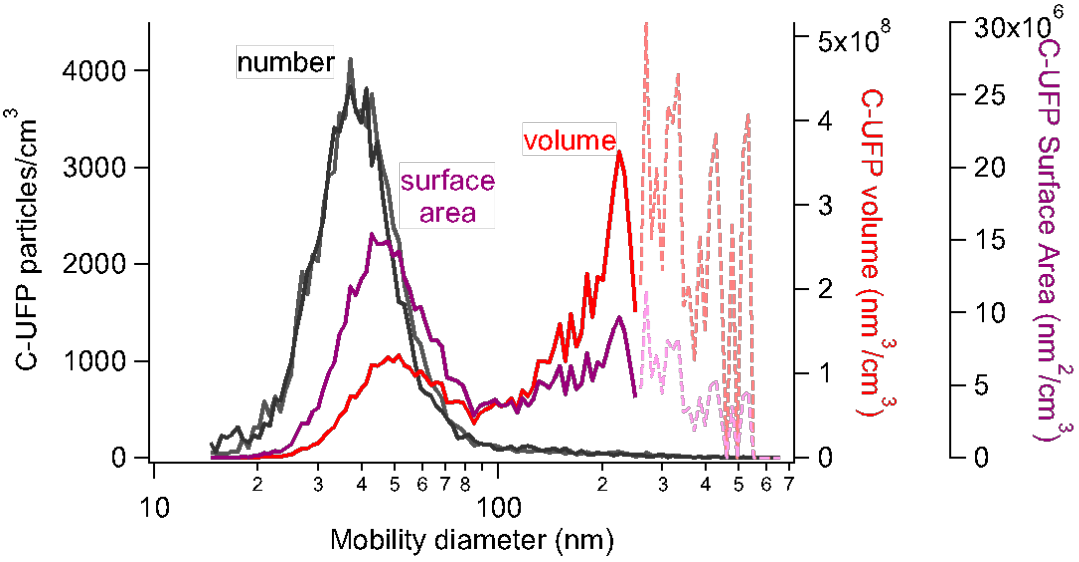

Figure 4.3 Particle number, surface area, and volume distributions
CAPs number (gray) distributions were compared to surface area (purple) and volume (red) distributions measured by SMPS. SMPS measurements above ~300 nm are typically inaccurate because large of corrections for particles with multiple charges

4.1.3 Particle Mass Concentration

Ambient PM_{10} mass concentration averaged 27.2 +/- 11.5 $\mu g/m^3$ (mean ± SD) for the nine weeks of exposure. The weekly average ambient mass concentration was generally steady with the exception of week six when there was one day with ~70 $\mu g/m^3$ ambient mass (Figure 4.4). The mass concentration of the exposure groups was unable to be calculated, because filter pre-weights and post-weights were inaccurate due to a miscalibrated microbalance. However, CAPs mass concentrations of the non-refractory species, which is typically about half of the total mass concentration, was 50 $\mu g/m^3$ ± 30.9.

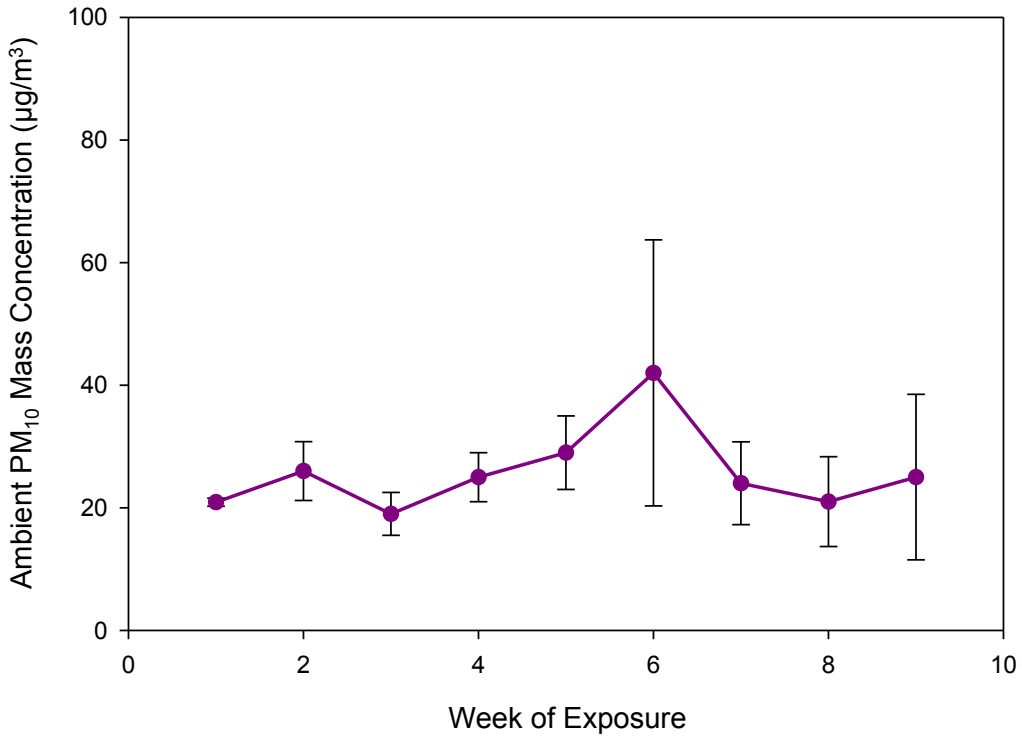

Figure 4.4. Ambient PM_{10} mass concentration.
Weekly average ambient mass concentration in $\mu g/m^3$ measured by Dustrak aerosol monitor with PM_{10} inlet. Data represents average of the daily mean ambient PM_{10} mass concentrations each week, with error bars indicating standard deviation.

4.2 Particle Characterization – Chemical Characteristics

4.2.1 Elemental and Organic Carbon

The CAPs aerosol contained the highest ratio of organic carbon (OC) to elemental carbon (EC) of the three particle containing aerosols (Figure 4.5). The deCAPs aerosol was composed of approximately the same amount of EC but about two-thirds the amount of OC as the CAPs aerosol (Figure 4.5), indicating that most of the carbon being volatized by the denuder was OC. The adjCAPs aerosol had non-significantly lower amounts of both OC and EC relative to the CAPs aerosol (Figure 4.5), although there was a greater difference in OC.

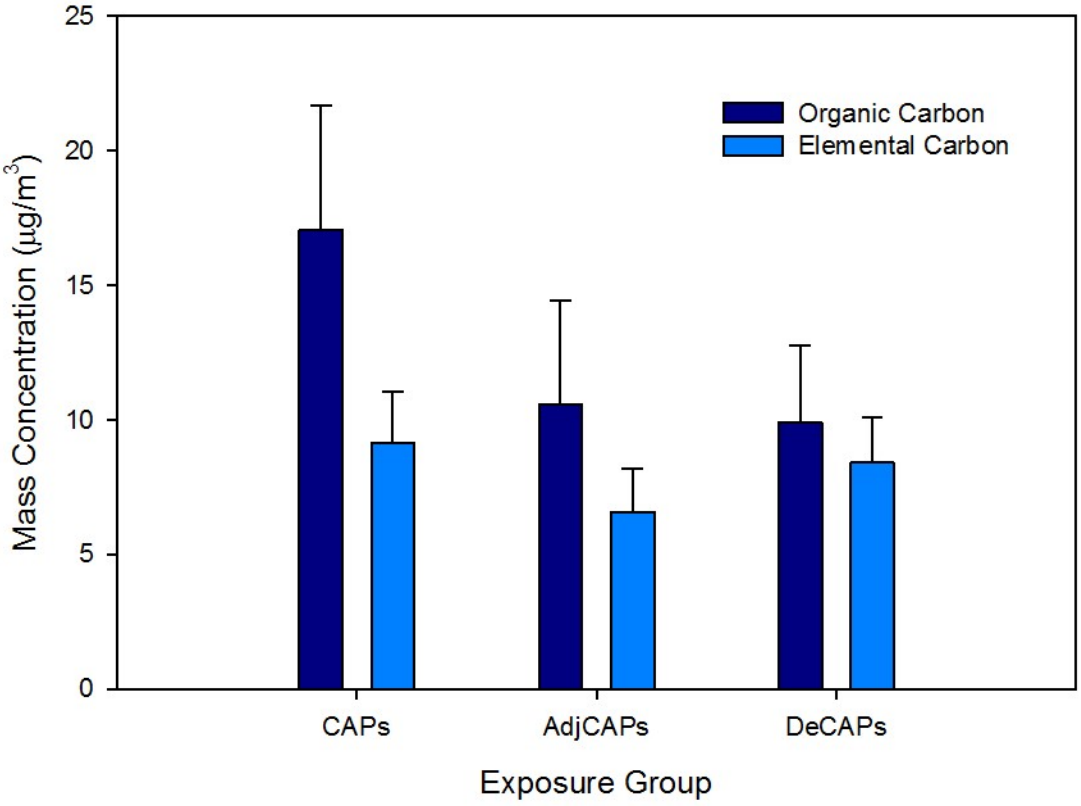

Figure 4.5 Study Average Elemental and Organic Carbon.
Mean of the weekly average EC and OC mass concentration of each PM exposure group measured from weekly collections of PM on quartz filters by a Thermal/Optical Transmittance Analyzer.

4.2.2 Percent Composition of Non-refractory Components of Concentrated PM

The percent composition of non-refractory (constituents of particles that can be vaporized by the AMS) components of concentrated particles is given in Figure 4.6. During a period when animals were not being exposed, the relative compositions of the CAPs, deCAPs, and adjCAPs aerosols were characterized by the AMS to evaluate the effects of denuding and adding dilution air to CAPs. The measurements were taken on the same day within the same sampling period to minimize meteorological or source related variations in particle composition.

CAPs contained mostly organics, and then smaller fractions of sulfate (SO_4^{2-}), ammonium (NH_4^+) and nitrate (NO_3^-). When CAPs were denuded at 120°C, the resultant deCAPs aerosol contains approximately 20% less organics, but larger relative fractions of nitrate, sulfate and ammonia (Figure 4.6). Therefore, it again appears that most of the material lost by denuding is in the organic fraction.

The adjCAPs fraction was tested to determine if adding various flow rates of dilution air that would be used during the animal exposures would impact the composition of the particles. At all three flow rates tested, there appeared to be minimal difference between adjCAPs and CAPs composition (Figure 4.6).

The AMS measured daily values of the mass concentration of non-refractory components of CAPs during the exposure. The averaged values of the mass concentration of each species are given in Table 4.1. The percent mass concentration of the total non-refractory mass for each species was also determined.

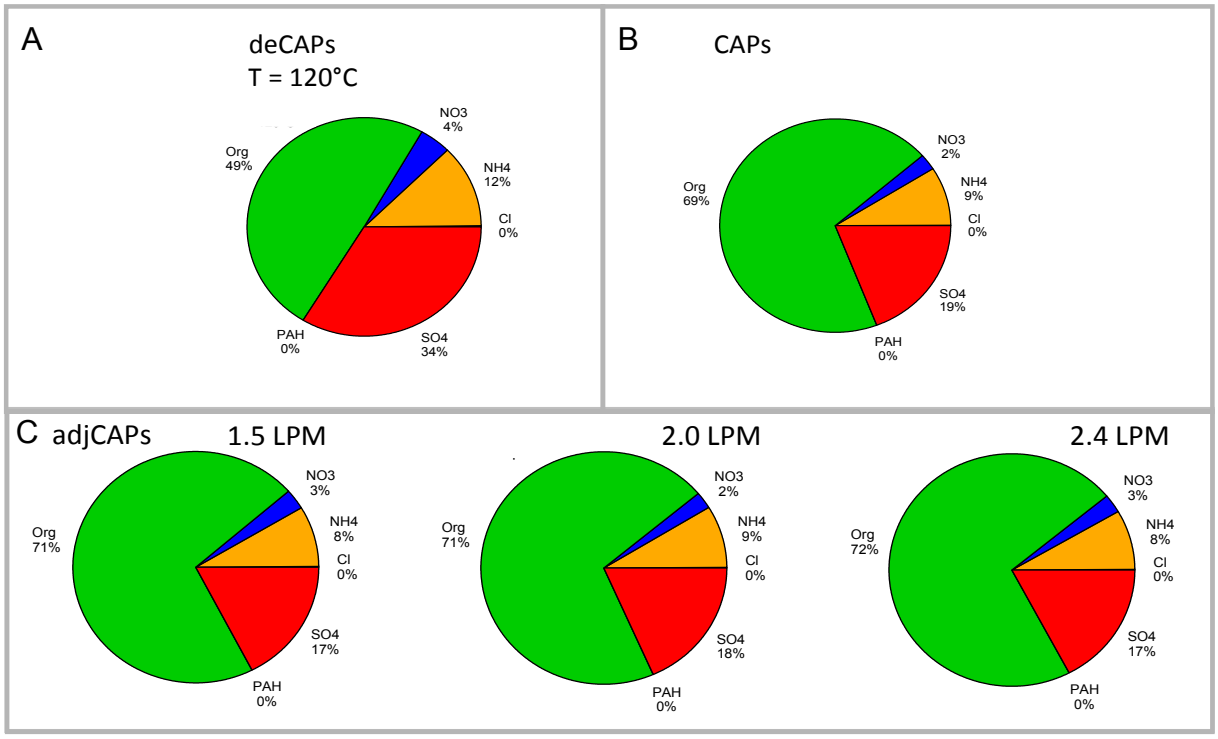

Figure 4.6 Percent Composition of Non-refractory Components of CAPs, DeCAPs, and AdjCAPs
Percentages of organics, NO_3^-, NH_4^+, Cl^-, SO_4^{2-}, and PAHs in A) deCAPs that were denuded at 120°C B) CAPs C) adjCAPs using 1.5, 2.0 or 2.4 LPM of dilution air. Data were collected using the AMS.

Table 4.1 Study Average Concentrations of Non-refractory Components of CAPs
Average mass and percent concentration of organics, sulfate (SO_4^{2-}), nitrate (NH_4^+), ammonium (NH_4^+), chloride (Cl^-) and total non-refractory components (Total) in CAPs measured by the AMS during the seventeen exposure days of the study that it was sampling. Percent mass is given as the mass of each species as a fraction of the total non-refractory mass.

	Total	Organics	SO_4^{2-}	NO_3^-	NH_4^+	Cl^-
Mass (μg/m^3)	50.3 ± 30.9	33.2 ± 19.3	7.7 ± 5.2	4.8 ± 7.0	4.2 ± 3.6	0.3 ± 0.4
Percent Mass (%)	-------	67.3 ± 10.1	17.0 ± 6.8	7.1 ± 5.5	8.2 ± 2.5	0.4 ± 0.4

4.2.3 Size Distributions of Non-Refractory Chemical Components

The size distributions of non-refractory components of concentrated particles are given in Figure 4.7 through Figure 4.10. During a period when animals were not being exposed, the mass size distributions of the CAPs, deCAPs, and adjCAPs aerosols were characterized by the AMS to evaluate the effects of denuding and adding dilution air to CAPs. The mass size distribution measurements were taken during two separate periods, one with a relatively larger (by mass) ultrafine mode, and the other with a relatively smaller ultrafine mode.

The size distributions as a function of mass of the organic, nitrate and sulfate components of CAPs are shown in Figure 4.7. The figure was generated from one day of measurements, but it is typical of the bimodal distribution of the CAPs aerosol, with an ultrafine mode that was almost completely organic and an accumulation mode that was mostly a mixture of sulfate and organics. The relative mass of each mode varied, with some days having a larger mass in the accumulation mode (Figure 4.9a) and others having more mass in ultrafine mode (Figure 4.9b).

The ultrafine mode had a larger proportion of less oxygenated species such as EC and hydrocarbons relative to the accumulation mode, which had a substantial amount of highly oxygenated acids (Figure 4.8a,b). The acid content of the organic components of the accumulation mode was higher in the aerosol that had a larger accumulation mode mass (Figure 4.8a), indicating that the acids may have made up a significant portion of this additional mass. In the aerosol with a larger ultrafine mode mass (Figure4.8b), there were a higher proportion of hydrocarbons.

The difference in relative proportions of the ultrafine and accumulation mode affected the presence of each mode following denuding. When there was a large accumulation mode, the ultrafine mode was easily removed by denuding at temperatures above 50°C and the remaining aerosol was primarily comprised of the accumulation mode (Figure 4.9a). If a large ultrafine mode was present, it took temperatures above 75°C to remove the ultrafine mode and the remaining aerosol was a single mode with a peak diameter between the ultrafine and accumulation modes (Figure 4.9b).

The CAPs and adjCAPs ultrafine and accumulation mode diameters were compared to determine if adding dilution air had an effect on the mass size distribution of the non-refractory components of the particles. There was no difference between CAPs and adjCAPs ultrafine and accumulation mode diameters (Figure 4.10).

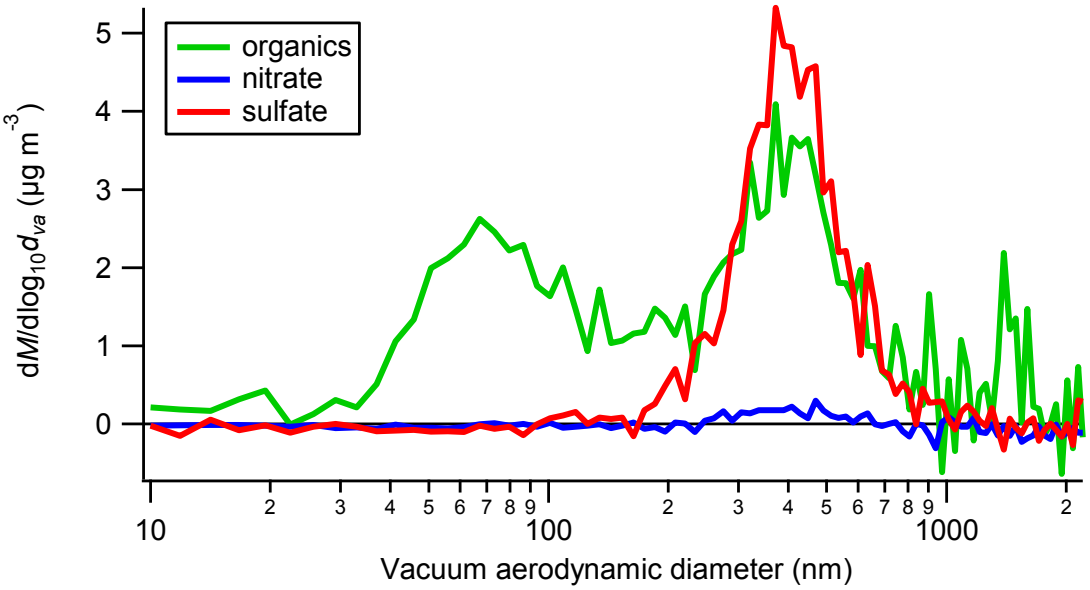

Figure 4.7 CAPs mass size distribution of organics, nitrate, and sulfate. Typical distribution of mass concentrations of organics, nitrate (NO_3^-), and sulfate (SO_4^{2-}) as a function of particle aerodynamic diameter measured by the AMS

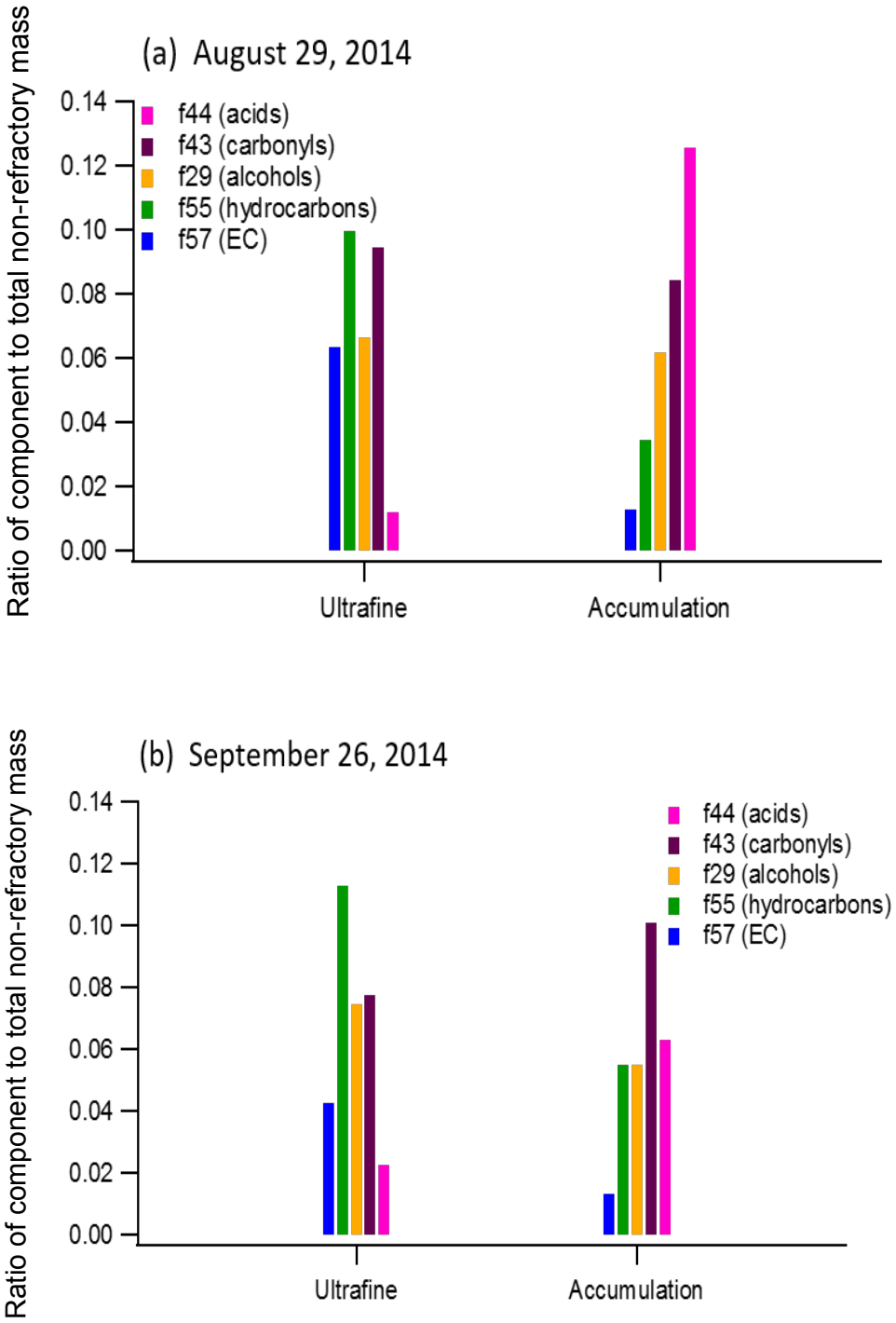

Figure 4.8 Composition of the ultrafine and accumulation modes of CAPs. Proportion of acids, carbonyls, alcohols, hydrocarbons, and elemental carbon (EC) measured by AMS in ultrafine and accumulation modes of CAPs on days with A) high mass concentration, low proportion of UF mode and B) low mass concentration, high proportion of UF mode

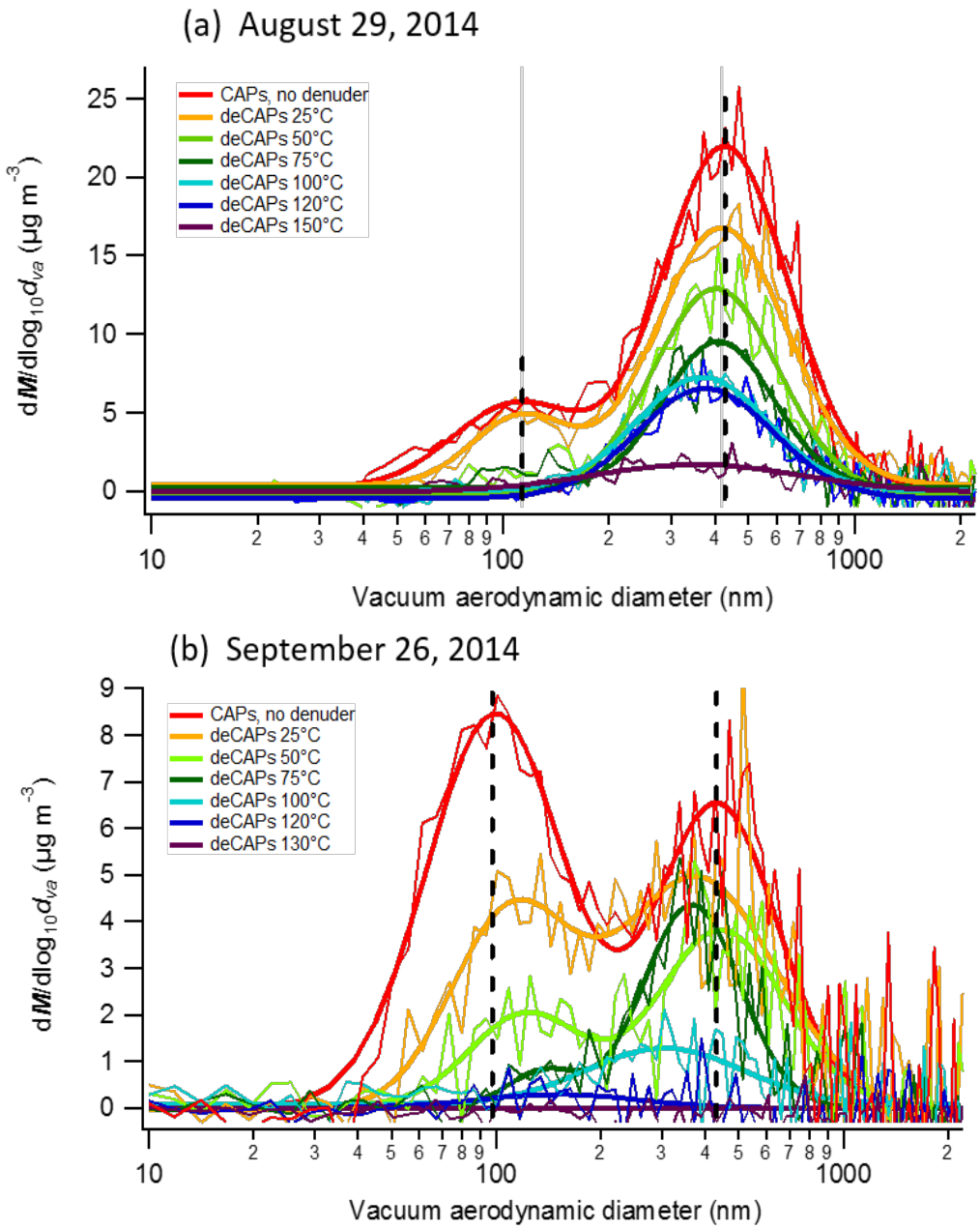

Figure 4.9 DeCAPs Mass Size Distribution at Increasing Denuder Temperatures. DeCAPs mass size distribution measured on days with A) high mass concentration, low proportion of UF mode and B) low mass concentration, high proportion of UF mode at conditions ranging from 25°C to 130°C. Unmodified CAPs measurements are also included in both graphs for comparison. Data collected using the AMS and represent averages of 3-5 measurements taken at each temperature during the same recording period.

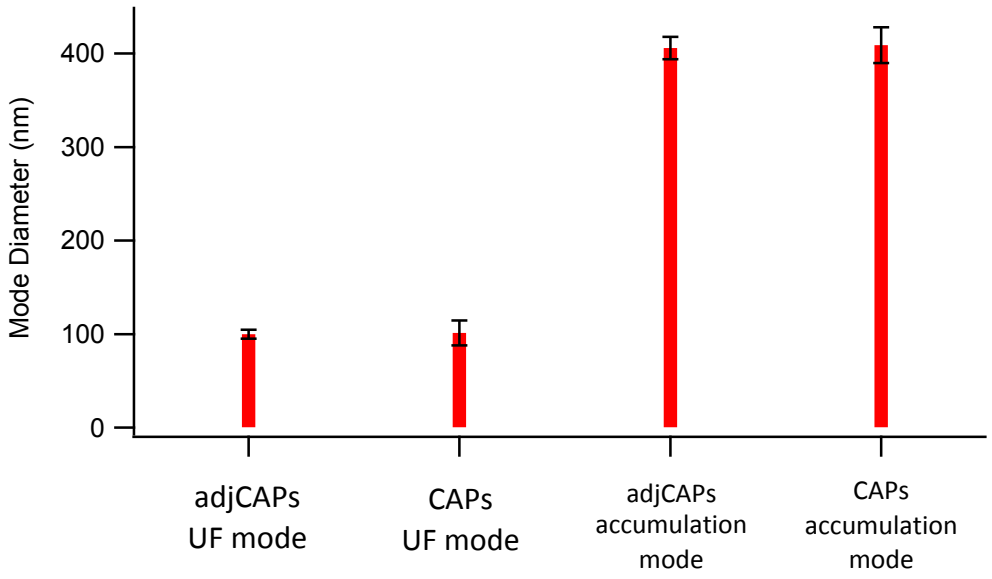

Figure 4.10 Aerodynamic diameter at peak mass concentration of CAPs and adjCAPs in the ultrafine and accumulation modes.
Mode diameter represents the aerodynamic diameter at peak mass concentration measured by the AMS in the ultrafine (UF) and accumulation modes for adjCAPs and CAPs exposures. Error bars represent two standard deviations of 45-60 minute collection averages.

4.2.4 Oxygen to Carbon and Hydrogen to Carbon Ratios

The oxygen to carbon (O:C) and hydrogen to carbon (H:C) ratios, which are characteristics of the families of organics comprising the organic fraction, of concentrated particles are given in Figure 4.11 and Figure 4.12. The O:C and H:C ratios of CAPs, deCAPs, and adjCAPs aerosols were characterized by the AMS during a period when animals were not being exposed to evaluate the effects of denuding and adding dilution air to CAPs. The O:C and H:C ratio measurements were taken during two separate periods, one with higher mass in the ultrafine mode and the other with most of the mass in the accumulation mode.

As hydrocarbon compounds are oxidized during atmospheric aging, the O:C ratio would increase and the H:C ratio would decrease. A typical progression would be hydrocarbon to alcohol to aldehyde to ketone to acid.

There was minimal change in the O:C and H:C ratios of CAPs by adding dilution air to create the adjCAPs aerosol (Figure 4.11). Denuding CAPs at 120°C substantially increased the O:C ratio and decreased the H:C ratio (Figure 4.11). The increase in O:C ratio and decrease in H:C ratio was more dramatic during the measurement with the larger ultrafine mode compared to the period with a larger accumulation mode (Figure 4.12).

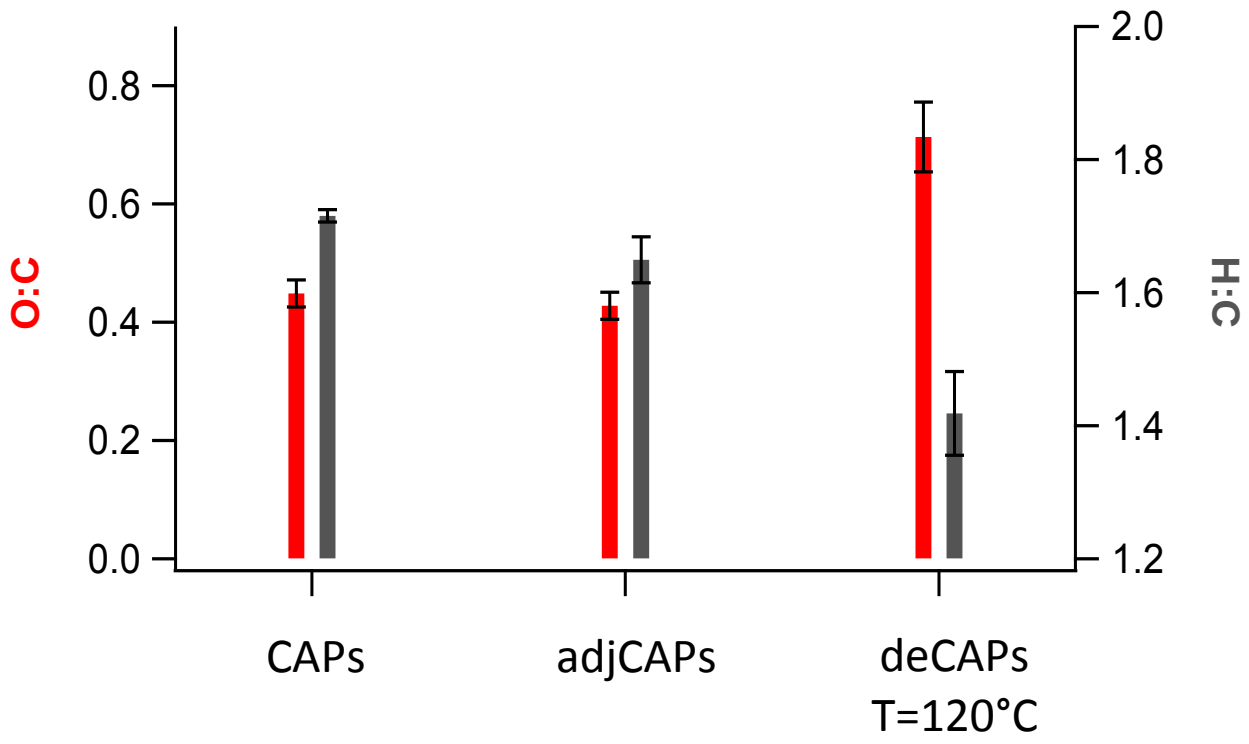

Figure 4.11 PM Oxygen to Carbon and Hydrogen to Carbon Ratios.
Oxygen to carbon (O:C, left axis) and hydrogen to carbon (H:C, right axis) ratios of CAPs, adjCAPs, and deCAPs measured by AMS. Error bars represent two standard deviations of 45-60 minute collection averages.

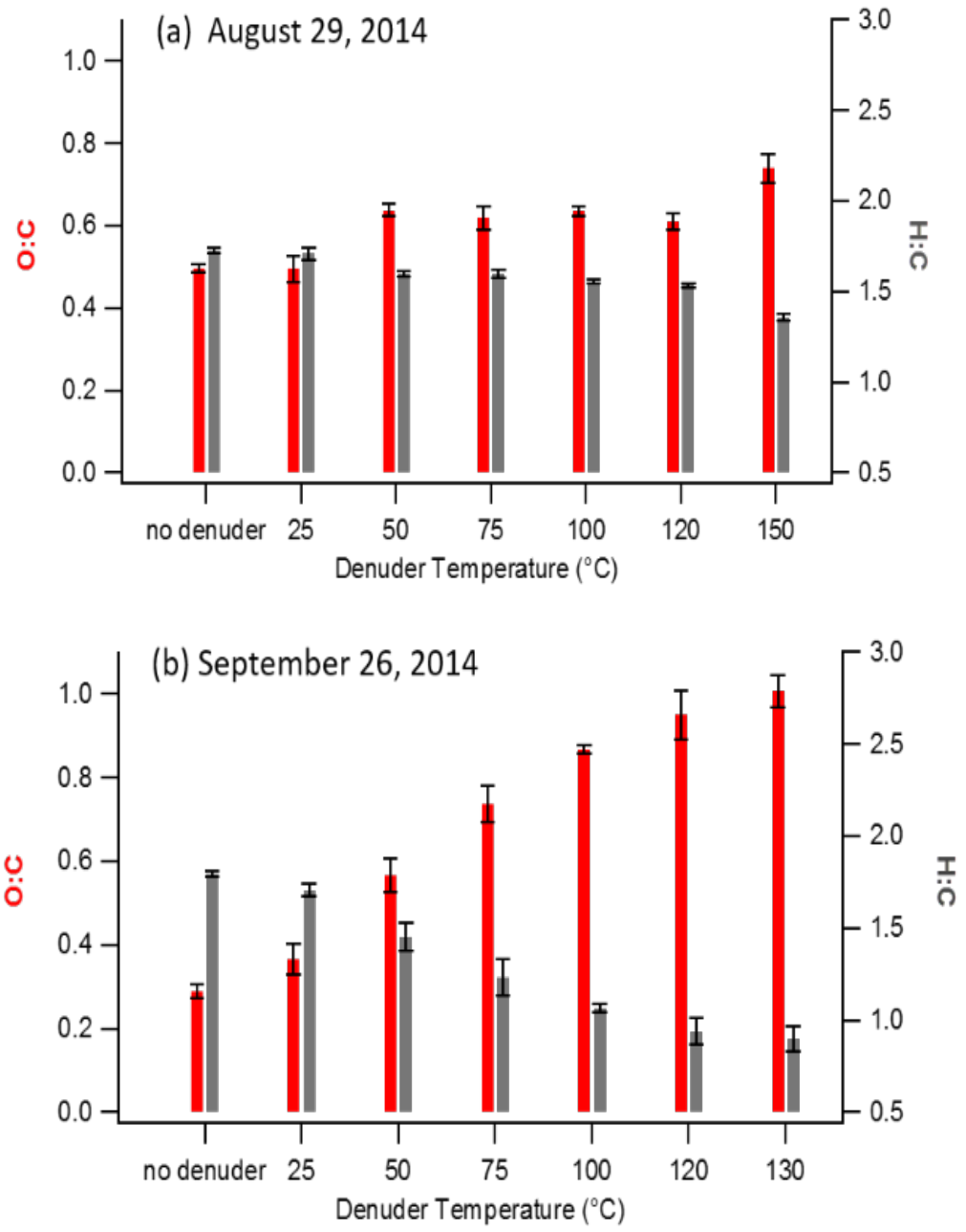

Figure 4.12 DeCAPs O:C and H:C Ratios at Increasing Denuder Temperatures
DeCAPs O:C and H:C ratio measured on days with A) high mass concentration, low proportion of UF mode and B) low mass concentration, high proportion of UF mode at conditions ranging from 25°C to 130°C. Data collected using AMS. Error bars represent two standard deviations of 20 minute collection averages at each temperature.

4.3 Progression of Atherosclerosis

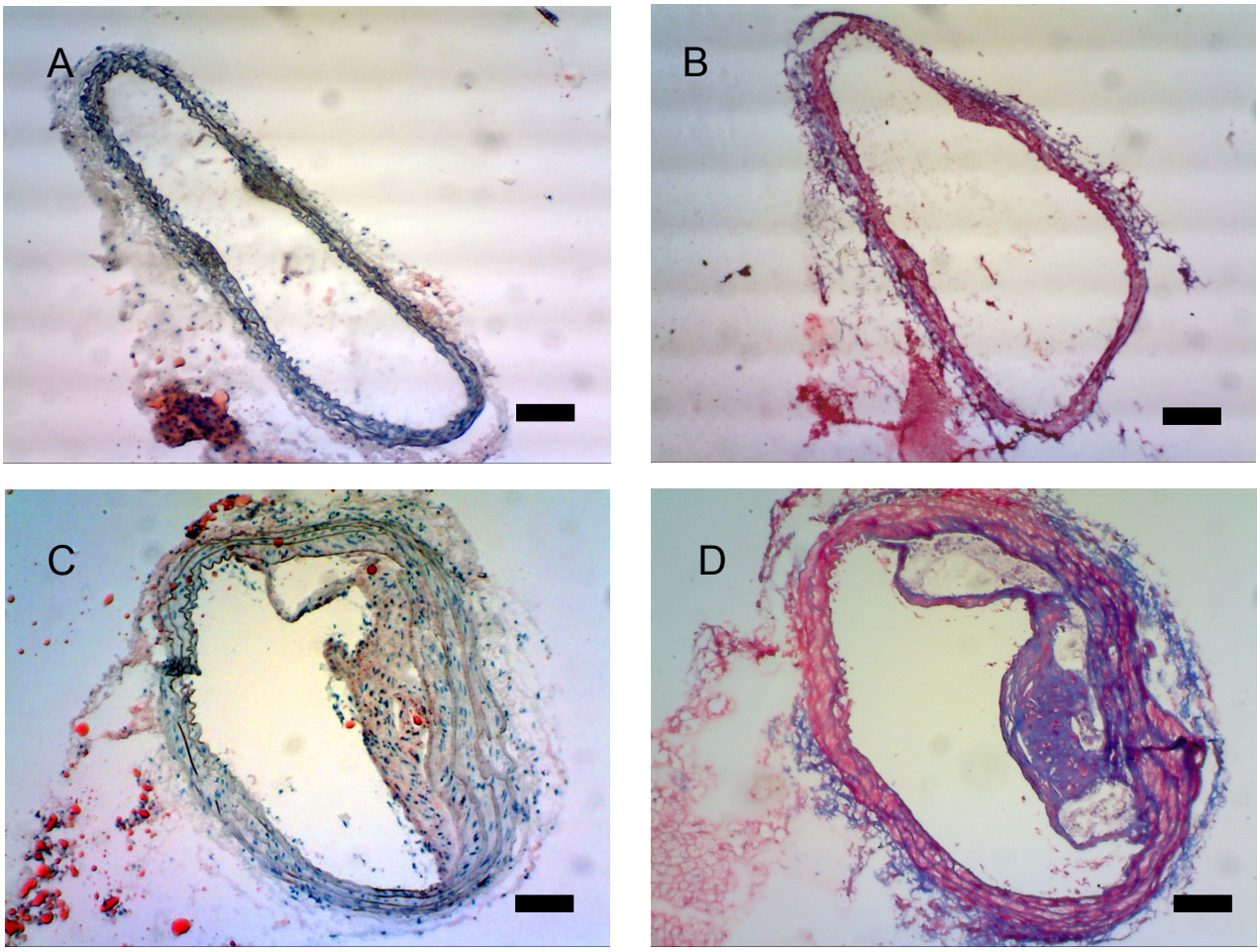

Figure 4.13 Representative images of brachiocephalic arteries without lesions
Representative images of brachiocephalic arteries from apoE -/- mice (A,B) without and (C,D) with atherosclerotic plaque formation. In (A,C) lipids are stained red with Oil Red O and in (B,D) collagen is stained blue with aniline blue as part of the Masson's trichrome stain. Black scale bars represent a distance of 100 μm.

Representative images of the brachiochephalic artery without (Figure 4.13a,b) and with (Figure 4.13c,d) atherosclerotic lesions show how the arteries with lesions have thickened arterial walls and occlusion of the lumen. Furthermore, the lesions contain high amounts of lipids (Figure 4.13c) and collagen (Figure 4.13d), neither of which are prevalent in the arterial walls that lack lesions (Figure 4.13a,b).

4.3.1 Brachiocephalic Artery

AdjCAPs exposed mice had significantly higher levels of atherosclerotic formation than clean air controls as measured by both occlusion of the lumen (Figure 4.14a) and thickening of the arterial wall (Figure 4.14b). Neither plaque size nor intima-media thickness in deCAPs exposed mice was different from the clean air control group. Furthermore, both the CAPs and adjCAPs exposed groups had plaques found in the brachiocephalic arteries of the majority of the mice, while the Air and deCAPs exposed groups had substantially lower percentages of mice with plaque (Table 4.2). Using a chi-square test, the distribution of lesion formation was related to the exposure group ($p=0.03$) with the adjCAPs exposure related to the presence of lesions ($p<0.05$) and the air group related to the absence of lesions ($p<0.05$).

CAPs exposed mice, despite being exposed to a higher concentration of CAPs than adjCAPs exposed mice, did not have significantly larger plaques, however they did have plaques with much higher levels of collagen than mice exposed to clean air (Figure 4.14c). There was no difference between the groups in lipid accumulation within the brachiocephalic lesions (Figure 4.14d).

Table 4.2 Percentage of Brachiocephalic Arteries with Atherosclerotic Lesions

Brachiocephalic Artery	Air	CAPs	AdjCAPs	DeCAPs
Total Arteries	14	14	12	15
Arteries with Lesion	4	8	10	6
% Arteries with Lesion	29	57	83	40

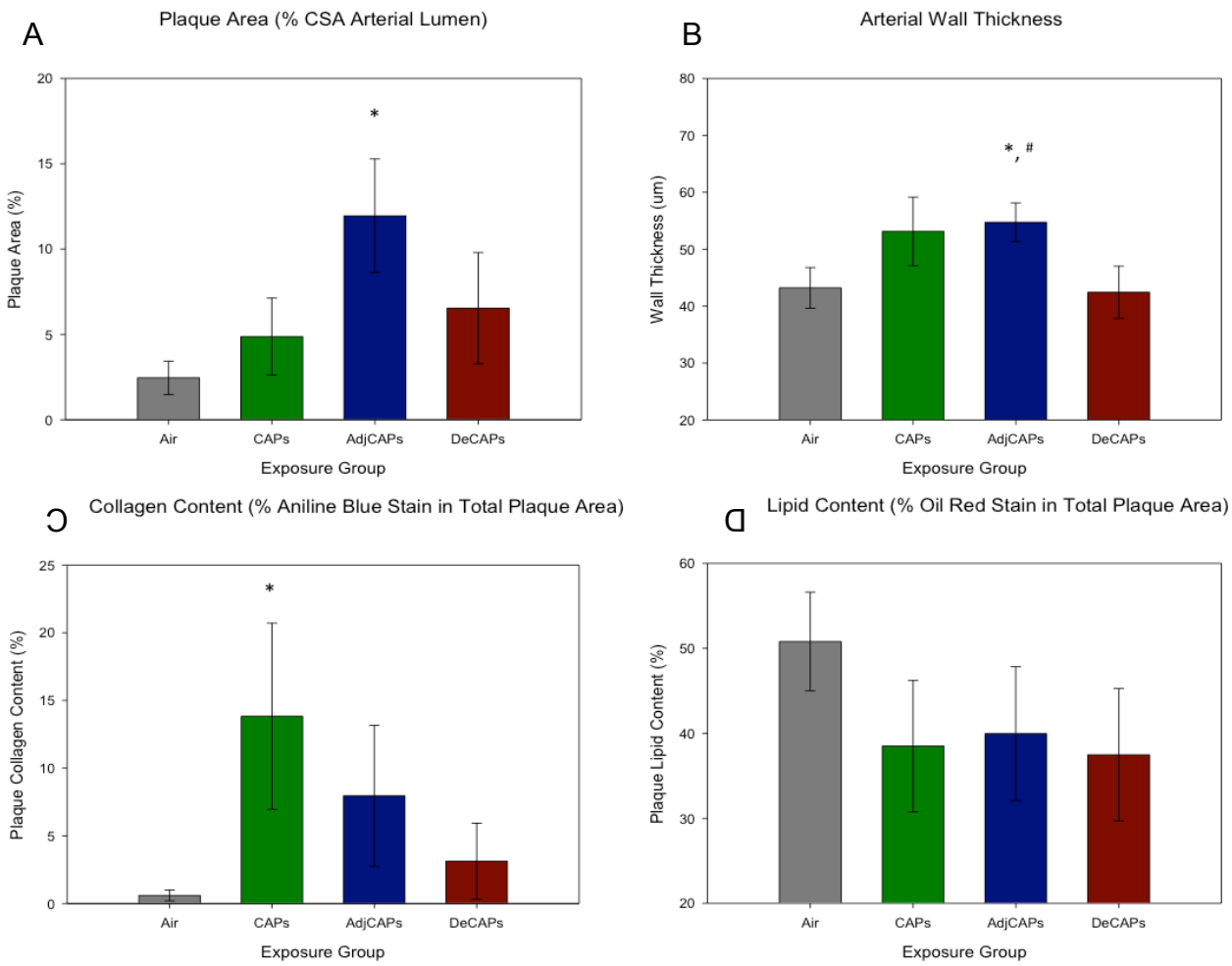

Figure 4.14 Measurements of Atherosclerotic Lesion Size and Composition for Brachiocephalic Artery.
A) Plaque size measured by area of lesion as a total percentage of the cross-sectional area of the arterial lumen B) Arterial intima-media thickness measured by the average distance between the lumenal wall of the intima to the adventitial surface of the media for each artery C) Collagen content measured by the percentage of blue pixels in each lesion divided by the number of pixels representing total lesion area D) Lipid content measured the same as C) except for red pixels. Each bar represents the mean of the values from all mice in each group with usable arteries and error bars representing standard error. *$p<0.05$ compared to Air, $^{\#}p<0.05$ compared to DeCAPs

4.3.2 Aortic Arch

There was no difference in plaque formation or composition among groups in plaques present in the aortic arch. Measurements of both aortic arch plaque area (Figure 4.15a) and intima-media thickness (Figure 4.15b) did not differ between exposure groups. Additionally, plaque lipid (Figure 4.15c) and collagen content (Figure 4.15d) was not different between exposure groups.

The AdjCAPs exposed group had the highest percentage of mice with plaques, however there was less of a disparity between groups as was found in the brachiocephalic artery (Table 4.3). There were also fewer mice with plaques across all groups in the aortic arch compared to the brachiocephalic artery. The plaques were much smaller although they did have similar collagen content and lipid content than plaques in the brachiocephalic artery.

Table 4.3 Percentage of Aortic Arches with Atherosclerotic Lesions

Aortic Arch	Air	CAPs	AdjCAPs	DeCAPs
Total Arteries	13	11	11	11
Arteries with Plaque	6	5	6	4
% Arteries with Plaque	46	45	55	36

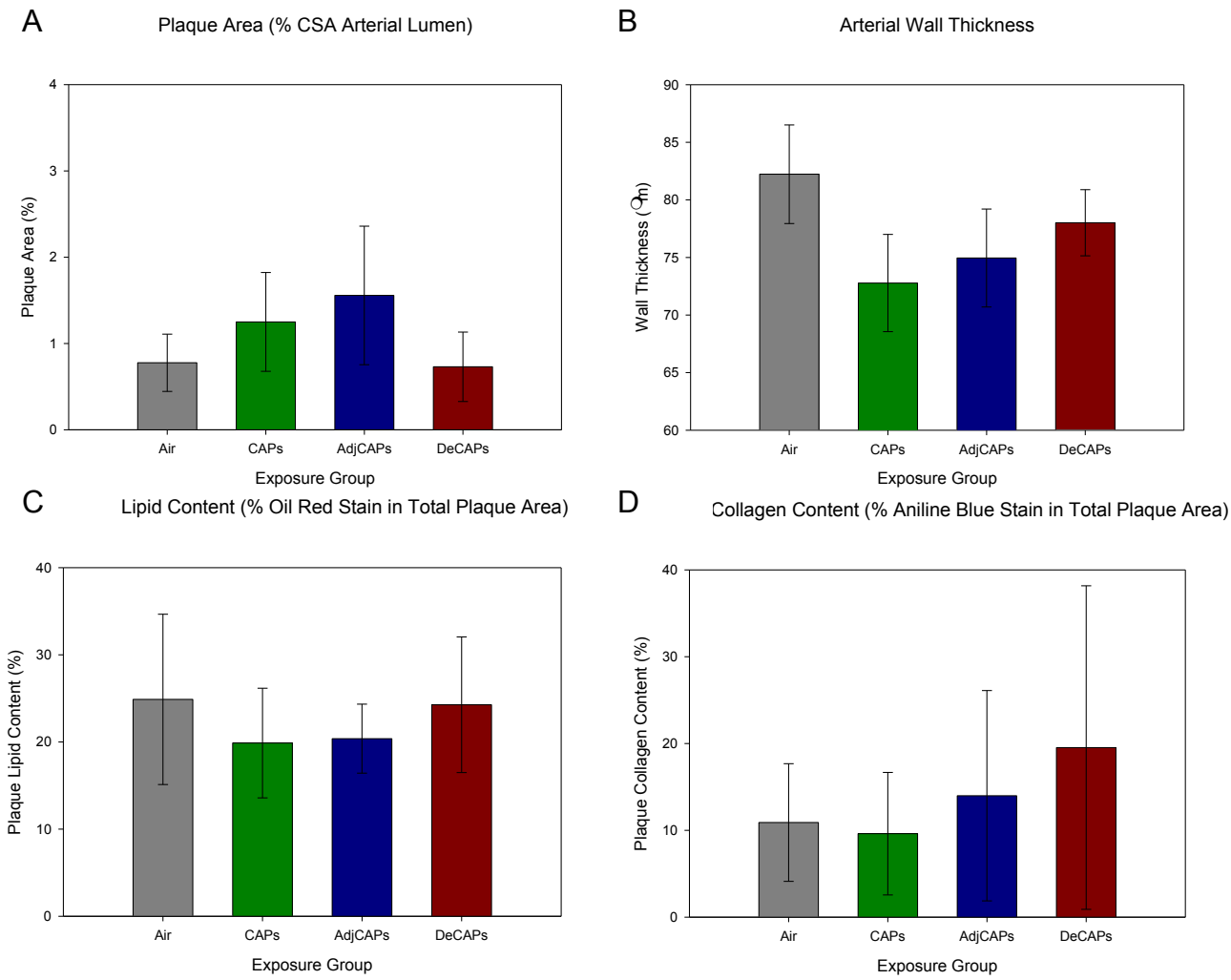

Figure 4.15 Measurements of Atherosclerotic Lesion Size and Composition for Aortic Arch.

A) Plaque size measured by area of lesion as a total percentage of the cross-sectional area of the arterial lumen B) Arterial intima-media thickness measured by the average distance between the lumenal wall of the intima to the adventitial surface of the media for each artery C) Lipid content measured by the percentage of red pixels in each lesion divided by the number of pixels representing total lesion area D) Collagen content measured the same as C) except for blue pixels. Each bar represents the mean of the values from all mice in each group with usable arteries and error bars representing standard error.

4.4 Serum Cholesterol

The ratio of total cholesterol (LDL + HDL cholesterol) to HDL cholesterol, a measure of the relative amounts of LDL and HDL cholesterol in the serum, was increased in mice exposed to adjCAPs compared to clean air control mice (Figure 4.16a). An increased ratio is considered a risk factor for atherosclerosis and coronary artery disease. The heightened ratio was attributable to a non-significant increase in LDL and decrease in HDL in the serum of adjCAPs exposed mice relative to the other exposure groups (Figure 4.16b). There was no difference in the cholesterol ratio or individual HDL and LDL concentrations between the CAPs and deCAPs groups and the clean air control group.

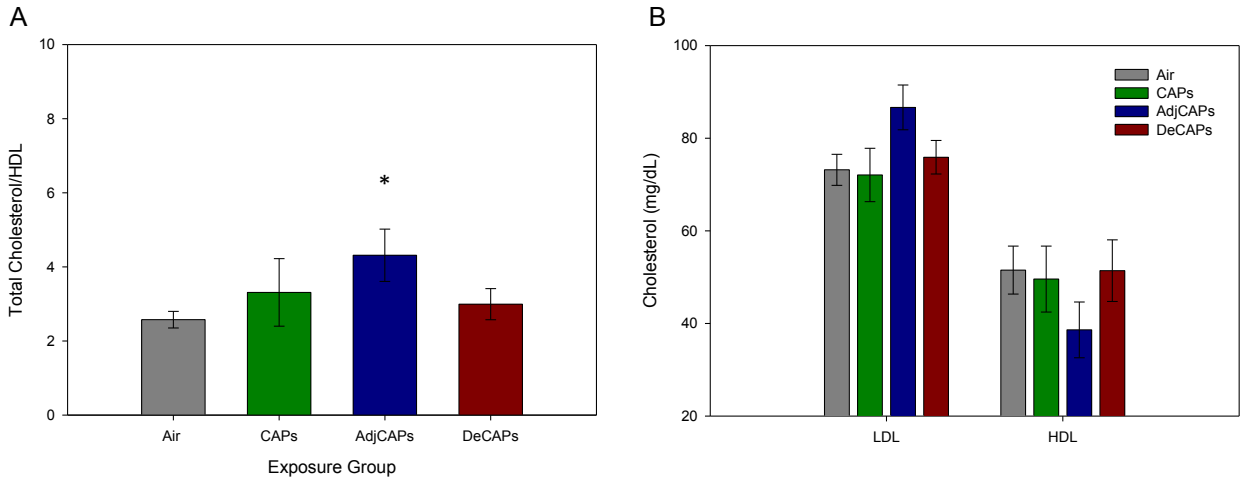

Figure 4.16 Serum LDL and HDL cholesterol.
A) Average ratio of total cholesterol (LDL + HDL cholesterol) to HDL cholesterol in serum of apoE -/- mice from each exposure group B) Average serum LDL and HDL concentrations. Values are expressed as mean of all mice in each group with error bars representing standard error. *p<0.05 compared to Air group.

4.5 Lipid Peroxidation

Malondialdehyde (MDA), a marker of lipid peroxidation, concentration was not significantly different among exposure groups in lung homogenate samples (Figure 4.17a). However, levels were non-significantly elevated in the adjCAPs exposed mice compared to the air group. There was also no difference in MDA concentration between exposure groups in homogenates of the descending aorta (Figure 4.17b). Homogenate samples were normalized by protein concentration to account for differences in the amount of tissue homogenized.

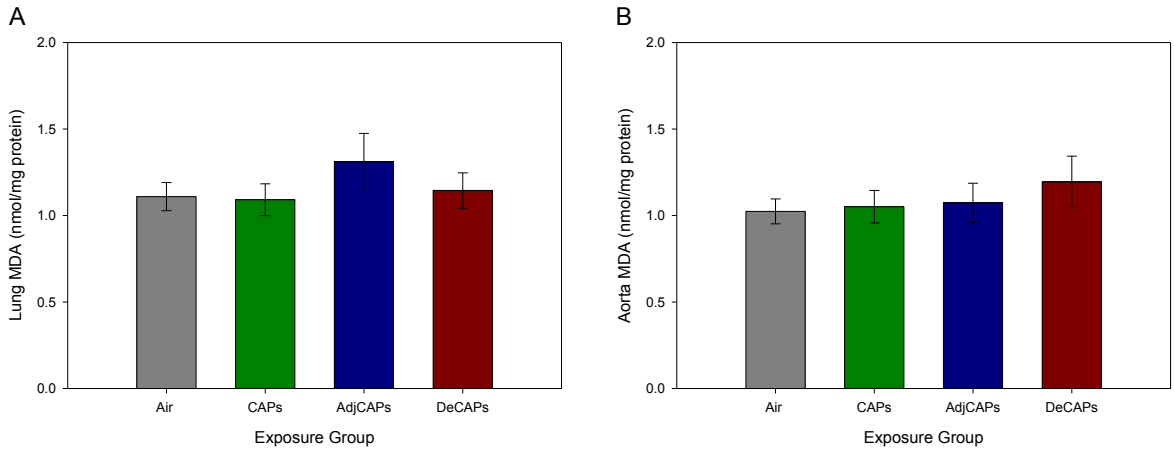

Figure 4.17 Malondialdhyde in lung and aorta tissue homogenate.
Average malondialdehyde (MDA) concentration in A) lung homogenate and B) descending aorta homogenate of apoE -/- mice from each exposure group. MDA concentrations were normalized by dividing MDA values by the protein concentration of each homogenate. Values are expressed as mean of all mice in each group with error bars representing standard error.

4.6 Serum Oxidized LDL

Serum oxidized LDL (OxLDL) concentrations were normalized to total serum LDL concentration to give the proportion of total LDL that was oxidized. The proportion of oxidized LDL (oxLDL) was significantly decreased in mice exposed to adjCAPs compared to mice receiving clean air (Figure 4.18). This could suggest either increased scavenging of oxLDL or the influence of the increased production of total LDL (Figure 4.16b). There was no difference in serum oxLDL between the clean air group and the CAPs or deCAPs groups.

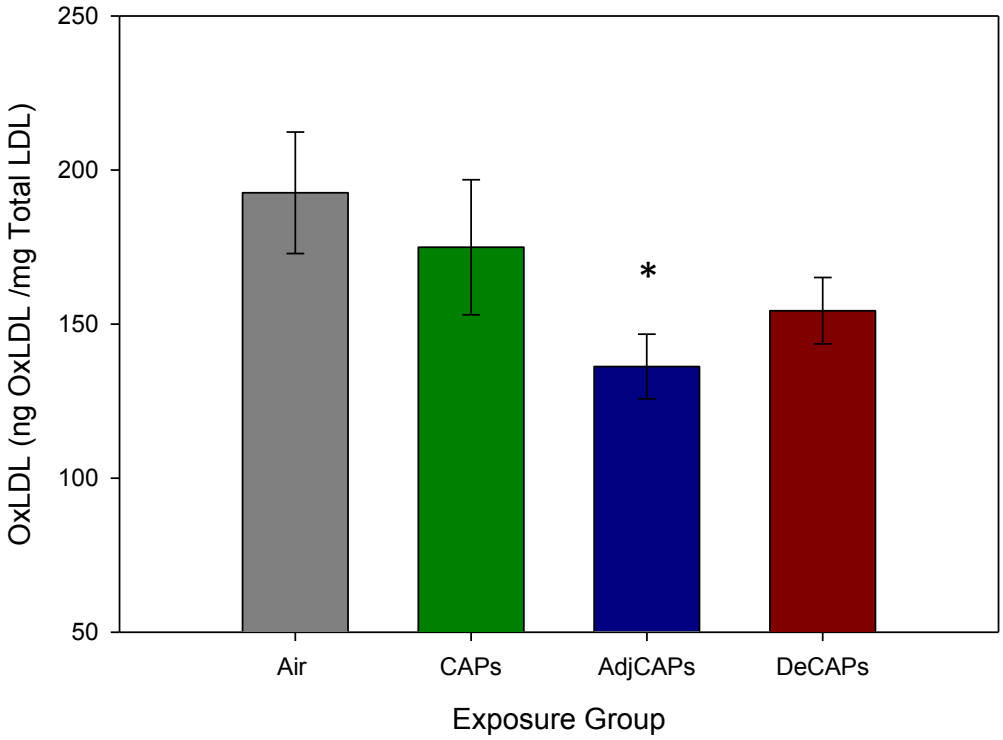

Figure 4.18 Serum Oxidized LDL.
Average oxidized LDL (oxLDL) concentration in the serum of apoE -/- mice from each exposure group. OxLDL concentrations were normalized by dividing oxLDL values by the overall serum LDL concentration. Values are expressed as mean of all mice in each group with error bars representing standard error. *$p<0.05$ compared to Air group.

4.7 Serum Biomarkers of Inflammation and Vascular Disease

Serum IL-6 concentrations were higher in mice exposed to adjCAPs compared to mice receiving deCAPs, however the adjCAPs group was not statistically different from clean air controls for either cytokine (Figure 4.19). Serum IL-10 was increased in mice exposed to deCAPs and was non-significantly increased in mice exposed to CAPs ($p<0.1$) There was no difference between groups for TNF-α or IL-1β.

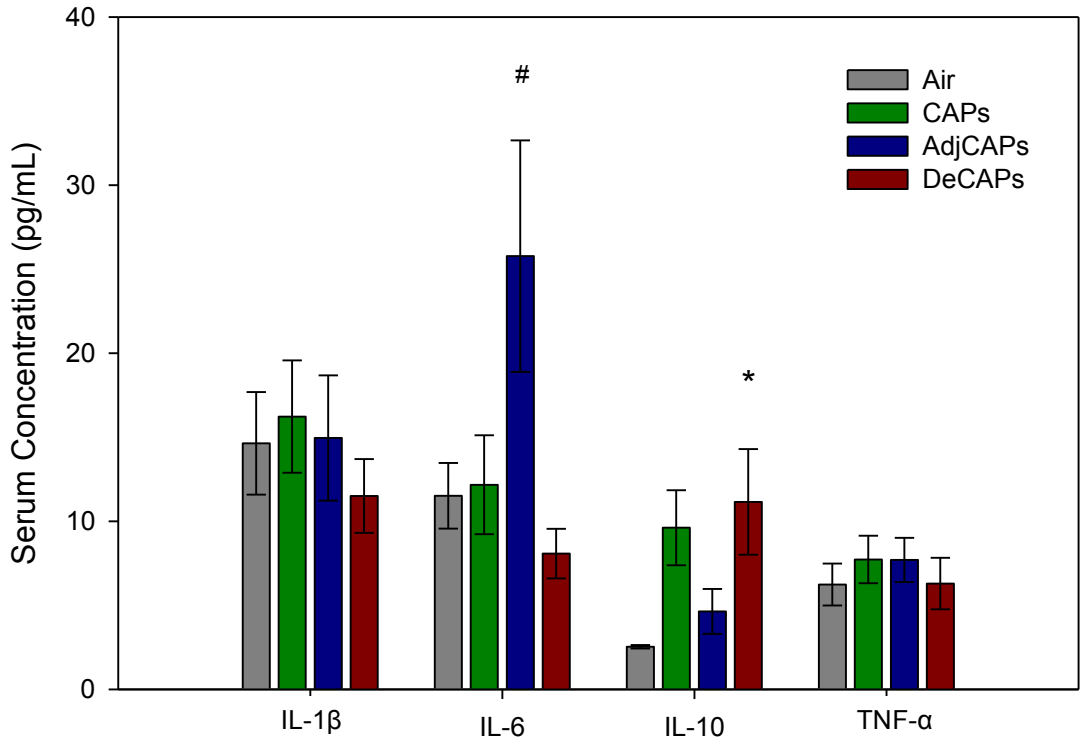

Figure 4.19 Serum Inflammatory Cytokines
Average IL-1β, IL-6, IL-10 and TNF-α concentrations in the serum of apoE -/- mice from each exposure group. Values are expressed as mean of all mice in each group with error bars representing standard error. $^{\#}p<0.05$ compared to DeCAPs group, $^{*}p<0.05$ compared to Air group.

There was no difference between CAPs, adjCAPs or deCAPs and clean air control concentrations of serum CRP. (Figure 4.20).

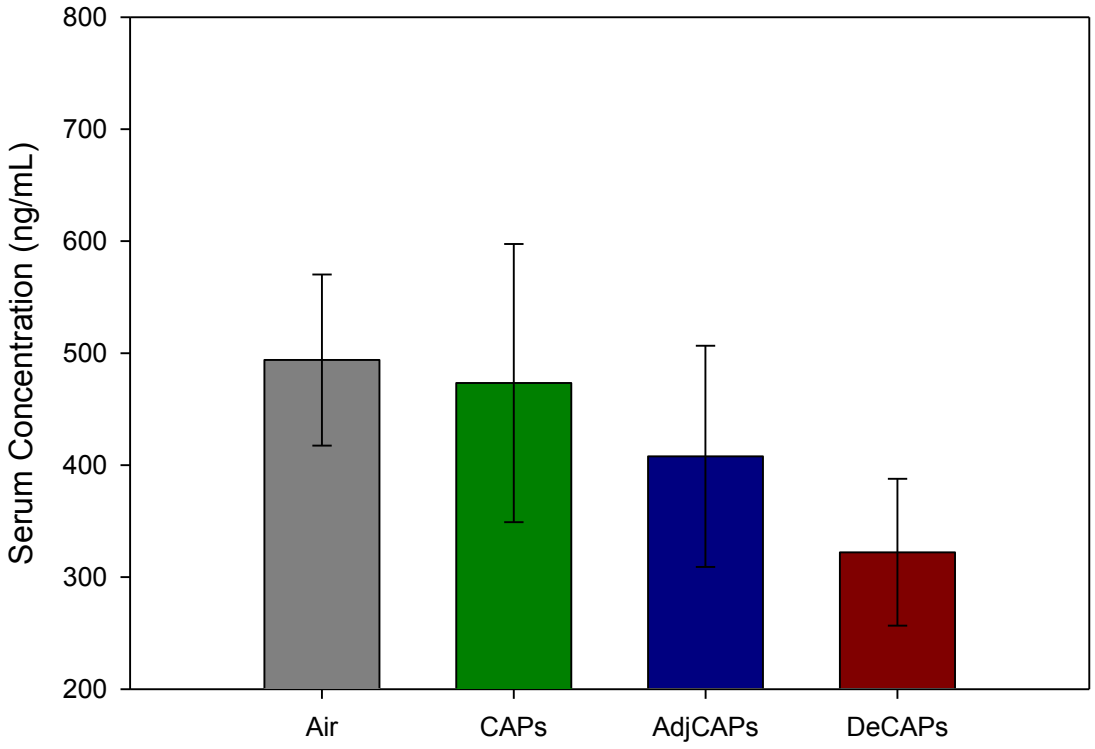

Figure 4.20 Serum C-Reactive Protein.
Average C-reactive protein (CRP) concentration in the serum of apoE -/- mice from each exposure group. Values are expressed as mean of all mice in each group with error bars representing standard error.

Serum concentrations of the soluble forms of cell adhesion molecules E-selectin (Figure 4.21a), P-selectin (Figure 4.21b), and ICAM-1 (Figure 4.21c) were not different between exposure groups, although CAPs and deCAPs groups had slightly elevated P-selectin ($p<0.1$). Similarly, PAI-1 and MMP-9, pro-atherogenic factors promoting thrombosis and vascular remodeling, respectively, were not present in the serum at significantly distinct concentrations between the various exposure groups (Figure 4.21d).

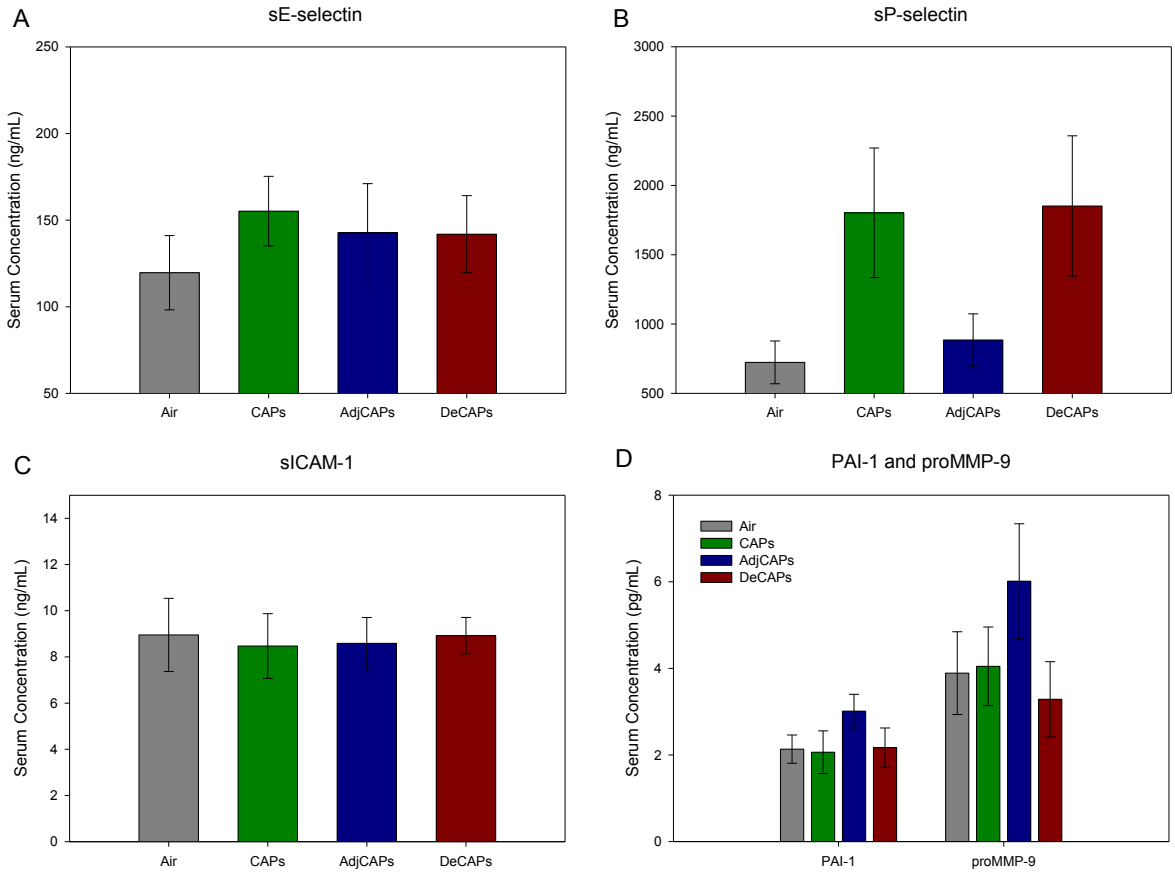

Figure 4.21 Other serum pro-atherogenic markers.
Average A) soluble E-selectin (sE-selectin), B) soluble P-selectin (sP-selectin), C) soluble ICAM-1 (sICAM-1), and D) plasminogen activator inhibitor-1 (PAI-1) and proMMP-9 concentrations in the serum of apoE -/- mice from each exposure group. Values are expressed as mean of all mice in each group with error bars representing standard error.

4.8 Heart Rate Variability

The post-exposure changes in heart rate variability (HRV) and heart rate (HR) are given in Figure 4.22-Figure 4.24. There was a decrease in power in the HF band of HRV (HF HRV) in mice exposed to CAPs during the post-exposure period (Figure 4.22a). HF HRV increased relative to baseline for the air exposed mice and DeCAPs exposed mice had a similar increase. All four exposure groups had lower heart rate (Figure 4.22d) and power in the LF band of HRV (LF HRV) (Figure 4.22b) following the exposures. LF/HF ratio decreased in the mice exposed to clean air and deCAPs due to the increased HF and decreased LF components while the reduction in the same direction for both CAPs and adjCAPs elicited minimal change in the LF/HF ratio (Figure 4.22c).

Looking at the time series of HF HRV over the nine weeks of exposure in Figure 4.23, there was no decreasing trend in the reduction in post-exposure HF HRV in the CAPs group, so there did not appear to be related to a cumulative change in HF HRV over time. However, there was a downward trend in HF HRV for the CAPs group within each week of exposure (Figure 4.24).

There was no difference between exposure groups for HRV parameters measured on days when no exposure occurred (Figure 4.25). These measurements took place during the same time period as the post-exposure measurements. The main difference from the post-exposure HRV values was that the Air and deCAPs groups did not have as pronounced of an increase from baseline in HF HRV and a decrease from baseline in LF/HF ratio.

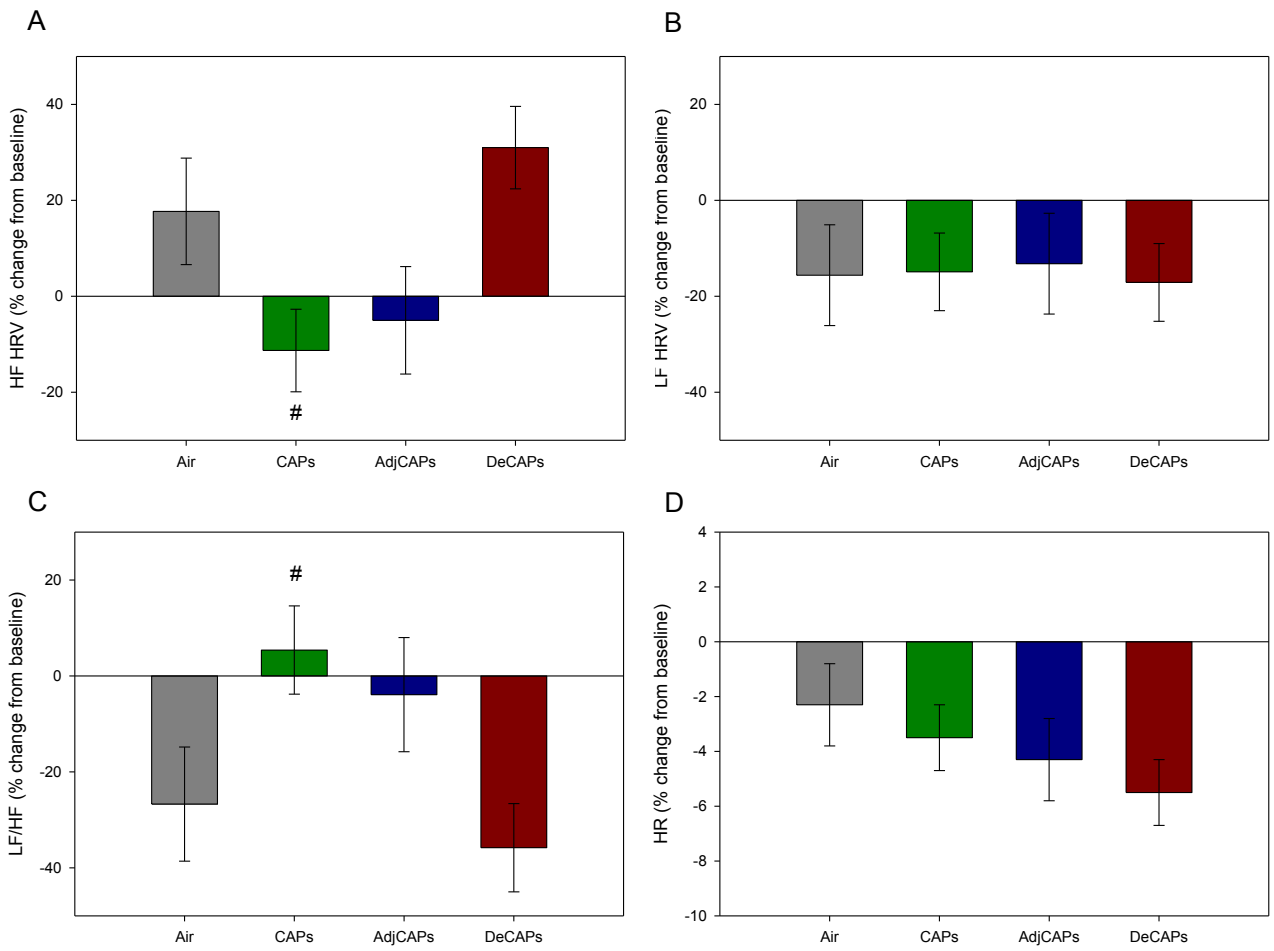

Figure 4.22 Study Average of Post-Exposure Heart Rate Variability.
A) High frequency power (HF HRV) B) Low frequency power (LF HRV) and C) Ratio of low frequency power to high frequency power (LF/HF) of heart rate variability D) Heart rate. Data were collected during the five hour post-exposure nighttime period. Data represent the mean change in each parameter from pre-exposure baseline for the mice in each group, with error bars indicating SEM. Group differences were determined by estimated mean differences from linear mixed models with the Bonferroni correction for multiple comparisons. $^{\#}p<0.05$ compared to deCAPs

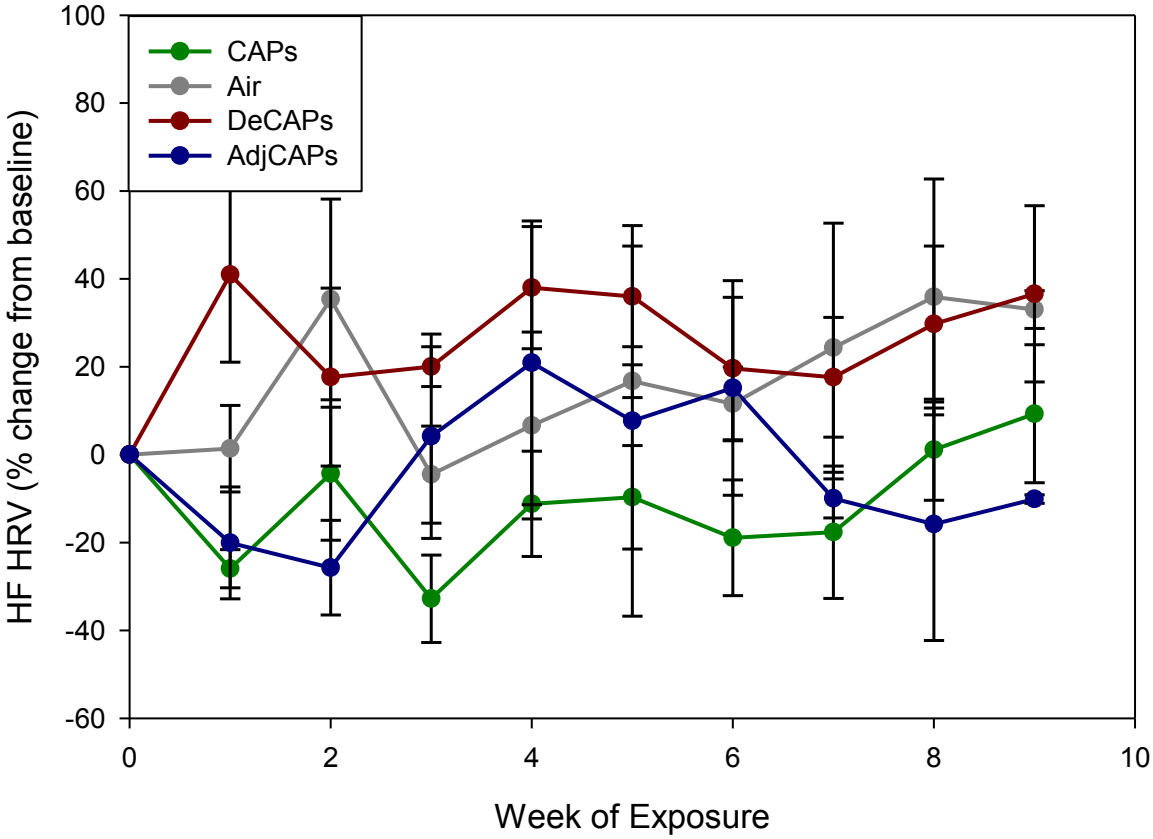

Figure 4.23 Weekly Average of Post-Exposure HF HRV.
Weekly mean high frequency power of heart rate variability (HF HRV) of mice in each exposure group expressed as change from pre-exposure baseline.

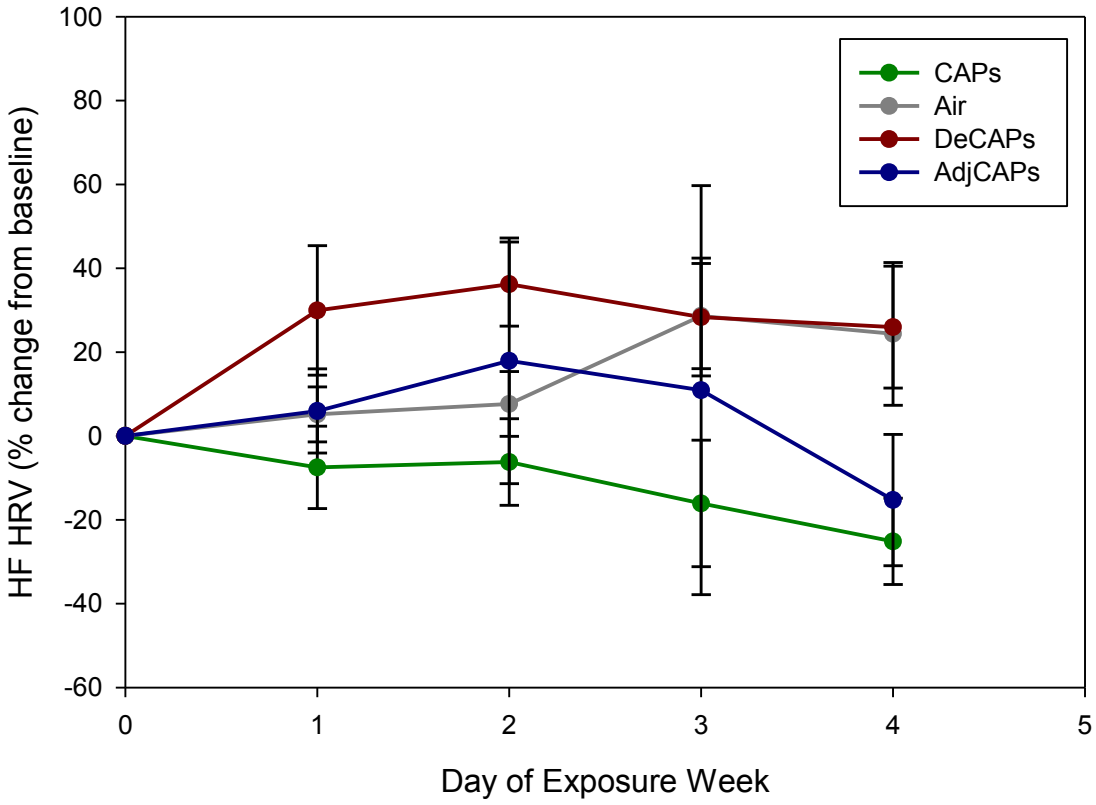

Figure 4.24 HF HRV Average Each Day of Exposure Week

Data were collected during the five hour post-exposure nighttime period. Data represent the mean high frequency power of heart rate variability (HF HRV) of the mice in each group on the first, second, third and fourth days of each exposure week, with error bars indicating SEM. Group differences were determined by estimated mean differences from linear mixed models with the Bonferroni correction for multiple comparisons.

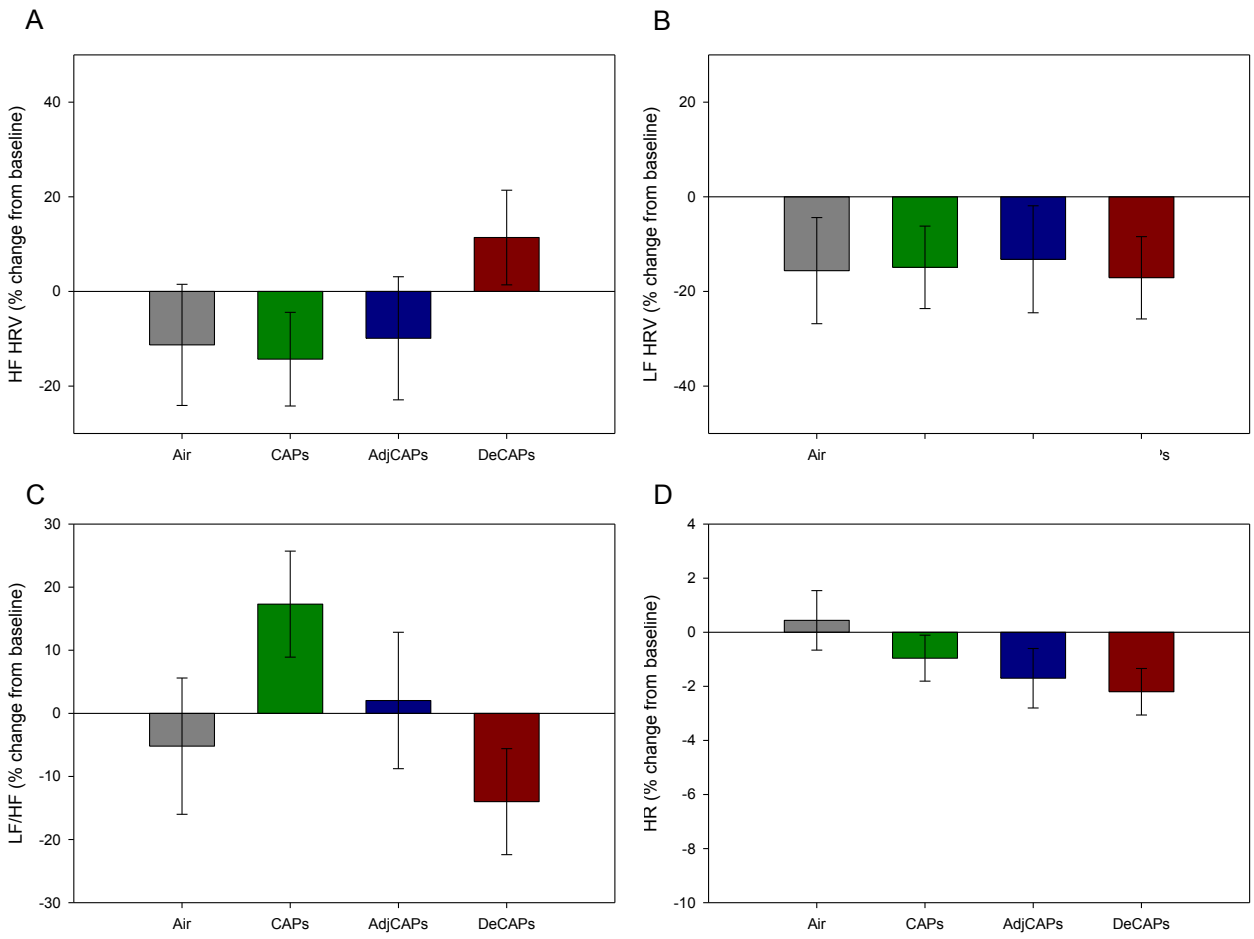

Figure 4.25 Heart Rate Variability on Days with No Exposure.
A) High frequency power (HF HRV) B) Low frequency power (LF HRV) and C) Ratio of low frequency power to high frequency power (LF/HF) of heart rate variability D) Heart rate. Data were collected during the five hour nighttime period of days with no exposure. Data represent the mean of the mice in each group with error bars indicating SEM. Group differences were determined by estimated mean differences from linear mixed models with the Bonferroni correction for multiple comparisons.

4.9 Heart Rate Variability Associations with Particle Composition

The daily change in HF power used for investigation of the association between particle characteristics and autonomic changes because it was significantly altered following CAPs exposure. Associations were investigated between HF HRV and daily changes in both physical and chemical parameters of CAPs including particle number concentration, particle mass concentration, fractions of non-refractory species, and particle oxygenation.

The daily change in post-exposure power of the HF component of HRV in mice exposed to CAPs was associated with daily changes in the level of oxygenation in the ultrafine mode. No associations were found between measures of the combined accumulation mode and ultrafine fractions (Figure 4.26a). However, when using the O:C ratio of only the ultrafine fraction, a significant positive association was found between ultrafine O:C ratio and HF HRV at O:C ratios below ~0.3:1 (Figure 4.26b). The O:C ratios below 0.3:1 are mostly associated with primary organic species such as PAHs, diesel/gasoline exhaust, and primary cooking aerosol. The more reduced fractions of secondary organic aerosol also fall into this range. Two data points that were well into the secondary organic aerosol range of O:C ratios (~0.4-0.5:1) were excluded from the association.

No other associations were found between daily HF HRV changes in CAPs exposed mice and daily changes in the physical or chemical characteristics of particles.

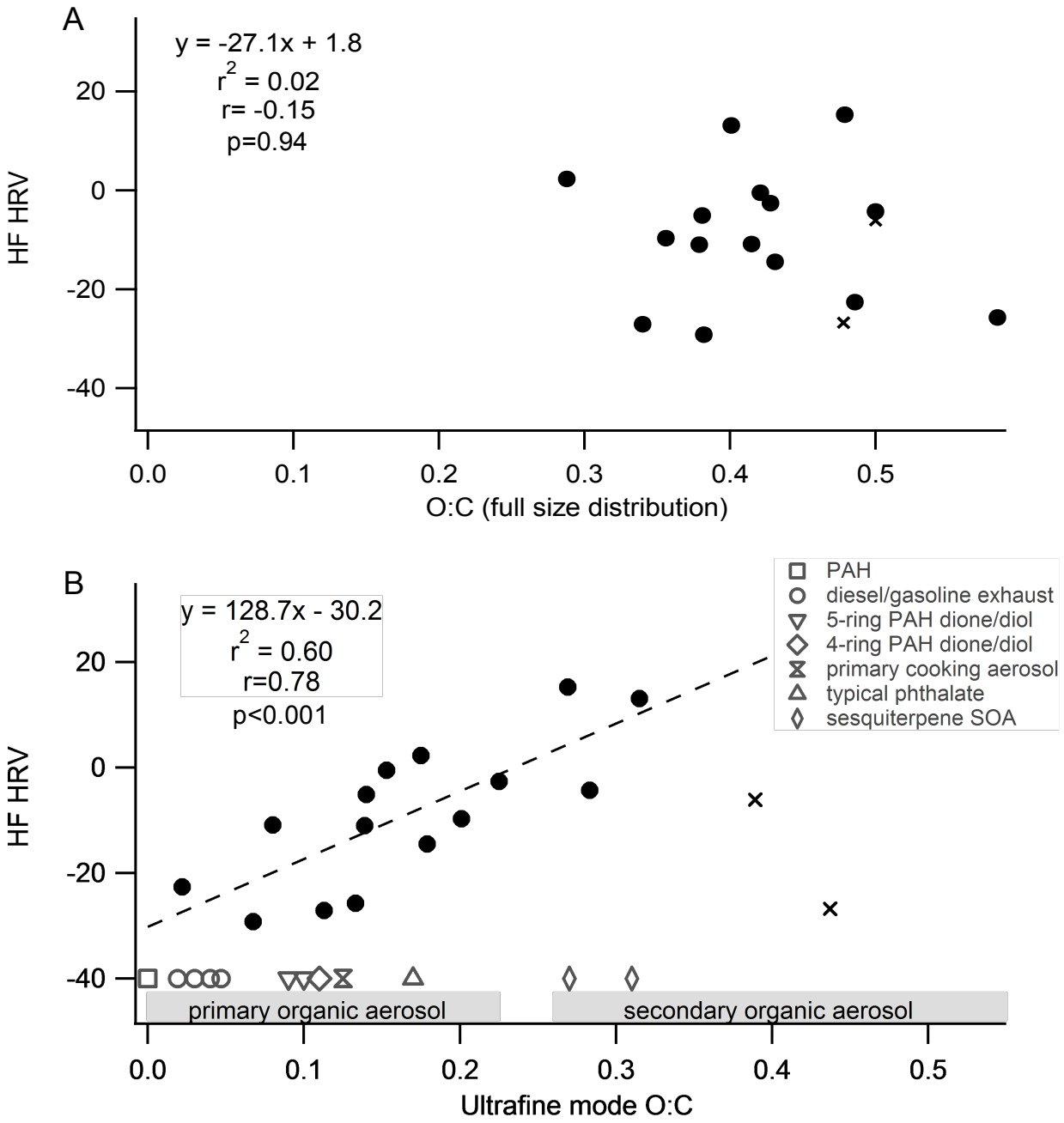

Figure 4.26 HF Heart Rate Variability Associations with O:C Ratio of CAPs. Association between HF HRV in CAPs exposed mice and O:C ratio of A) the combined accumulation and ultrafine modes of CAPs and B) the ultrafine mode of CAPs. There was no association between daily changes in the O:C ratio of the whole aerosol and HF HRV (r^2=0.02, p=0.94). When only taking the O:C ratio of the ultrafine fraction, there is a significant positive association between daily changes in O:C ratio and HF HRV (r^2=0.60, p<0.001). Two days with very high ultrafine O:C ratios were excluded from the association and are marked by "x". Characteristic O:C ratios of various primary organic aerosol and secondary organic aerosol species are listed on the x-axis.

5 Discussion

5.1 Particle Chemistry

The chemical composition of CAPs during this study was typical of Southern California summertime urban aerosol[18,24]. The non-refractory fraction of particles was mostly composed of organics, followed by a smaller fraction of sulfate and a lesser fraction of nitrate. Both nitrate and sulfate were present as ammonium nitrate and ammonium sulfate, respectively. CAPs consisted of a bimodal mass size distribution that included an ultrafine mode comprised entirely of organics, and an accumulation mode that was a mix of organics, sulfate, and a small amount of nitrate. The composition of bimodal distribution did not change over the course of the study, but there were daily variations in mass concentration present in each mode.

The O:C ratio of CAPs during the study was determined to range from 0.2 to 0.5, which would make the CAPs characteristic of POA or SV-OOA[33]. The days with lower O:C likely had a larger proportion of POA, while the days with higher O:C had a higher percentage of aged SOA due to atmospheric oxidation. The variation was probably due to daily changes in meteorological conditions such as wind, sunlight and precipitation that affected the amount of particle transport and photochemical oxidation. The ultrafine mode contained substantially higher levels of more reduced organic species such as hydrocarbons, and therefore the O:C ratio of just the ultrafine mode was predominately less than 0.4. The low O:C ratios indicated that the majority of the ultrafine mode particles most likely resulted from primary traffic emissions, which are the main

contributor to POA in Southern California $PM_{2.5}$[140]. New particle formation may have also been a contributor to ultrafine particle formation, but prior collection of SMPS data in the exposure location indicated that new particle formation events were rare, so nucleation of fresh SOA was not expected to be a contributor to the ultrafine mode.

The accumulation mode consisted of more highly oxidized species that the ultrafine mode. The main difference in chemical species between the accumulation mode and the ultrafine mode was the presence of a high amount of organic acids in the accumulation mode. Oxidized species are typically associated with the accumulation mode and characteristic of aged SOA that undergoes hours to days of photochemical oxidation in the atmosphere[33]. Although the accumulation mode made up a minimal portion of the CAPs particle number concentration, it comprised a substantial proportion of the mass concentration, indicating that there were a few large particles present in the aerosol that dominated CAPs mass concentration, either due to oxidized combustion-related particles that had grown into the accumulation mode size range or natural dust particles in the atmosphere.

The properties of the ultrafine and accumulation mode fractions of CAPs strongly impacted its response to denuding. The ultrafine fraction was, by mass, able to be removed much more readily by denuding than the accumulation mode. This indicated a higher presence of more volatile species in the ultrafine fraction relative to the accumulation mode. The ultrafine mode was mostly made up of semi-volatile organic species in prior studies, so the prevalence of more semi-volatile species in that fraction is consistent with those findings[72,141]. Highly aged organic aerosol, in particular LV-OOA, is much less volatile than POA or SV-OOA[9], so the presence of these species in

the accumulation mode may contribute to its lower volatility. Sulfate and nitrate, which were predominately present in the accumulation mode, were more refractory than the organic fraction in denuded CAPs and therefore also contributed to the persistence of the accumulation mode.

The less oxygenated organic species in the ultrafine fraction were primarily removed by the stripping of semi-volatile species in denuded CAPs, and this supports previous findings that SVOCs such as PAHs, which have a very low O:C ratio of less than 0.1, were removed through denuding. However, this conclusion is limited by the fact that PAHs were not directly measured. PAH concentrations in PM were reduced by 60% with a thermodenuder at 120°C in an experiment to measure the oxidant potential of PM[72]. PAHs were not directly measured so the true Also, PAHs were mostly removed in a prior study of the effects of SVOCs on the progression of atherosclerosis[68]. Denuding did not impact the mass concentrations of elemental carbon in CAPs. The persistence of elemental carbon is consistent with previous denuder studies showing that it was refractory[68,72]. Although the concentration of metals was not measured in this study, it was expected that the metal content would be conserved in the denuded CAPs based on previous experiments that found minimal loss of metals through the thermodenuder[68,72].

5.2 Progression of Atherosclerosis

The progression of atherosclerosis was enhanced in the arteries of mice exposed to CAPs containing SVOCs relative to mice that were exposed to denuded particles at

the same concentration. Additionally, the groups of mice exposed to CAPs containing SVOCs had a higher percentage of mice with lesions than the groups exposed to particles without SVOCs. The increased progression of atherosclerosis with CAPs exposure agrees with previous findings of the importance of SVOCs in the exacerbation of atherosclerosis[68], but this is the first study to show that atherosclerotic progression is attenuated in mice receiving denuded particles at the same concentration. This supports that our previous findings of attenuated plaque formation in mice exposed to denuded particles were primarily due to compositional differences between CAPs and DeCAPs, not because the CAPs particle concentration was an approximately three times higher than the DeCAPs concentration. However, an unexpected finding was that while the mice exposed to adjCAPs had increased lesion size, but the mice exposed to CAPs, the higher CAPs concentration, did not. The possible mechanisms of why this occurred will be discussed in section 5.3.

Compositionally, lesions of mice exposed to the higher CAPs concentration were more advanced than mice exposed to clean air. It appeared that, in this study, the level in fibrosis was related to the concentration of PM associated SVOCs on the particles. The lesions of mice exposed to CAPs were more fibrotic than lesions in air control or deCAPs exposed mice that received very little SVOC exposure, in which the lesions were more characteristic of small foam cells. Collagen within advanced lesions is important marker for the migration and proliferation of SMCs. An increase in SMCs related to elevated inflammatory signaling following CAPs exposure is one possible mechanism for the increase in collagen. This is consistent with findings that heightened collagen deposition in plaques of apoE -/- mice exposed to diesel exhaust[66].

5.3 Mechanisms of Plaque Formation

5.3.1 Inflammation

Plaque size was increased in mice exposed to the lower concentration of CAPs but the mice exposed to the higher CAPs concentration in this study did not have larger plaques relative to clean air or DeCAPs exposed mice. A similar biphasic dose-response occurred in a prior study of apoE -/- mice in which exposure to a 25 $\mu g/m^3$ CAPs elicited a significantly greater activation of MAP kinases in the central nervous system than exposure to a 125 $\mu g/m^3$ CAPs[142]. MAP kinases are involved in activating transcription factor NF-κB, which induces the production of many pro-inflammatory cytokines and adhesion molecules[143], including IL-6 which was increased in the serum of mice exposed to the lower CAPs concentration in the present study. One explanation for this biphasic response could be that higher concentrations of CAPs may activate anti-oxidant or anti-inflammatory pathways that don't promote sustained enhanced systemic inflammation that was found with the lower concentration CAPS exposure. Additionally, cytotoxic pathways could be activated at higher concentrations that may not produce the same type of systemic inflammatory response.

SVOCs may promote atherosclerosis through the elevation of circulating IL-6, because IL-6 was elevated in the serum of mice exposed to whole CAPs but not denuded CAPs. IL-6 is an important inflammatory player in the progression of atherosclerosis because it promotes both early lesion formation and plaque growth by influencing a number of pro-atherogenic events. IL-6 promotes endothelial dysfunction, SMC proliferation and migration as well as recruitment and activation of inflammatory

cells, thereby perpetuating vascular inflammation [83]. IL-6 was implicated in up-regulation of pro-inflammatory cytokines TNF-α and IL-1 in apoE -/- mice, especially when they were fed a high fat diet[144]. IL-6 affects the local the expression of the scavenger receptors involved in the uptake of modified LDL and thus promotes the formation of macrophage-derived foam cells [84].

Increased IL-6 is consistent with human biomarker studies of PM exposure. In one study, increased IL-6 was related to higher long-term concentrations of $PM_{2.5}$ in study of adults from major American cities[91]. Plasma concentrations of CRP and IL-6 were associated with PM exposure in a panel of elderly subjects with coronary artery disease[96]. They found a significant positive association of IL-6 with ultrafine fraction mass concentration and primary OC, but an inverse relationship of IL-6 with mass concentration of the accumulation mode and secondary OC. The association of IL-6 with the ultrafine fraction and primary OC supports our finding that SVOCs, most of which were primary OC in the ultrafine fraction, are likely responsible for increased IL-6 response. CAPs exposed mice in our study, however, did not have a change in serum levels of CRP. This may be related to the differences in human and mouse physiology because CRP is not a main acute phase protein in mice[145], and the knockout of CRP in mice does not reduce the progression of atherosclerosis[146].

IL-6 can also have effects on atherosclerosis through altered lipid metabolism, although the specific mechanisms remain to be fully understood. The ratio of LDL to HDL cholesterol was increased in adjCAPs exposed mice, and this group of mice also had a greater progression of atherosclerosis and serum IL-6 concentrations. IL-6 administration in humans altered total cholesterol levels[147,148], and studies with IL-6 -/-

mice indicated that IL-6 production decreases circulating cholesterol[144]. Circulating IL-6 was associated with low HDL cholesterol levels in the plasma of elderly adults[149] and in healthy individuals[150].

IL-6 regulation of MMP-9 could be responsible for the effects of IL-6 on lipid metabolism. MMP-9 concentrations were non-significantly elevated in mice exposed to adjCAPs, and these mice also had significantly increased serum IL-6 concentrations and elevated total cholesterol to HDL ratio. This is consistent with findings that IL-6 promotes MMP-9 production[151], and that MMP-9 is associated with increased LDL and decreased HDL in the serum[152], making this a plausible pathway for pro-inflammatory alterations to lipid metabolism that lead to increased atherosclerosis.

IL-10 was increased in the serum of mice exposed to unmodified CAPs and mice that received denuded CAPs. IL-10 is an anti-inflammatory cytokine that is atheroprotective. IL-10 inhibits the production of pro-inflammatory cytokines IL-1B, TNF-α, and IL-8 from monocytes[89]. It also prevents monocyte recruitment to the arterial wall by preventing the expression of MCP-1 and ICAM-1, possibly through the suppression of the NF-kB activation[89]. IL-10 also modifies lipid metabolism in macrophages to prevent lipid accumulation and foam cell formation[153].

It is unclear why IL-10 levels were elevated in mice exposed to unmodified CAPs and deCAPs, but were not increased by adjCAPs. However, the increased levels of IL-10 in the CAPs and deCAPs exposures could implicate refractory components as being important to this response. There is limited evidence on the relationship between PM exposure and circulating IL-10 levels that would help explain this result. IL-10 expression was reduced in vascular $F4/80^{+}$ cells in a 10-week exposure to $PM_{2.5}$ CAPs

in a diet-induced obesity mouse model[154] indicating a pro-inflammatory effect of CAPs exposure. Conversely, an anti-inflammatory response occurred in mice exposed to PM with high and low metal content through oropharyngeal aspiration that had similarly increased serum concentrations of IL-10 relative to control[155]. The inconsistencies in effects of CAPs exposure on systemic IL-10 concentrations and the downstream effects on associated disease states will require more investigation to understand the various responses.

Markers of plaque vulnerability were increased in mice exposed to adjCAPs. Elevated IL-6 levels are related to increased plaque vulnerability[156], in part because IL-6 can induce the production of MMP-9 and PAI-1, both of which are also associated with higher plaque risk. IL-6 stimulates the production of MMP-9 in macrophages[157], which can lead to degradation of the fibrotic cap and enhanced risk of plaque rupture. Generation of PAI-1, a pro-thrombotic factor that inhibits fibrinolysis, is also promoted by IL-6[158]. The increased levels of IL-10 in mice exposed to unmodified CAPs may have promoted plaque stability by the inhibition of an increase in MMP-9[89] that enhanced levels of plaque fibrosis.

One limitation of the impact of CAPs on biomarkers of inflammation in this study is that the background levels of the biomarkers related to atherosclerosis are high in many cases because these animals are already susceptible to developing the disease. Therefore, the ability to see significant differences in certain biomarkers with CAPs exposure may be blunted, especially with endpoint measurements. Repeated measurements of serum biomarkers using serial blood draws may be one way to

counteract this problem by determining the trend of these markers over time and by comparing them to a pre-exposure baseline.

Another limitation in the complete applicability of these findings to human health is that the PM-related changes in atherosclerosis were found in a diseased mouse model. The mice used in this study were already susceptible to developing atherosclerosis because of the knockout of the apoE -/- gene and would have probably eventually developed the disease. However, the exposure to particulate matter enhanced the atherosclerotic progression in these mice, and in humans this would be relevant to people who are already at risk of developing atherosclerotic lesions due to other genetic and environmental risk factors.

5.3.2 Cholesterol

Mice exposed to the adjCAPs had a high ratio of total cholesterol to HDL. Total cholesterol to HDL ratio is a clinical measure of the relative amounts of circulating HDL and LDL cholesterol. An increase in the ratio is associated with increased risk of ischemic heart disease due to increased pro-atherogenic LDL and decreased cardioprotective HDL[159]. In humans, a ratio lower than 3.5:1 is considered healthy. In mice, the pro-atherogenic cutoff for the ratio is lower because they have much higher levels of circulating HDL cholesterol and lesser LDL[160]. Mice exposed to the adjCAPs had an average serum total to HDL cholesterol ratio of 4:1, which is pro-atherogenic even by human standards, and was significantly higher than mice receiving clean air.

The altered cholesterol ratio following adjCAPs exposure was consistent with findings that PM alters circulating cholesterol levels. In a population based cohort study

in Israel, three-month average PM_{10} concentrations were associated with increased blood LDL and decreased blood HDL[103]. Additionally, a study of diabetic Mexican Americans found that short-term $PM_{2.5}$ exposure was associated with decreased HDL to LDL ratio[161]. Long-term exposure to Beijing $PM_{2.5}$ also increased serum LDL in apoE -/- mice that had accelerated atherosclerotic plaque formation[65]. Although the mechanism of how PM exposure alters the cholesterol ratio has not yet been fully understood, exposure related changes in lipid metabolism in the adipose tissue[162] and the liver[163] have been observed following $PM_{2.5}$ inhalation.

5.3.3 Reactive Oxygen Species

Oxidized LDL was reduced in the serum of mice exposed to adjCAPs compared to clean air controls. This was an unexpected result as oxLDL is typically associated with increased atherosclerosis[164]. It was also expected that the particle associated SVOCs might be atherogenic because of its ability to cause oxidative damage in the vasculature that would promote formation of oxLDL. One possible explanation for the reduction in serum oxLDL was that there might have been increased scavenging of oxLDL by the arteries due to increased IL-6 signaling. To some extent the increased amount of total LDL in this group could have contributed to the reduced normalized level in the adjCAPs mice. Alternatively, oxidation of LDL could occur in the arterial wall rather than the plasma, meaning that plasma concentrations may not necessarily reflect the amount of lesion associated oxLDL, which is present at much higher concentrations than in the serum. A study of human carotid plaque oxLDL concentrations found that plaque concentrations were approximately 70 times higher than in plasma[165].

Lipid peroxidation in descending aorta homogenate was measured to determine if there was an increase in oxidized lipids in the arterial wall due to CAPs exposure. There was no difference in MDA, a marker for lipid peroxidation, between the exposure groups. However, the descending aorta is not a primary location of atherosclerotic plaque formation but it is also not totally void of lesion formation. The arteries that are more prone to lesion formation were used for histology, so the descending aorta was the best available option for the analysis. Testing for lipid peroxidation using an artery that is more susceptible to lesion development, or a immunohistochemical stain for oxLDL may give a better indication of increased oxidatively modified lipids in the arterial wall proximal to lesions due to CAPs exposure.

There was no difference in lipid peroxidation between lung homogenate samples from each exposure group. Systemic inflammatory signaling or particle translocation to the vascular does not necessarily need to be associated with markers of oxidative lung alterations to tissue components. The presence of redox-active SVOC compounds in CAPs would predict that oxidative stress in the lungs would occur, but that may not have been reflected in the lipid peroxidation measurements because the anti-oxidant response may have prevented measurable lipid peroxidation in the lung[70]. Further investigation into the anti-oxidant responses in the lung may determine that there was depletion of anti-oxidant molecules that may reflect pro-oxidant activity of the SVOCs in the lungs. Additionally, investigating markers of oxidative stress in the lungs after shorter-term exposures may yield a response that was masked by compensatory mechanisms that may have been activated after nine weeks of exposures.

5.4 Autonomic Effects of PM Exposure on the Progression of Atherosclerosis

5.4.1 Changes in Heart Rate Variability

HF HRV power was decreased post-exposure in mice exposed to CAPs. We observed a similar decrease in HF power with CAPs exposure in our previous study[68]. Decreased HF power is indicative of parasympathetic withdrawal, and this autonomic imbalance has been linked to a number of cardiovascular diseases, including atherosclerosis [127,166]. The HF HRV reduction in CAPs exposed mice was present following exposure and seemed to trend downward with each successive day of exposure during the exposure week, indicating that the acute response was cumulative over the course of daily repeated exposures. The post-exposure changes, however, were not cumulative week to week, so the weekend recovery period with no exposures may have allowed for a compensatory response to counteract the HF HRV reductions. Further investigation would be necessary to determine if HF HRV would continue to decline with further exposures beyond four days, or if the response would plateau over continuous repeated exposures.

There was no change in HF HRV in mice exposed to adjCAPs, which could be related to the lower exposure concentration, however those mice did also not have an increase in HF power from baseline as did the clean air and deCAPs exposed mice. It appears there may have been a dose effect on HF power relative to control related to the presence of the SVOCs. The CAPs exposed mice, with high levels of SVOCs, had the greatest reduction in HRV power while the adjCAPs mice, with less SVOCs, had a

smaller reduction and the deCAPs mice, with little to no SVOCs had the same response as control.

CAPs exposure may be related to acute reductions in HF power by altering parasympathetic response due to the activation of pulmonary C-fibers, which can be stimulated by pro-oxidative species within CAPs[108,109]. Given that SVOCs contain species such as PAHs that promote oxidative stress in the lungs, the presence of these species in the whole CAPs and absence in the denuded CAPs likely explain the differing acute responses in HF HRV. The decreased parasympathetic activity may promote increased atherosclerosis through alterations to hemodynamics or by promotion of cytokine release. Disruptions in normal vascular autonomic control of blood flow may alter shear stress on the vessel walls through increased turbulent flow, which has been linked to the progression of atherosclerosis[118]. The vagus nerve inhibits pro-inflammatory cytokine release and is protective against systemic inflammation[119], so a reduction in parasympathetic activity could minimize its atheroprotective effects.

One limitation of using HRV analysis a measure parasympathetic activity is the influence of respiratory changes on HF power. Respiratory sinus arrhythmia (RSA) is the primary driver of vagal control of the heart and, consequently, HF power under normal conditions[167]. Post-exposure reductions in HF power that were found in the present study could be related to a CAPs induced change in respiratory parameters such as respiratory rate or tidal volume. Alterations in both of these respiratory parameters have been linked to HRV changes[168], and future investigations may attempt

to determine if there is any impact of CAPs exposure on respiration and if it influences HRV in this mouse model.

Another way to look at the frequency domain parameters of HRV is to compare the relative contributions of LF and HF HRV by measuring the ratio of LF power to HF power. This measure was used in the past to designate the balance between the sympathetic and parasympathetic branches of the autonomic nervous system, which are associated with LF and HF HRV, respectively, but recent research has indicated that the LF component does not solely represent sympathetic input because LF activity is still present following sympathetic blockade[169]. Furthermore, noradrenaline spillover into cardiac venous drainage, a measure of sympathetic cardiac outflow, is not correlated with an increase in LF power or LF/HF ratio[170]. Also, increased sympathetic outflow due to disease or pharmacological intervention has been associated with decreased LF power[170]. Therefore, interpreting the LF/HF ratio as a measure of sympathovagal balance is dubious. The increase in the measure does indicate, however, that the HF power decreased following CAPs exposure at a greater magnitude than other frequency components, reinforcing the finding that the decrease in parasympathetic activity is the most prominent change following CAPs exposure relative to other, albeit undefined, autonomic processes that control the other components.

Another proposed physiological correlate for the contributions of the LF component of HRV is the cardiac autonomic outflow due to baroreflex[167,170] and the difference between sympathetic or parasympathetic cardiac autonomic outflow is not distinguished. The evidence for this correlate comes from several studies that show a severe reduction in LF power with impaired baroreflex function even when there is

normal cardiac sympathetic outflow[170]. Therefore, the decrease in LF power found in all groups in this study could be related to a blunting of the baroreflex response with increased age in apoE -/- mice. The decrease in LF power may also be related to the decrease in heart rate observed in all four groups, as LF power has been associated with mean heart rate[169].

Although the HRV findings are significant, they are limited in that they only look at a small timeframe of about five hours out of the day. The timeframe was chosen to minimize the effects of external influences on HRV that could mask the effects of the exposure. If there are sudden changes in heart rate or skipped beats caused by external stimuli, then the frequency domain HRV calculation is measuring the frequency of those effects on heart rate rather than the autonomic control of heart rate.

Data was not used from during the exposure because of the chamber stress and frequent noise from the presence of the technician monitoring the exposure system. The period immediately after the exposure was not desirable for HRV analysis because the mice were recovering from the stress of exposure and the excitement of being handled. Late afternoon and early evening were also not ideal because there was typically a severe drop in HRV during the switch from light to dark. Therefore, the 8PM-1AM timeframe was chosen to get a five-hour stable post-exposure period that minimized influences unrelated to the exposure. Future studies can minimize these external influences to get more immediate effects during and post-exposure by developing chambers that mice can stay in post-exposure and by better isolating the animals from external stimuli in the chambers during the exposure.

5.4.2 Associations of HF HRV with Particle Chemistry

The daily changes in post-exposure HF HRV in mice exposed to CAPs were positively associated with daily changes in the level of oxygenation of the particles and PAH content. During the 2014 study, comparisons were made between HF power and the total O:C ratio of the combined ultrafine and accumulation modes and no association was found. This may be because the O:C ratios were being influenced by the mass of a few larger accumulation mode particles that were present in the aerosol when most of the particles by number were present in the ultrafine range. Because of this, and the finding that the effect on HF power was related to the SVOCs present in the ultrafine mode, the association between HF power and oxygenation of just the ultrafine fraction was tested. An association was found between HF power and ultrafine O:C ratio at ratios of ~0.25:1 and lower.

The association between HF power and a low ultrafine O:C ratio strongly implicated SVOCs in being responsible for daily acute changes to autonomic control. The AMS measurements found that deCAPs had substantially increased O:C ratios after removal of SVOCs, meaning that the SVOCs in the original aerosol had relatively low O:C ratios. This finding is consistent with measurements of many components of primary organic aerosol, including PAHs, diesel and gasoline exhaust, and cooking aerosol, indicating that levels of primary organic aerosol may have been driving the effects on the autonomic nervous system. O:C ratios of SOA are greater than 0.25:1, and the difference in the type of particles above that cutoff may be responsible for the loss of the trend between O:C ratio and HF HRV during the few days of high UF O:C ratios. These findings were consistent with human biomarkers studies in which markers

of inflammation and cardiovascular disease were differentially associated with primary and secondary organics in PM[34,96].

PAHs are thought to be a main driver of oxidative stress induced by particle exposure because they can be biotransformed to reactive species in the lung. The resultant oxidative stress may then activate afferent pulmonary C-fibers that signal alterations of autonomic control of the heart. These findings are consistent with a number of epidemiological studies that link PAH exposure to reductions in HRV[171-173]. However, investigations into the chemical components of ambient PM that are related to HRV changes in humans are not as clear. Changes in HRV have been linked to metals[174], organic carbon[175], or no associations with $PM_{2.5}$ have been found at all[176]. The differences are probably related to regionally dependent compositions of the particles and subject related variations in the studies.

6 Conclusions

It is becoming increasingly apparent that exposure to particulate matter is related to changes in the progression of atherosclerosis and that the nature of these changes are dependent on particle concentration and composition. In this study we were able to link the exacerbation of atherosclerosis to exposure to semi-volatile constituents of PM that are primarily found in the ultrafine fraction of the aerosol. Our investigation may help explain why there is increasing evidence that cardiovascular effects of PM exposure are associated with the ultrafine fraction. Exposure to undenuded PM

(adjCAPs) at the same concentration as for denuded PM confirmed our earlier finding that removal of SVOCs from the aerosol by denuding significantly reduced atherogenicity. However, there were less atherogenic effects at a higher concentration of PM. This could suggest a change in the balance of pro-oxidant and anti-oxidant factors produced by higher levels of PM exposure.

PM-related SVOC exposure was associated with increased inflammatory markers and alterations to cholesterol levels, but no increased oxidative stress was found. IL-6 is a main pro-inflammatory cytokine involved in the normal pathophysiology of atherosclerosis and it appears that PM-related SVOCs promote atherosclerotic formation via its activation. Pro-atherogenic LDL cholesterol was also increased relative to anti-atherogenic HDL cholesterol in mice exposed to SVOCs in PM. The increase in inflammation related to PM exposure is likely altering lipid metabolism, and this is an emerging area of research into the effects of PM on the cardiovascular system with a number of recent studies also finding altered levels of LDL and HDL cholesterol. Although SVOCs have been linked to the pro-oxidant activity of PM, no increased markers of oxidative stress were measured. However, this study was limited to only looking at oxidative changes to lipids and does not completely discount that the particles may promote oxidative stress via another mechanism such as the depletion of anti-oxidants.

Alterations to autonomic function also appear to play a role in the exacerbation of atherosclerosis by PM exposure. Reductions in parasympathetic activity, a consequence associated with a number of cardiovascular diseases, were associated with exposure to SVOCs, and this reduction may be related to pro-atherogenic

increases in blood pressure and oxidative stress and inflammation in the vasculature. The most powerful aspect of analyzing daily changes in autonomic function by measures of heart rate variability is the ability to associate those changes with daily changes in particle characteristics. These associations implicated low-oxygenated organics that are characteristic of primary emissions as driving the effects on autonomic function. This supports the idea that semi-volaltile species such as PAHs are responsible for the toxic effects of PM on the cardiovascular system.

The findings of this project support the idea that regulatory controls of exposure to PM should take into account other particle characteristics in addition to particle size and mass concentration. The importance of ultrafine particles, the prevalence of which are not well described by measures of mass concentration, in the enhancement of atherosclerosis supports the need for better monitoring and regulation of these particles in the air. Furthermore, the finding that the chemical composition of primary emissions is potentially contributing to its enhanced toxicity can inform other researchers and decision makers on how better to protect public health either through controls and technologies to limit semi-volatile emissions or public planning to limit exposures to freshly emitted particles.

7 References

1. Phalen R. The Particulate Air Pollution Controversy: A Case Study and Lessons Learned. Boston: Kluwer Academic Publishers; 2002.

2. Pope CA, Burnett RT, Thurston GD, et al. Cardiovascular mortality and long-term exposure to particulate air pollution: epidemiological evidence of general pathophysiological pathways of disease. Circulation 2004;109:71-7.

3. Laden F, Schwartz J, Speizer FE, Dockery DW. Reduction in fine particulate air pollution and mortality: Extended follow-up of the Harvard Six Cities study. Am J Respir Crit Care Med 2006;173:667-72.

4. Schwartz J. Is there harvesting in the association of airborne particles with daily deaths and hospital admissions? Epidemiology 2001;12:55-61.

5. Burnett RT, Dales R, Krewski D, Vincent R, Dann T, Brook JR. Associations between ambient particulate sulfate and admissions to Ontario hospitals for cardiac and respiratory diseases. Am J Epidemiol 1995;142:15-22.

6. Dockery DW, Pope CA, Xu X, et al. An association between air pollution and mortality in six U.S. cities. N Engl J Med 1993;329:1753-9.

7. Miller F, Gardner D, Graham J, Lee R, Wilson W, Bachmann J. Size Considerations for Establishing A Standard for Inhalable Particles. Journal of the Air Pollution Control Association 1979;29:610-5.

8. EPA US. Integrated Review Plan for the National Ambient Air Quality Standards for Particulate Matter. Triangle Park, NC: Office of Air Quality Planning and Standards, U.S. Environmental Protection Agency; 2016.

9. Hester R, Harrison R. Airborne Particulate Matter: Sources, Atmospheric Processes and Health. Cambridge, United Kingdom: The Royal Society of Chemistry; 2016.

10. Guo ZG, Feng JL, Fang M, Chen HY, Lau KH. The elemental and organic characteristics of PM2.5 in Asian dust episodes in Qingdao, China, 2002. Atmospheric Environment 2004;38:909-19.

11. Paasonen P, Asmi A, Petaja T, et al. Warming-induced increase in aerosol number concentration likely to moderate climate change. Nature Geoscience 2013;6:438-42.

12. Stanier CO, Khlystov AY, Pandis SN. Nucleation events during the Pittsburgh air quality study: Description and relation to key meteorological, gas phase, and aerosol parameters. Aerosol Science and Technology 2004;38:253-64.

13. Hasheminassab S, Daher N, Ostro BD, Sioutas C. Long-term source apportionment of ambient fine particulate matter (PM2.5) in the Los Angeles Basin: A focus on emissions reduction from vehicular sources. Environmental Pollution 2014;193:54-64.

14. Fann N, Lamson AD, Anenberg SC, Wesson K, Risley D, Hubbell BJ. Estimating the national public health burden associated with exposure to ambient PM2.5 and ozone. Risk Anal 2012;32:81-95.

15. Garcia CA, Yap PS, Park HY, Weller BL. Association of long-term PM2.5 exposure with mortality using different air pollution exposure models: impacts in rural and urban California. Int J Environ Health Res 2016;26:145-57.

16. Hasheminassab S, Daher N, Saffari A, Wang D, Ostro BD, Sioutas C. Spatial and temporal variability of sources of ambient fine particulate matter (PM2.5) in California. Atmospheric Chemistry and Physics 2014;14:12085-97.

17. Arhami M, Sillanpaa M, Hu SH, Olson MR, Schauer JJ, Sioutas C. Size-Segregated Inorganic and Organic Components of PM in the Communities of the Los Angeles Harbor. Aerosol Science and Technology 2009;43:145-60.

18. Kim B, Teffera S, Zeldin M. Characterization of PM2.5 and PM10 in the South Coast Air Basin of southern California: Part 1 - Spatial variations. Journal of the Air & Waste Management Association 2000;50:2034-44.

19. ATSDR (Agency for Toxic Substances and Disease Registry): Toxicological Profile for Polycyclic Aromatic Hydrocarbons (PAHs). Atlanta, GA: U.S. Department of Health and Human Services, Public Health Service; 1995.

20. Eiguren-Fernandez A, Avol EL, Thurairatnam S, Hakami M, Froines JR, Miguel AH. Seasonal influence on vapor- and particle-phase polycyclic aromatic hydrocarbon concentrations in school communities located in Southern California. Aerosol Science and Technology 2007;41:438-46.

21. Eiguren-Fernandez A, Miguel AH, Froines JR, Thurairatnam S, Avol EL. Seasonal and spatial variation of polycyclic aromatic hydrocarbons in vapor-phase and PM 2.5 in Southern California urban and rural communities. Aerosol Science and Technology 2004;38:447-55.

22. Sawant AA, Na K, Zhu XN, Cocker DR. Chemical characterization of outdoor PM2.5 and gas-phase compounds in Mira Loma, California. Atmospheric Environment 2004;38:5517-28.

23. Singh M, Bowers K, Sioutas C. Seasonal and spatial trends in particle number concentrations and size distributions at the children's health study sites in Southern California. Journal of Exposure Science and Environmental Epidemiology 2006;16:3-18.

24. Chow J, Watson J, Fujita E, Lu Z, Lawson D, Ashbaugh L. Temporal and Spatial Variations of $PM_{2.5}$ and PM_{10} Aerosol in the Southern California Air-Quality Study. Atmospheric Environment 1994;28:2061-80.

25. Lough G, Schauer J, Park J, Shafer M, Deminter J, Weinstein J. Emissions of metals associated with motor vehicle roadways. Environmental Science & Technology 2005;39:826-36.

26. Chow JC. Measurement methods to determine compliance with ambient air quality standards for suspended particles. J Air Waste Manag Assoc 1995;45:320-82.

27. Krudysz M, Froines J, Fine P, Sioutas C. Intra-community spatial variation of size-fractionated PM mass, OC, EC, and trace elements in the Long Beach, CA area. Atmospheric Environment 2008;42:5374-89.

28. Robinson AL, Grieshop AP, Donahue NM, Hunt SW. Updating the Conceptual Model for Fine Particle Mass Emissions from Combustion Systems. Journal of the Air & Waste Management Association 2010;60:1204-22.

29. Zhang Q, Jimenez JL, Canagaratna MR, et al. Ubiquity and dominance of oxygenated species in organic aerosols in anthropogenically-influenced Northern Hemisphere midlatitudes. Geophysical Research Letters 2007;34.

30. Robinson AL, Donahue NM, Shrivastava MK, et al. Rethinking organic aerosols: Semivolatile emissions and photochemical aging. Science 2007;315:1259-62.

31. Shrivastava MK, Lane TE, Donahue NM, Pandis SN, Robinson AL. Effects of gas particle partitioning and aging of primary emissions on urban and regional organic aerosol concentrations. Journal of Geophysical Research-Atmospheres 2008;113.

32. Canagaratna MR, Jimenez JL, Kroll JH, et al. Elemental ratio measurements of organic compounds using aerosol mass spectrometry: characterization, improved calibration, and implications. Atmospheric Chemistry and Physics 2015;15:253-72.

33. Ng NL, Canagaratna MR, Zhang Q, et al. Organic aerosol components observed in Northern Hemispheric datasets from Aerosol Mass Spectrometry. Atmospheric Chemistry and Physics 2010;10:4625-41.

34. Delfino RJ, Staimer N, Tjoa T, et al. Associations of primary and secondary organic aerosols with airway and systemic inflammation in an elderly panel cohort. Epidemiology 2010;21:892-902.

35. Rager JE, Lichtveld K, Ebersviller S, et al. A toxicogenomic comparison of primary and photochemically altered air pollutant mixtures. Environ Health Perspect 2011;119:1583-9.

36. Herrington W, Lacey B, Sherliker P, Armitage J, Lewington S. Epidemiology of Atherosclerosis and the Potential to Reduce the Global Burden of Atherothrombotic Disease. Circ Res 2016;118:535-46.

37. Rathore SS, Hinn AR, Cooper LS, Tyroler HA, Rosamond WD. Characterization of incident stroke signs and symptoms: findings from the atherosclerosis risk in communities study. Stroke 2002;33:2718-21.

38. Stang PE, Carson AP, Rose KM, et al. Headache, cerebrovascular symptoms, and stroke: the Atherosclerosis Risk in Communities Study. Neurology 2005;64:1573-7.

39. Steinberg D. Low density lipoprotein oxidation and its pathobiological significance. J Biol Chem 1997;272:20963-6.

40. Vora DK, Fang ZT, Liva SM, et al. Induction of P-selectin by oxidized lipoproteins. Separate effects on synthesis and surface expression. Circ Res 1997;80:810-8.

41. Cushing SD, Berliner JA, Valente AJ, et al. Minimally modified low density lipoprotein induces monocyte chemotactic protein 1 in human endothelial cells and smooth muscle cells. Proc Natl Acad Sci U S A 1990;87:5134-8.

42. Gu L, Okada Y, Clinton SK, et al. Absence of monocyte chemoattractant protein-1 reduces atherosclerosis in low density lipoprotein receptor-deficient mice. Mol Cell 1998;2:275-81.

43. Fielding CJ, Fielding PE. Molecular physiology of reverse cholesterol transport. J Lipid Res 1995;36:211-28.

44. Nofer JR, Kehrel B, Fobker M, Levkau B, Assmann G, von Eckardstein A. HDL and arteriosclerosis: beyond reverse cholesterol transport. Atherosclerosis 2002;161:1-16.

45. Barter PJ, Puranik R, Rye KA. New insights into the role of HDL as an anti-inflammatory agent in the prevention of cardiovascular disease. Curr Cardiol Rep 2007;9:493-8.

46. Leitinger N, Schulman IG. Phenotypic polarization of macrophages in atherosclerosis. Arterioscler Thromb Vasc Biol 2013;33:1120-6.

47. Lusis AJ. Atherosclerosis. Nature 2000;407:233-41.

48. Kragel AH, Reddy SG, Wittes JT, Roberts WC. Morphometric analysis of the composition of atherosclerotic plaques in the four major epicardial coronary arteries in acute myocardial infarction and in sudden coronary death. Circulation 1989;80:1747-56.

49. Clarke MC, Bennett MR. Cause or consequence: what does macrophage apoptosis do in atherosclerosis? Arterioscler Thromb Vasc Biol 2009;29:153-5.

50. Clarke MC, Figg N, Maguire JJ, et al. Apoptosis of vascular smooth muscle cells induces features of plaque vulnerability in atherosclerosis. Nat Med 2006;12:1075-80.

51. Otsuka F, Sakakura K, Yahagi K, Joner M, Virmani R. Has our understanding of calcification in human coronary atherosclerosis progressed? Arterioscler Thromb Vasc Biol 2014;34:724-36.

52. Bentzon JF, Otsuka F, Virmani R, Falk E. Mechanisms of plaque formation and rupture. Circ Res 2014;114:1852-66.

53. Kolodgie FD, Burke AP, Farb A, et al. The thin-cap fibroatheroma: a type of vulnerable plaque: the major precursor lesion to acute coronary syndromes. Curr Opin Cardiol 2001;16:285-92.

54. Badimon L, Padró T, Vilahur G. Atherosclerosis, platelets and thrombosis in acute ischaemic heart disease. Eur Heart J Acute Cardiovasc Care 2012;1:60-74.

55. Rosenfeld ME, Polinsky P, Virmani R, Kauser K, Rubanyi G, Schwartz SM. Advanced atherosclerotic lesions in the innominate artery of the ApoE knockout mouse. Arterioscler Thromb Vasc Biol 2000;20:2587-92.

56. Plump AS, Smith JD, Hayek T, et al. Severe hypercholesterolemia and atherosclerosis in apolipoprotein E-deficient mice created by homologous recombination in ES cells. Cell 1992;71:343-53.

57. Nakashima Y, Plump AS, Raines EW, Breslow JL, Ross R. ApoE-deficient mice develop lesions of all phases of atherosclerosis throughout the arterial tree. Arterioscler Thromb 1994;14:133-40.

58. Schwartz SM, Galis ZS, Rosenfeld ME, Falk E. Plaque rupture in humans and mice. Arterioscler Thromb Vasc Biol 2007;27:705-13.

59. Adar SD, Sheppard L, Vedal S, et al. Fine particulate air pollution and the progression of carotid intima-medial thickness: a prospective cohort study from the multi-ethnic study of atherosclerosis and air pollution. PLoS Med 2013;10:e1001430.

60. Diez Roux AV, Auchincloss AH, Franklin TG, et al. Long-term exposure to ambient particulate matter and prevalence of subclinical atherosclerosis in the Multi-Ethnic Study of Atherosclerosis. Am J Epidemiol 2008;167:667-75.

61. Künzli N, Jerrett M, Mack WJ, et al. Ambient air pollution and atherosclerosis in Los Angeles. Environ Health Perspect 2005;113:201-6.

62. Kälsch H, Hennig F, Moebus S, et al. Are air pollution and traffic noise independently associated with atherosclerosis: the Heinz Nixdorf Recall Study. Eur Heart J 2014;35:853-60.

63. Sun Q, Wang A, Jin X, et al. Long-term air pollution exposure and acceleration of atherosclerosis and vascular inflammation in an animal model. JAMA 2005;294:3003-10.

64. Araujo JA, Barajas B, Kleinman M, et al. Ambient particulate pollutants in the ultrafine range promote early atherosclerosis and systemic oxidative stress. Circ Res 2008;102:589-96.

65. Chen T, Jia G, Wei Y, Li J. Beijing ambient particle exposure accelerates atherosclerosis in ApoE knockout mice. Toxicol Lett 2013;223:146-53.

66. Campen MJ, Lund AK, Knuckles TL, et al. Inhaled diesel emissions alter atherosclerotic plaque composition in ApoE(-/-) mice. Toxicol Appl Pharmacol 2010;242:310-7.

67. Leitinger N. Oxidized phospholipids as modulators of inflammation in atherosclerosis. Curr Opin Lipidol 2003;14:421-30.

68. Keebaugh AJ, Sioutas C, Pakbin P, Schauer JJ, Mendez LB, Kleinman MT. Is atherosclerotic disease associated with organic components of ambient fine particles? Sci Total Environ 2015;533:69-75.

69. Dellinger B, Pryor WA, Cueto R, Squadrito GL, Hegde V, Deutsch WA. Role of free radicals in the toxicity of airborne fine particulate matter. Chem Res Toxicol 2001;14:1371-7.

70. Li N, Hao M, Phalen RF, Hinds WC, Nel AE. Particulate air pollutants and asthma. A paradigm for the role of oxidative stress in PM-induced adverse health effects. Clin Immunol 2003;109:250-65.

71. Donaldson K, Brown DM, Mitchell C, et al. Free radical activity of PM10: iron-mediated generation of hydroxyl radicals. Environ Health Perspect 1997;105 Suppl 5:1285-9.

72. Verma V, Pakbin P, Cheung KL, et al. Physicochemical and oxidative characteristics of semi-volatile components of quasi-ultrafine particles in an urban atmosphere. Atmospheric Environment 2011;45:1025-33.

73. Tao F, Gonzalez-Flecha B, Kobzik L. Reactive oxygen species in pulmonary inflammation by ambient particulates. Free Radic Biol Med 2003;35:327-40.

74. Valko M, Leibfritz D, Moncol J, Cronin MT, Mazur M, Telser J. Free radicals and antioxidants in normal physiological functions and human disease. Int J Biochem Cell Biol 2007;39:44-84.

75. Brook RD. Cardiovascular effects of air pollution. Clin Sci (Lond) 2008;115:175-87.

76. Harrison D, Griendling KK, Landmesser U, Hornig B, Drexler H. Role of oxidative stress in atherosclerosis. Am J Cardiol 2003;91:7A-11A.

77. Kampfrath T, Maiseyeu A, Ying Z, et al. Chronic fine particulate matter exposure induces systemic vascular dysfunction via NADPH oxidase and TLR4 pathways. Circ Res 2011;108:716-26.

78. Araujo JA, Nel AE. Particulate matter and atherosclerosis: role of particle size, composition and oxidative stress. Part Fibre Toxicol 2009;6:24.

79. Furnkranz A, Schober A, Bochkov VN, et al. Oxidized phospholipids trigger atherogenic inflammation in murine arteries. Arterioscler Thromb Vasc Biol 2005;25:633-8.

80. Boesten LS, Zadelaar AS, van Nieuwkoop A, et al. Tumor necrosis factor-alpha promotes atherosclerotic lesion progression in APOE*3-Leiden transgenic mice. Cardiovasc Res 2005;66:179-85.

81. Schreyer SA, Vick CM, LeBoeuf RC. Loss of lymphotoxin-alpha but not tumor necrosis factor-alpha reduces atherosclerosis in mice. J Biol Chem 2002;277:12364-8.

82. Chew M, Zhou J, Daugherty A, et al. Thalidomide inhibits early atherogenesis in apoE-deficient mice. APMIS Suppl 2003:113-6.

83. Schuett H, Luchtefeld M, Grothusen C, Grote K, Schieffer B. How much is too much? Interleukin-6 and its signalling in atherosclerosis. Thromb Haemost 2009;102:215-22.

84. Keidar S, Heinrich R, Kaplan M, Hayek T, Aviram M. Angiotensin II administration to atherosclerotic mice increases macrophage uptake of oxidized ldl: a possible role for interleukin-6. Arterioscler Thromb Vasc Biol 2001;21:1464-9.

85. Huber SA, Sakkinen P, Conze D, Hardin N, Tracy R. Interleukin-6 exacerbates early atherosclerosis in mice. Arterioscler Thromb Vasc Biol 1999;19:2364-7.

86. Kirii H, Niwa T, Yamada Y, et al. Lack of interleukin-1beta decreases the severity of atherosclerosis in ApoE-deficient mice. Arterioscler Thromb Vasc Biol 2003;23:656-60.

87. Cesari M, Penninx BW, Newman AB, et al. Inflammatory markers and onset of cardiovascular events: results from the Health ABC study. Circulation 2003;108:2317-22.

88. Paffen E, DeMaat MP. C-reactive protein in atherosclerosis: A causal factor? Cardiovasc Res 2006;71:30-9.

89. Han X, Boisvert WA. Interleukin-10 protects against atherosclerosis by modulating multiple atherogenic macrophage function. Thromb Haemost 2015;113:505-12.

90. Han X, Kitamoto S, Wang H, Boisvert WA. Interleukin-10 overexpression in macrophages suppresses atherosclerosis in hyperlipidemic mice. FASEB J 2010;24:2869-80.

91. Hajat A, Allison M, Diez-Roux AV, et al. Long-term exposure to air pollution and markers of inflammation, coagulation, and endothelial activation: a repeat-measures analysis in the Multi-Ethnic Study of Atherosclerosis (MESA). Epidemiology 2015;26:310-20.

92. Pope CA, Hansen ML, Long RW, et al. Ambient particulate air pollution, heart rate variability, and blood markers of inflammation in a panel of elderly subjects. Environ Health Perspect 2004;112:339-45.

93. Seaton A, Soutar A, Crawford V, et al. Particulate air pollution and the blood. Thorax 1999;54:1027-32.

94. Tsai DH, Amyai N, Marques-Vidal P, et al. Effects of particulate matter on inflammatory markers in the general adult population. Part Fibre Toxicol 2012;9:24.

95. Dai J, Sun C, Yao Z, Chen W, Yu L, Long M. Exposure to concentrated ambient fine particulate matter disrupts vascular endothelial cell barrier function via the IL-6/HIF-1 α signaling pathway. FEBS Open Bio 2016;6:720-8.

96. Delfino RJ, Staimer N, Tjoa T, et al. Circulating biomarkers of inflammation, antioxidant activity, and platelet activation are associated with primary combustion aerosols in subjects with coronary artery disease. Environ Health Perspect 2008;116:898-906.

97. Cui Y, Sun Q, Liu Z. Ambient particulate matter exposure and cardiovascular diseases: a focus on progenitor and stem cells. J Cell Mol Med 2016;20:782-93.

98. Kita T, Kume N, Minami M, et al. Role of oxidized LDL in atherosclerosis. Ann N Y Acad Sci 2001;947:199-205; discussion -6.

99. Liu L, Ruddy T, Dalipaj M, et al. Effects of indoor, outdoor, and personal exposure to particulate air pollution on cardiovascular physiology and systemic mediators in seniors. J Occup Environ Med 2009;51:1088-98.

100. Sørensen M, Daneshvar B, Hansen M, et al. Personal PM2.5 exposure and markers of oxidative stress in blood. Environ Health Perspect 2003;111:161-6.

101. Soares SR, Carvalho-Oliveira R, Ramos-Sanchez E, et al. Air pollution and antibodies against modified lipoproteins are associated with atherosclerosis and vascular remodeling in hyperlipemic mice. Atherosclerosis 2009;207:368-73.

102. Ramanathan G, Yin F, Speck M, et al. Effects of urban fine particulate matter and ozone on HDL functionality. Part Fibre Toxicol 2016;13:26.

103. Yitshak Sade M, Kloog I, Liberty IF, Schwartz J, Novack V. The Association Between Air Pollution Exposure and Glucose and Lipids Levels. J Clin Endocrinol Metab 2016;101:2460-7.

104. Triposkiadis F, Karayannis G, Giamouzis G, Skoularigis J, Louridas G, Butler J. The sympathetic nervous system in heart failure physiology, pathophysiology, and clinical implications. J Am Coll Cardiol 2009;54:1747-62.

105. Olshansky B, Sabbah HN, Hauptman PJ, Colucci WS. Parasympathetic nervous system and heart failure: pathophysiology and potential implications for therapy. Circulation 2008;118:863-71.

106. Middlekauff HR, Park J, Moheimani RS. Adverse effects of cigarette and noncigarette smoke exposure on the autonomic nervous system: mechanisms and implications for cardiovascular risk. J Am Coll Cardiol 2014;64:1740-50.

107. Widdicombe J, Lee LY. Airway reflexes, autonomic function, and cardiovascular responses. Environ Health Perspect 2001;109 Suppl 4:579-84.

108. Bautista DM, Jordt SE, Nikai T, et al. TRPA1 mediates the inflammatory actions of environmental irritants and proalgesic agents. Cell 2006;124:1269-82.

109. Bessac BF, Jordt SE. Breathtaking TRP channels: TRPA1 and TRPV1 in airway chemosensation and reflex control. Physiology (Bethesda) 2008;23:360-70.

110. Lin YS, Hsu CC, Bien MY, Hsu HC, Weng HT, Kou YR. Activations of TRPA1 and P2X receptors are important in ROS-mediated stimulation of capsaicin-sensitive lung vagal afferents by cigarette smoke in rats. J Appl Physiol (1985) 2010;108:1293-303.

111. Hazari MS, Haykal-Coates N, Winsett DW, et al. TRPA1 and sympathetic activation contribute to increased risk of triggered cardiac arrhythmias in hypertensive rats exposed to diesel exhaust. Environ Health Perspect 2011;119:951-7.

112. Carll AP, Hazari MS, Perez CM, et al. Whole and particle-free diesel exhausts differentially affect cardiac electrophysiology, blood pressure, and autonomic balance in heart failure-prone rats. Toxicol Sci 2012;128:490-9.

113. Simula S, Laitinen T, Vanninen E, et al. Baroreflex sensitivity in asymptomatic coronary atherosclerosis. Clin Physiol Funct Imaging 2013;33:70-4.

114. Pham H, Bonham AC, Pinkerton KE, Chen CY. Central neuroplasticity and decreased heart rate variability after particulate matter exposure in mice. Environ Health Perspect 2009;117:1448-53.

115. Mack WJ, Islam T, Lee Z, Selzer RH, Hodis HN. Environmental tobacco smoke and carotid arterial stiffness. Prev Med 2003;37:148-54.

116. Wauters A, Dreyfuss C, Pochet S, et al. Acute exposure to diesel exhaust impairs nitric oxide-mediated endothelial vasomotor function by increasing endothelial oxidative stress. Hypertension 2013;62:352-8.

117. Amiya E, Watanabe M, Komuro I. The Relationship between Vascular Function and the Autonomic Nervous System. Ann Vasc Dis 2014;7:109-19.

118. Heo KS, Fujiwara K, Abe J. Shear stress and atherosclerosis. Mol Cells 2014;37:435-40.

119. Pavlov VA, Tracey KJ. The cholinergic anti-inflammatory pathway. Brain Behav Immun 2005;19:493-9.

120. Bernstein IM, Damron D, Schonberg AL, Sallam RM, Shapiro R. The relationship of plasma volume, sympathetic tone, and proinflammatory cytokines in young healthy nonpregnant women. Reprod Sci 2009;16:980-5.

121. Spengler RN, Allen RM, Remick DG, Strieter RM, Kunkel SL. Stimulation of alpha-adrenergic receptor augments the production of macrophage-derived tumor necrosis factor. J Immunol 1990;145:1430-4.

122. Pongratz G, Straub RH. The sympathetic nervous response in inflammation. Arthritis Res Ther 2014;16:504.

123. Rhoden CR, Wellenius GA, Ghelfi E, Lawrence J, González-Flecha B. PM-induced cardiac oxidative stress and dysfunction are mediated by autonomic stimulation. Biochim Biophys Acta 2005;1725:305-13.

124. Ghelfi E, Rhoden CR, Wellenius GA, Lawrence J, Gonzalez-Flecha B. Cardiac oxidative stress and electrophysiological changes in rats exposed to concentrated ambient particles are mediated by TRP-dependent pulmonary reflexes. Toxicol Sci 2008;102:328-36.

125. Heart rate variability: standards of measurement, physiological interpretation and clinical use. Task Force of the European Society of Cardiology and the North American Society of Pacing and Electrophysiology. Circulation 1996;93:1043-65.

126. Rowan WH, Campen MJ, Wichers LB, Watkinson WP. Heart rate variability in rodents: uses and caveats in toxicological studies. Cardiovasc Toxicol 2007;7:28-51.

127. Simula S, Vanninen E, Lehto S, et al. Heart rate variability associates with asymptomatic coronary atherosclerosis. Clin Auton Res 2014;24:31-7.

128. Huikuri HV, Jokinen V, Syvänne M, et al. Heart rate variability and progression of coronary atherosclerosis. Arterioscler Thromb Vasc Biol 1999;19:1979-85.

129. Wellenius GA, Saldiva PH, Batalha JR, et al. Electrocardiographic changes during exposure to residual oil fly ash (ROFA) particles in a rat model of myocardial infarction. Toxicol Sci 2002;66:327-35.

130. Tankersley CG, Campen M, Bierman A, Flanders SE, Broman KW, Rabold R. Particle effects on heart-rate regulation in senescent mice. Inhal Toxicol 2004;16:381-90.

131. Corey LM, Baker C, Luchtel DL. Heart-rate variability in the apolipoprotein E knockout transgenic mouse following exposure to Seattle particulate matter. J Toxicol Environ Health A 2006;69:953-65.

132. Lamb CM, Hazari MS, Haykal-Coates N, et al. Divergent electrocardiographic responses to whole and particle-free diesel exhaust inhalation in spontaneously hypertensive rats. Toxicol Sci 2012;125:558-68.

133. Farraj AK, Haykal-Coates N, Winsett DW, et al. Increased non-conducted P-wave arrhythmias after a single oil fly ash inhalation exposure in hypertensive rats. Environ Health Perspect 2009;117:709-15.

134. Carll AP, Haykal-Coates N, Winsett DW, et al. Cardiomyopathy confers susceptibility to particulate matter-induced oxidative stress, vagal dominance, arrhythmia and pulmonary inflammation in heart failure-prone rats. Inhal Toxicol 2015;27:100-12.

135. Chen LC, Hwang JS. Effects of subchronic exposures to concentrated ambient particles (CAPs) in mice. IV. Characterization of acute and chronic effects of ambient air fine particulate matter exposures on heart-rate variability. Inhal Toxicol 2005;17:209-16.

136. Kim S, Jaques PA, Chang MC, et al. Versatile aerosol concentration enrichment system (VACES) for simultaneous in vivo and in vitro evaluation of toxic

effects of ultrafine, fine and coarse ambient particles - Part II: Field evaluation. Journal of Aerosol Science 2001;32:1299-314.

137. Kim S, Jaques PA, Chang MC, Froines JR, Sioutas C. Versatile aerosol concentration enrichment system (VACES) for simultaneous in vivo and in vitro evaluation of toxic effects of ultrafine, fine and coarse ambient particles - Part I: Development and laboratory characterization. Journal of Aerosol Science 2001;32:1281-97.

138. Oldham MJ, Phalen RF, Robinson RJ, Kleinman MT. Performance of a portable whole-body mouse exposure system. Inhalation Toxicology 2004;16:657-62.

139. Folz RJ, Abushamaa AM, Suliman HB. Extracellular superoxide dismutase in the airways of transgenic mice reduces inflammation and attenuates lung toxicity following hyperoxia. J Clin Invest 1999;103:1055-66.

140. Schauer JJ. Evaluation of elemental carbon as a marker for diesel particulate matter. J Expo Anal Environ Epidemiol 2003;13:443-53.

141. Biswas S, Verma V, Schauer JJ, Cassee FR, Cho AK, Sioutas C. Oxidative potential of semi-volatile and non volatile particulate matter (PM) from heavy-duty vehicles retrofitted with emission control technologies. Environ Sci Technol 2009;43:3905-12.

142. Kleinman MT, Araujo JA, Nel A, et al. Inhaled ultrafine particulate matter affects CNS inflammatory processes and may act via MAP kinase signaling pathways. Toxicol Lett 2008;178:127-30.

143. Hoesel B, Schmid JA. The complexity of NF- κ B signaling in inflammation and cancer. Mol Cancer 2013;12:86.

144. Schieffer B, Selle T, Hilfiker A, et al. Impact of interleukin-6 on plaque development and morphology in experimental atherosclerosis. Circulation 2004;110:3493-500.

145. Szalai AJ, McCrory MA. Varied biologic functions of C-reactive protein: lessons learned from transgenic mice. Immunol Res 2002;26:279-87.

146. Teupser D, Weber O, Rao TN, Sass K, Thiery J, Fehling HJ. No reduction of atherosclerosis in C-reactive protein (CRP)-deficient mice. J Biol Chem 2011;286:6272-9.

147. Veldhuis GJ, Willemse PH, Sleijfer DT, et al. Toxicity and efficacy of escalating dosages of recombinant human interleukin-6 after chemotherapy in patients with breast cancer or non-small-cell lung cancer. J Clin Oncol 1995;13:2585-93.

148. Lyngsø D, Simonsen L, Bülow J. Metabolic effects of interleukin-6 in human splanchnic and adipose tissue. J Physiol 2002;543:379-86.

149. Zuliani G, Volpato S, Blè A, et al. High interleukin-6 plasma levels are associated with low HDL-C levels in community-dwelling older adults: the InChianti study. Atherosclerosis 2007;192:384-90.

150. Gomaraschi M, Basilico N, Sisto F, et al. High-density lipoproteins attenuate interleukin-6 production in endothelial cells exposed to pro-inflammatory stimuli. Biochim Biophys Acta 2005;1736:136-43.

151. Kusano K, Miyaura C, Inada M, et al. Regulation of matrix metalloproteinases (MMP-2, -3, -9, and -13) by interleukin-1 and interleukin-6 in mouse calvaria: association of MMP induction with bone resorption. Endocrinology 1998;139:1338-45.

152. Furenes EB, Seljeflot I, Solheim S, Hjerkinn EM, Arnesen H. Long-term influence of diet and/or omega-3 fatty acids on matrix metalloproteinase-9 and pregnancy-associated plasma protein-A in men at high risk of coronary heart disease. Scand J Clin Lab Invest 2008;68:177-84.

153. Han X, Kitamoto S, Lian Q, Boisvert WA. Interleukin-10 facilitates both cholesterol uptake and efflux in macrophages. J Biol Chem 2009;284:32950-8.

154. Sun Q, Yue P, Deiuliis JA, et al. Ambient air pollution exaggerates adipose inflammation and insulin resistance in a mouse model of diet-induced obesity. Circulation 2009;119:538-46.

155. Cuevas AK, Niu J, Zhong M, et al. Metal rich particulate matter impairs acetylcholine-mediated vasorelaxation of microvessels in mice. Part Fibre Toxicol 2015;12:14.

156. Yamagami H, Kitagawa K, Nagai Y, et al. Higher levels of interleukin-6 are associated with lower echogenicity of carotid artery plaques. Stroke 2004;35:677-81.

157. Kothari P, Pestana R, Mesraoua R, et al. IL-6-mediated induction of matrix metalloproteinase-9 is modulated by JAK-dependent IL-10 expression in macrophages. J Immunol 2014;192:349-57.

158. Cesari M, Pahor M, Incalzi RA. Plasminogen activator inhibitor-1 (PAI-1): a key factor linking fibrinolysis and age-related subclinical and clinical conditions. Cardiovasc Ther 2010;28:e72-91.

159. Lemieux I, Lamarche B, Couillard C, et al. Total cholesterol/HDL cholesterol ratio vs LDL cholesterol/HDL cholesterol ratio as indices of ischemic heart disease risk in men: the Quebec Cardiovascular Study. Arch Intern Med 2001;161:2685-92.

160. Pendse AA, Arbones-Mainar JM, Johnson LA, Altenburg MK, Maeda N. Apolipoprotein E knock-out and knock-in mice: atherosclerosis, metabolic syndrome, and beyond. J Lipid Res 2009;50 Suppl:S178-82.

161. Chen Z, Salam MT, Toledo-Corral C, et al. Ambient Air Pollutants Have Adverse Effects on Insulin and Glucose Homeostasis in Mexican Americans. Diabetes Care 2016;39:547-54.

162. Liu C, Bai Y, Xu X, et al. Exaggerated effects of particulate matter air pollution in genetic type II diabetes mellitus. Part Fibre Toxicol 2014;11:27.

163. Liu C, Xu X, Bai Y, et al. Air pollution-mediated susceptibility to inflammation and insulin resistance: influence of CCR2 pathways in mice. Environ Health Perspect 2014;122:17-26.

164. Li D, Mehta JL. Oxidized LDL, a critical factor in atherogenesis. Cardiovasc Res 2005;68:353-4.

165. Nishi K, Itabe H, Uno M, et al. Oxidized LDL in carotid plaques and plasma associates with plaque instability. Arterioscler Thromb Vasc Biol 2002;22:1649-54.

166. Zanobetti A, Gold DR, Stone PH, et al. Reduction in heart rate variability with traffic and air pollution in patients with coronary artery disease. Environ Health Perspect 2010;118:324-30.

167. Draghici AE, Taylor JA. The physiological basis and measurement of heart rate variability in humans. J Physiol Anthropol 2016;35:22.

168. Hirsch JA, Bishop B. Respiratory sinus arrhythmia in humans: how breathing pattern modulates heart rate. Am J Physiol 1981;241:H620-9.

169. Billman GE. The LF/HF ratio does not accurately measure cardiac sympatho-vagal balance. Front Physiol 2013;4:26.

170. Goldstein DS, Bentho O, Park MY, Sharabi Y. Low-frequency power of heart rate variability is not a measure of cardiac sympathetic tone but may be a measure of modulation of cardiac autonomic outflows by baroreflexes. Exp Physiol 2011;96:1255-61.

171. Yang B, Deng Q, Zhang W, et al. Exposure to Polycyclic Aromatic Hydrocarbons, Plasma Cytokines, and Heart Rate Variability. Sci Rep 2016;6:19272.

172. Li X, Feng Y, Deng H, et al. The dose-response decrease in heart rate variability: any association with the metabolites of polycyclic aromatic hydrocarbons in coke oven workers? PLoS One 2012;7:e44562.

173. Deng Q, Guo H, Deng N, et al. Polycyclic aromatic hydrocarbon exposure, miR-146a rs2910164 polymorphism, and heart rate variability in coke oven workers. Environ Res 2016;148:277-84.

174. Magari SR, Schwartz J, Williams PL, Hauser R, Smith TJ, Christiani DC. The association of particulate air metal concentrations with heart rate variability. Environ Health Perspect 2002;110:875-80.

175. Chuang KJ, Chan CC, Su TC, Lin LY, Lee CT. Associations between particulate sulfate and organic carbon exposures and heart rate variability in patients with or at risk for cardiovascular diseases. J Occup Environ Med 2007;49:610-7.

176. Bartell SM, Longhurst J, Tjoa T, Sioutas C, Delfino RJ. Particulate air pollution, ambulatory heart rate variability, and cardiac arrhythmia in retirement community residents with coronary artery disease. Environ Health Perspect 2013;121:1135-41.